SPATIAL MODELLING OF MONTHLY CLIMATE ACROSS MOUNTAINOUS TERRAIN IN SOUTHERN YUKON AND NORTHERN BRITISH COLUMBIA

HANNAH ACKERMAN

Thesis submitted to the University of Ottawa
in partial fulfillment of the requirements for the
Master of Science degree in Geography

Department of Geography, Environment and Geomatics
Faculty of Arts
University of Ottawa

© Hannah Ackerman, Ottawa, Canada, 2022

TABLE OF CONTENTS

ABSTRACT v
ACKNOWLEDGEMENTS vii
LIST OF FIGURES viii
LIST OF TABLES xiii
LIST OF ABBREVIATIONS xv
CHAPTER 1: INTRODUCTION 1
1.1 Introduction 1
1.2 Research Goals and Objectives 5
1.3 Background 6
1.3.1 Climate of southern Yukon and northern British Columbia 6
1.3.2 Modelling MMAT through lapse rates in complex terrains 7
1.3.3 FDD and TDD in TTOP modelling 11
1.4 Thesis structure 11
CHAPTER 2: STUDY REGION AND AREAS 12
2.1 Regional setting and permafrost distribution 12
2.2 Environment and Climate Change Canada sites & homogenization 16
2.3 Study area specific information 18
CHAPTER 3: MEAN MONTHLY AIR TEMPERATURE MODELLING IN SOUTHERN YUKON AND NORTHERN BRITISH COLUMBIA USING LAPSE RATES AND DEGREE OF CONTINENTALITY 19
3.1 Abstract 19
3.2 Introduction 20
3.3 Methods 21
3.3.1 Methods overview 22
3.3.2 Digital Elevation Model (DEM) preparation 23
3.3.3 Treeline model 24
3.3.4 Data processing 24
3.3.5 Spatial modelling of MMAT 32
3.3.6 MMAT model validation 34
3.4 Results 35
3.4.1 Monthly lapse rates 35

3.4.2 Mean monthly and seasonal air temperature 36
3.4.3 Evaluation of the MMAT models 58
3.4.4 Mean Annual Air Temperature 62
3.5 Discussion 64
3.5.1 Factors affecting model validity 64
3.5.2 Comparison with other temperature profile maps 65
3.5.3 Relationship between July MMAT and treeline 72
3.6 Conclusions 75
3.7 References 76
CHAPTER 4: FREEZING DEGREE DAY AND THAWING DEGREE DAY MODELLING IN SOUTHERN YUKON AND NORTHERN BRITISH COLUMBIA USING LAPSE RATES AND DEGREE OF CONTINENTALITY 79
4.1 Abstract 79
4.2 Introduction 80
4.3 Methods 80
4.3.1 Methods overview 81
4.3.2 Digital Elevation and treeline models 82
4.3.3 Data processing 82
4.3.4 Spatial modelling of FDD and TDD 87
4.3.5 FDD and TDD model validation 88
4.4 Results 90
4.4.1 Freezing and Thawing Degree Day maps 90
4.4.2 Evaluation of FDD and TDD models 93
4.4.3 Mean Annual Air Temperature 96
4.5 Discussion 98
4.5.1 Factors affecting model validity 98
4.5.2 Comparison with other FDD and TDD maps 99
4.5.3 MAAT maps 103
4.6 Conclusions 107
4.7 References 108
CHAPTER 5: CONCLUSIONS 110
5.1 Introduction 110
5.2 Summary of findings 110

5.3 Research limitations ... 111

5.4 Future research ... 112

BIBLIOGRAPHY ... 113

APPENDICES ... 117

Appendix A: Excluded data statistics ... 117

Appendix B: Lapse rate values ... 147

Appendix C: Government weather station data ... 148

Appendix D: Measured and modelled MMAT ... 150

Appendix E: Measured and modelled FDD and TDD ... 153

ABSTRACT

Two measures of air temperature trends across southern Yukon and northern British Columbia were modelled based on measurements from 83 monitoring sites across seven areas, operating for up to 14 years. Both mean monthly air temperature (MMAT) and freezing and thawing degree days (FDD and TDD, respectively) were modelled across this area (59 °N to 64.5 °N) at elevations ranging from 330-1480 m asl. Lapse rates in this region show inversions in the winter months (November – March) varying in inversion strength and length in relation to degree of continentality. The spatial and elevation range of these sites allowed for regional lapse rate modelling at the monthly scale for MMAT and at the annual scale for FDD and TDD. Lapse rates below treeline were found to be correlated ($p < 0.1$) with degree of continentality in the colder months (November – April) and August. In these months, lapse rates were modelled using kriging trend surfaces. In months where degree of continentality was not found to have a significant impact on lapse rates ($p > 0.1$) (May – October, excluding August), an average lapse rate calculated from the seven study regions was used across the study region. A combination of lapse rate trend surfaces, elevation, and temperatures at sea level were used to model MMAT and F/TDD below treeline. A treeline trend surface was created using a 4th order polynomial, allowing for temperatures at treeline to be determined. MMAT and F/TDD above treeline were calculated using a constant lapse rate of -6 °C/km, elevation, and temperature at treeline. The above and below treeline models were combined to create continuous models of MMAT and F/TDD.

Modelled MMAT showed a high degree of homogeneity across the study region in warmer months. Inversions in lapse rates are evident in the colder months, especially December through February, when colder temperatures are easily identified in valley bottoms, increasing to treeline, and decreasing above treeline. Modelled MMAT values were validated using 20 sites across the study region, using both Environment and Climate Change Canada and University of Ottawa sites. The RMSE between modelled and observed MMAT was highest in January (4.4 °C) and lowest in June (0.7 °C). Sites below treeline showed a stronger relationship between modelled and observed values than sites above treeline. Edge effects of the model were evident in the northeast of the study region as well as in the ice fields in the southwest along the Alaska border. The new MMAT maps can be used to help understand species range change, underlying permafrost conditions, and climate patterns over time.

FDD values were found to be highly influenced by both degree of continentality as well as latitude, whereas TDD values were mainly dependent on elevation, with degree of continentality and latitude being lesser influences. FDD and TDD were validated using the same 20 sites across the study region, with FDD showing a larger RMSE (368 degree days) between modelled and observed values than TDD (150 degree days). TDD modelling performed better on average, with a lower average absolute difference (254 degree days) between modelled and observed values at the validation sites than FDD modelling (947 degree days). The models of FDD and TDD represent a component of temperature at top of permafrost (TTOP) modelling for future studies.

Two mean annual air temperature (MAAT) maps were created, one calculated from the MMAT models, and the other from the F/TDD models. Most of the study region showed negative MAAT, mainly between -6 °C and 0 °C for both methods. The average MAAT calculated from FDD and TDD values was -2.4 ºC, whereas the average MAAT calculated from MMAT values was -2.8 ºC. Models of MAAT were found to be slightly warmer than in previous studies, potentially indicating warming temperature trends.

ACKNOWLEDGEMENTS

Thank you to the University of Ottawa community for the continued support throughout my Masters. Thank you to Dr. Phillip Bonnaventure at the University of Lethbridge for providing treeline data and to Alex Bevington for providing further temperature data at the Monarch study area.

Thank you to my supervisor, Dr. Antoni Lewkowicz, for your continued support and patience in my progression of my Masters. Our conversations of theories and modelling processes were always enriching and although sometimes confusing, allowed me to grow in my understanding of GIS and climate patterns. Toni, it has been an honour to work with you in the last few years of your career. I appreciate all you have done for me and wish you the best in your retirement.

I would also like to thank my committee members, Dr. Konrad Gajewski and Dr. André Viau, for their input on my project. Thank you, Konrad, for your assistance in modelling using GIS properties as well as your input on final map outputs. Thank you, André, for your support in determining the best way to work with incomplete datasets. The methodology of the project was greatly improved through yours and Toni's contributions.

Thank you to my friends for supporting me while I worked on this project and reminding me to take a break when I was feeling overwhelmed or stuck. Thank you especially to Nic Desjardins for helping me figure out where I went wrong with simple math. Although COVID caused a lot of social distancing and a complete change in our lives, your support through small get togethers and video calls added brightness to an otherwise isolating time.

Finally, thank you to my family for listening to me discuss a project that you did not fully understand. Thank you to Nikki Blair for reviewing my earliest drafts of my project and helping me find areas where I made assumptions of common knowledge. The biggest thanks go to my Mom and Dad for listening to presentations either before or after and letting me go on about my project as much as I would like. Your unwavering support has been invaluable.

LIST OF FIGURES

Figure 1-1. Topographic map of study area located in northern British Columbia and southern Yukon (ArcGIS Pro, 2020, Government of Canada, 2016; ESRI Data and Maps, 2021; Government of Canada, 2019a; ArcGIS Pro, 2020). 3

Figure 1-2. Mean annual air temperature predicted across the study region of northern British Columbia (59–60° N) and the southern half of the Yukon (60–65° N) (Lewkowicz et al., 2012)... 5

Figure 1-3. January mean daily temperature (Wahl et al., 1987). 9

Figure 1-4. July mean daily temperature (Wahl et al., 1987). 10

Figure 2-1. Study regions and validation sites in study area of southern Yukon and northern British Columbia, Canada. Study region locations are based on geographic centres of the individual sites within a study region (Government of Canada, 2016; ESRI Data and Maps, 2021; Government of Canada, 2018; ArcGIS Pro, 2020). 13

Figure 2-2. Area above and below treeline within the study area. 79% of the study area is located below treeline, 21% is located above treeline. These values exclude areas covered by glaciers or ice fields, where the model was not used to predict temperatures. The seven study areas used in creating the model are shown. Map based on treeline model and DEM from Chapter 3. 15

Figure 2-3. Map of the study region showing the locations of the Johnson's Crossing (JC), Sa Dena Hes (SDH), Faro (F), Keno (K) and Dawson (D) study areas in relation to permafrost zones (Heginbottom et al., 1995) and climatic regions (Wahl et al., 1987) (Bonnaventure & Lewkowicz, 2012). 16

Figure 3-1. Mean monthly air temperature methods overview. Solid boxes correspond to inputs or outputs. Dashed boxes correspond to ArcGIS Pro tools or Excel calculations.Blue boxes outline the steps of the DEM preparation, green outlines the steps to create a treeline model, red outlines the data processing, and purple outlines the MMAT modelling process. 22

Figure 3-2. Study regions and validation sites in study area of southern Yukon and northern British Columbia, Canada. Study region locations are based on geographic centres of the individual sites within a study region (Government of Canada, 2016; ESRI Data and Maps, 2021; Government of Canada, 2018; ArcGIS Pro, 2020). 26

Figure 3-3. Government weather stations (Appendix C, Table C-1 and C-2) within the study region as well as surrounding areas used to build the models of mean annual air temperature based on calculated lapse rates and temperatures at sea level and treeline. (Government of Canada, 2016; Government of Canada, 2019c; ESRI Data and Maps, 2021; NCEI, n.d.). 29

Figure 3-4. Monthly lapse rates at the seven study areas used to create models of MMAT. The Zero line is the threshold for inverted lapse rates. The global average annual lapse rate of -6.5°C/km is also shown. The degree of continentality for each study area is given in the legend. Specific monthly lapse rate values can be found in Appendix B. 36

Figure 3-5. Annual cycle of MMAT across the study region. Maximum and minimum values are the warmest and coldest modelled MMAT grid cells, respectively, in a given month, while the *average is the mean of all the grid cells.Mean MMAT is shown as the horizontal line within the boxes ± one SD on either side. The lines extending from the box represent the maximum and minimum MMAT value for the month across the entirety of the study region.* *37*

Figure 3-6. Modelled winter (December – February) mean air temperature across study region in northern British Columbia and southern Yukon, from 50 – 64.5° N. The seven study areas used in building the model are shown. Whitehorse (not shown) is located approximately 10 km northeast of Wolf Creek. *39*

Figure 3-7. Predicted December mean air temperature (MMAT) values across study region in northern British Columbia and Southern Yukon, from 59 – 64.5° N. The seven study areas used in building the model are shown. Whitehorse (not shown) is located approximately 10 km northeast of Wolf Creek. Average MMAT across the study region was calculated to be -15.5 °C. *40*

Figure 3-8. Predicted mean January air temperature (MMAT) values across study region in northern British Columbia and Southern Yukon, from 59 – 64.5° N. The seven study areas used in building the model are shown. Whitehorse (not shown) is located approximately 10 km northeast of Wolf Creek. Average MMAT across the study region was calculated to be -17 °C. *41*

Figure 3-9. Predicted mean February air temperature (MMAT) values across study region in northern British Columbia and Southern Yukon, from 59 – 64.5° N. The seven study areas used in building the model are shown. Whitehorse (not shown) is located approximately 10 km northeast of Wolf Creek. Average MMAT across the study region was calculated to be -14.6 °C. *42*

Figure 3-10. Modelled spring (March - May) mean air temperature across study region in northern British Columbia and Southern Yukon, from 59 – 64.5° N. The seven study areas used in building the model are shown. Whitehorse (not shown) is located approximately 10 km northeast of Wolf Creek. *44*

Figure 3-11. Predicted mean March air temperature (MMAT) values across study region in northern British Columbia and Southern Yukon, from 59 – 64.5° N. The seven study area used in building the model are shown. Whitehorse (not shown) is located approximately 10 km northeast of Wolf Creek. Average MMAT across the study region was calculated to be -9.8 °C. *45*

Figure 3-12. Predicted mean April air temperature (MMAT) values across study region in northern British Columbia and Southern Yukon, from 59 – 64.5° N. The seven study areas used in building the model are shown. Whitehorse (not shown) is located approximately 10 km northeast of Wolf Creek. Average MMAT across the study region was calculated to be -2.4 °C. *46*

Figure 3-13. Predicted mean May air temperature (MMAT) values across study region in northern British Columbia and Southern Yukon, from 59 – 64.5° N. The seven study areas used in building the model are shown. Whitehorse (not shown) is located approximately 10 km northeast of Wolf Creek. Average MMAT across the study region was calculated to be 4.8 °C. *47*

Figure 3-14. Modelled summer (June – August) mean air temperature across study region in northern British Columbia and Southern Yukon, from 59 – 64.5° N. The seven study areas used in building the model are shown. Whitehorse (not shown) is located approximately 10 km northeast of Wolf Creek. *49*

Figure 3-15. Predicted mean June air temperature (MMAT) values across study region in northern British Columbia and Southern Yukon, from 59 – 64.5° N. The seven study areas used in building the model are shown. Whitehorse (not shown) is located approximately 10 km northeast of Wolf Creek. Average MMAT across the study region was calculated to be 7 °C. *50*

Figure 3-16. Predicted mean July air temperature (MMAT) values across study region in northern British Columbia and Southern Yukon, from 59 – 64.5° N. The seven study areas used in building the model are shown. Whitehorse (not shown) is located approximately 10 km northeast of Wolf Creek. Average MMAT across the study region was calculated to be 12.4 °C. *51*

Figure 3-17. Predicted mean August air temperature (MMAT) values across study region in northern British Columbia and Southern Yukon, from 59 – 64.5° N. The seven study areas used in building the model are shown. Whitehorse (not shown) is located approximately 10 km northeast of Wolf Creek. Average MMAT across the study region was calculated to be 10.1 °C. *52*

Figure 3-18. Modelled autumn (September – November) mean air temperature across study region in northern British Columbia and Southern Yukon, from 59 – 64.5° N. The seven study areas used in building the model are shown. Whitehorse (not shown) is located approximately 10 km northeast of Wolf Creek. *54*

Figure 3-19. Predicted mean September air temperature (MMAT) values across study region in northern British Columbia and Southern Yukon, from 59 – 64.5° N. The seven study areas used in building the model are shown. Whitehorse (not shown) is located approximately 10 km northeast of Wolf Creek. Average MMAT across the study region was calculated to be 4.6 °C. *55*

Figure 3-20. Predicted mean October air temperature (MMAT) values across study region in northern British Columbia and Southern Yukon, from 59 – 64.5° N. The seven study areas used in building the model are shown. Whitehorse (not shown) is located approximately 10 km northeast of Wolf Creek. Average MMAT across the study region was calculated to be -3.5 °C. *56*

Figure 3-21. Predicted mean November air temperature (MMAT) values across study region in northern British Columbia and Southern Yukon, from 59 – 64.5° N. The seven study areas used in building the model are shown. Whitehorse (not shown) is located approximately 10 km northeast of Wolf Creek. Average MMAT across the study region was calculated to be -13.2 °C. *57*

Figure 3-22. Modelled and measured MMAT values for four validation sites located below treeline. A – AINA Base Camp (UO site) (RMSE 0.92), B – Beaver Creek Palsa (UO site) (RMSE 1.33), C – Carmacks (ECCC site) (RMSE 1.43), D – Hour Lake (ECCC site) (RMSE 1.98). Measured values are an average of a minimum of three years of data. Bars represent the SD of measured MMAT temperatures during the collection period. *59*

Figure 3-23. Modelled and measured MMAT values for four validation sites located above treeline. A – Alpine Burwash Backup (UO site) (RMSE 4.69), B – Macmillan Pass (ECCC site) (RMSE 4.03), C – Northern Dancer Backup (UO site) (RMSE 1.76), D – 60 Mile Backup (UO site) (RMSE 1.45). Measured values were averages of a minimum of three years of data. Bars represent the SD of measured MMAT temperatures during the collection period. *60*

Figure 3-24. Modelled mean annual air temperature (MAAT) values calculated as the average of all MMAT maps. Whitehorse (not shown) is located approximately 10 km northeast of Wolf Creek. Average MAAT across the study region was calculated to be -2.8 °C. 63

Figure 3-25. January MMAT values for Yukon Territory. Isotherm map (A) created by Wahl et al. (1987). (B) Gridded 90 x 90 m cell map created using modelled lapse rates below treeline and standard -6 °C/km lapse rate above treeline. Symbology has been matched as closely as possible for comparison to the map by Wahl et al. (1987). Red was used to indicate warmer temperatures than the top of the scale used by Wahl et al. (1987). 67

Figure 3-26. July MMAT values for Yukon Territory. Isotherm map (A) created by Wahl et al. (1987). Gridded 90 x 90 m cell map (B) created using modelled lapse rates below treeline and standard -6 °C/km lapse rate above treeline. Symbology has been matched as closely as possible for comparison to the map by Wahl et al. (1987). Purple was used to indicate colder temperatures than the end of the scale used by Wahl et al. (1987). 68

Figure 3-27. MAAT values for Yukon Territory. Isotherm map (A) created by Wahl et al. (1987). (B) Gridded 90 x 90 m cell map created using modelled lapse rates below treeline and standard -6 °C/km lapse rate above treeline. Symbology has been matched as closely as possible for comparison to the map by Wahl et al. (1987). Red was used to indicate warmer temperatures than the top of the scale used by Wahl et al. (1987). 69

Figure 3-28. MAAT values for Yukon Territory. Gridded map (A) created by Lewkowicz et al. (2012). Gridded 90 x 90 m cell map (B) created using modelled lapse rates below treeline and standard -6 °C/km lapse rate above treeline. 71

Figure 3-29. July MMAT values above and below treeline and the 10 °C threshold across study region in northern British Columbia and Southern Yukon, from 59 – 64.5° N. A – Below treeline and >10 °C, B – Below treeline and <10 °C, C – Above treeline and >10 °C, D – Above treeline and <10 °C. The seven study areas used in building the model are shown. 74

Figure 4-1. Freezing and thawing degree day methods overview. Solid boxes correspond to inputs or outputs. Dashed boxes correspond to ArcGIS Pro tools or Excel calculations. Blue boxes outline the steps of the DEM preparation, green outlines the steps to create a treeline model, red outlines the data processing, and purple outlines the FDD and TDD modelling process. 81

Figure 4-2. Study regions and validation sites in study area of southern Yukon and northern British Columbia, Canada. Study region locations are based on geographic centers of the individual sites within a study region (Government of Canada, 2016; ESRI Data and Maps, 2021; Government of Canada, 2018; ArcGIS Pro, 2020). 83

Figure 4-3. Measured FDD (A) and TDD (B) lapse rates below treeline and degree of continentality at seven study areas. The linear regression line for the two variables is shown. Regressions are significant at p = 0.1. FDD and DOC regression slope = -0.079. TDD and DOC regression slope = 0.028. Three areas (Johnson's Crossing, Wolf Creek, Monarch) were found to have no significant FDD lapse rate below treeline, these sites were given a lapse rate of 0 degree days/m. Sa Dena Hes was excluded from the calculation of TDD lapse rate due to a lack of data. 85

Figure 4-4. Government weather stations (Appendix C, Table C-1) within the study region as well as surrounding areas used to build the models of freezing and thawing degree days based on calculated FDD and TDD lapse rates and values at sea level and treeline. (Government of Canada, 2016; Government of Canada, 2019; ESRI Data and Maps, 2021). 89

Figure 4-5. Predicted freezing degree days (FDD) across study region in northern British Columbia and Southern Yukon, from 59 – 64.5º N. The seven study areas used in building the model are shown. Whitehorse (not shown) is located approximately 10 km northeast of Wolf Creek. Average FDD across the study region was calculated to be 2272 degree days. 91

Figure 4-6. Predicted thawing degree days (TDD) across study region in northern British Columbia and Southern Yukon, from 59 – 64.5º N. The seven study areas used in building the model are shown. Whitehorse (not shown) is located approximately 10 km northeast of Wolf Creek. Average TDD across the study region was calculated to be 1399 degree days. 92

Figure 4-7. Measured and modelled (A) FDD and (B) TDD values at the 20 validation sites. A 1:1 reference line is shown as a comparison guide. One validation site below treeline, Alaska Highway MP681 (848 m asl), did not have a measured value for comparison and was therefore excluded. 94

Figure 4-8. Predicted mean annual air temperature (MAAT) values across study region in northern British Columbia and Southern Yukon, from 59 – 64.5º N. Calculated from modelled FDD and TDD values. Whitehorse (not shown) is located approximately 10 km northeast of Wolf Creek. Average MAAT across the study region was calculated to be -2.4 ºC. 97

Figure 4-9. Climate Atlas of Canada FDD days in comparison to modelled FDD days at 14 sites in Yukon and British Columbia. Climate Atlas of Canada based on FDD values calculated from data collected between 1976 – 2005. Modelled FDD values calculated from data collected between 2006 – 2019. Average difference calculated to be 275 freezing degree days............................ 102

Figure 4-10. MAAT map calculated using MMAT values (A) by Lewkowicz et al. (2012) and MAAT map calculated using FDD and TDD values (B). 104

Figure 4-11. Difference in mean annual air temperature predictions calculated by subtracting the FDD and TDD-based MAAT values from the MMAT-based MAAT values. Whitehorse (not shown) is located approximately 10 km northeast of Wolf Creek. The average difference in MAAT models across the study region was calculated to be -0.4 ºC. 106

LIST OF TABLES

Table 2-1. Study regions in Yukon and British Columbia paired with nearest homogenized Environment and Climate Change Canada weather stations (Government of Canada, 2017; Government of Canada, 2018). *17*

Table 2-2. Study area information for number of usable sites within each area, minimum and maximum elevation of sites within the area, general vegetation cover, and the start date of data collection. *18*

Table 3-1. Root Mean Square Error and regression slope coefficients for modelled vs. observed MMAT values at 20 validation sites *58*

Table 3-2. Areas with July MMAT above and below 10 ºC in relation to treeline. *72*

Table 3-3. Percent of area above treeline where modelled July MMAT exceeds 10°C at half degree intervals *72*

Table 4-1. FDD, TDD, and difference values for two pairs of sites spanning treeline. *88*

Table 4-2. Modelled and measured FDD and TDD values for four sites below treeline. Difference values were calculated as measured minus modelled *95*

Table 4-3. Modelled and measured FDD and TDD values for four sites above treeline. Difference values were calculated as modelled minus measured *95*

Table 4-4. RMSE and slope coefficient. *96*

Table 4-5. Percent area of difference between MAAT maps created using MMAT and FDD and TDD values. *105*

Table A-1. Months missing data excluded from MMAT, FDD, and TDD calculations. Months were only excluded if missing more than 8 days of data. The number of months missing data is across all 83 sites collecting data from 2006 – 2019. .... *117*

Table A-2. Excluded or missing data from Dawson sites located below treeline used in lapse rate modelling. Green indicates data that was used. Red indicates missing data where a minimum of 8 days of data was missing. No fill indicates time outside of the data collection period for the site. *118*

Table A-3. Excluded or missing data from Faro sites located below treeline used in lapse rate modelling. Green indicates data that was used. Red indicates missing data where a minimum of 8 days of data was missing. No fill indicates time outside of the data collection period for the site. *123*

Table A-4. Excluded or missing data from Johnson Crossing sites located below treeline used in lapse rate modelling. Green indicates data that was used. Red indicates missing data where a minimum of 8 days of data was missing. No fill indicates time outside of the data collection period for the site. *125*

Table A-5. Excluded or missing data from Keno sites located below treeline used in lapse rate modelling. Green indicates data that was used. Red indicates missing data where a minimum of 8 *days of data was missing. No fill indicates time outside of the data collection period for the site. 130*

Table A-6. Excluded or missing data from Monarch sites located below treeline used in lapse rate modelling. Green indicates data that was used. Red indicates missing data where a minimum of 8 days of data was missing. No fill indicates time outside of the data collection period for the site. 135

Table A-7. Excluded or missing data from Sa Dena Hes sites located below treeline used in lapse rate modelling. Green indicates data that was used. Red indicates missing data where a minimum of 8 days of data was missing. No fill indicates time outside of the data collection period for the site. 139

Table A-8. Excluded or missing data from Wolf Creek sites located below treeline used in lapse rate modelling. Green indicates data that was used. Red indicates missing data where a minimum of 8 days of data was missing. No fill indicates time outside of the data collection period for the site. 141

Table B-1. Monthly lapse rate at the seven study areas used to create kriging trend surfaces of lapse rate for MMAT modelling across the study region. The global average annual value is -6.5°C/km. 147

Table C-1. Environment and Climate Change Canada (Government of Canada, 2022b) weather station elevations and coordiates (WGS 1984). 148

Table C-2. National Centers for Environmental Information (NCEI, n.d.) weather station elevations and coordinates (WGS 1984). 149

Table D-1. Elevation (m asl) and coordinates (WGS 1984) for the validations sites. 150

Table D-2. Measured MMAT and MAAT values at 20 validation sites within the study region. Measured values are based on either ECCC or University of Ottawa temperature monitoring stations. Data was collected between 2006 – 2019, with a minimum of 3 years of data............ 151

Table D-3. Modelled MMAT and MAAT values at 20 validation sites within the study region. Modelled values were based on values from Chapter 3.4. 152

Table E-1. Measured FDD, TDD, amd MAAT values at 20 validation sites within the study region. Measured values are based on either ECCC or University of Ottawa temperature monitoring stations. Data was collected between 2006 – 2019, with a minimum of 3 years of data............ 153

Table E-2. Modelled FDD, TDD, and MAAT values at 20 validation sites within the study region. Modelled values were based on values from Chapter 4.4. 154

LIST OF ABBREVIATIONS

DEM	digital elevation model
ECCC	Environment and Climate Change Canada
FDD	freezing degree days
IPCC	Intergovernmental Panel on Climate Change
MAAT	mean annual air temperature
MMAT	mean monthly air temperature
NCEI	National Centers for Environmental Information
TDD	thawing degree days
TTOP	temperature at top of permafrost
UTM WGS84	Universal Transverse Mercator World Geodetic System 1984

CHAPTER 1: INTRODUCTION

1.1 Introduction

Over the past several decades polar amplification and increased water vapour in the atmosphere have caused polar regions to warm twice as rapidly on average as the rest of the world (Walsh, 2014), amplified through positive feedback loops created by decreased snow and sea ice cover (IPCC, 2019). The atmosphere is warming with increased greenhouse gas emissions, caused by building heating and cooling, transportation, manufacturing, agriculture, and forestry, among other factors (Bush & Lemmen, 2019). This has resulted in global climate change that is disproportionately affecting polar regions (IPCC, 2019). For example, average winter temperatures in the Arctic in 2016 and 2018 were 6 ºC warmer than the 1981-2010 30-year average (IPCC, 2019).

Warming polar regions will result in major changes in the cryosphere, causing water to be released from ice shelves, glaciers, icebergs, and ice-rich permafrost. Northern British Columbia and southern Yukon Territory are underlain by permafrost ranging from isolated patches to continuous permafrost (Bonnaventure & Lewkowicz, 2012). Over the past decade, permafrost in high mountain areas has seen an increase of 0.19 ºC ± 0.05 ºC in ground temperature due to climate change, decreasing permafrost thickness and causing some ground ice melt (IPCC, 2019).

Increased ocean water levels from glacier melt and warmer ocean water will result in flooding of coastal areas as well as changes to drainage basins in northern communities where permafrost thaw occurs. Degradation of ice-rich permafrost can also cause multiple issues with infrastructure as the ground becomes less stable, destroying or destabilizing roadways, buildings, pipelines, and train tracks (Larsen *et al.*, 2008; Melvin *et al.*, 2016). The degradation of permafrost has been linked to increased frequency, magnitude, and location of natural disasters from mud or rockslides through increased active layer thickness and decreased stability along mountain slopes (IPCC, 2019; Bush & Lemmen, 2019). Snow cover, glaciers, sea ice, and permafrost are projected to continue to decline throughout the 21st century to varying degrees based on all RCP models (IPCC, 2019).

Climate indices currently used to define the climate in Yukon and northern British Columbia have been based on Environment and Climate Change Canada (ECCC) weather station data (Government of Canada, 2019c; Wahl *et al.*, 1987). While the ECCC stations have the advantage of long records, they are limited by being sparse and located predominantly at low elevations in valley bottoms (Government of Canada, 2018). As a result, the current weather station network does not allow for a full spatial representation of the climate in the region's complex, mountainous terrain. Furthermore, climate indices for the study area need to be updated to take into account the increased annual and seasonal average temperatures. These have increased rapidly across Canada in recent decades with the greatest differences occurring in the winter months and in northern Canada (Bush & Lemmen, 2019).

As a general trend, air temperatures decrease with increasing elevation at a global average lapse rate of 6.5 °C/km (Encyclopædia Britannica, Inc., n.d.). For the purposes of this study, the normal lapse rate will be expressed as -6.5 °C/km, indicating a decrease in air temperature with increasing elevations. Inversions in lapse rates will therefore be expressed as positive values. Air temperature lapse rates vary spatially across the terrain in northern British Columbia and southern Yukon, however, as a result of the complex landscape (*Figure 1-1*). Mountain ranges block warm, moist maritime air from reaching valleys. This can cause cold air to be trapped in valleys in winter while the higher elevations remain warmer, making it challenging to accurately represent temperature profiles (Wahl *et al.*, 1987). Once the cold, dense air mass has settled in the valley, there is very little vertical mixing, so that warmer air can sit atop colder air, creating an inverted and irregular temperature profile. Inverted lapse rates occur in other mountainous areas (Kattel *et al.*, 2013; Rolland, 2003), but the northern location of the study region and the height of the mountains limits the amount of incoming solar radiation that can reach the valley bottom and warm the air, especially in winter.

Local cold air drainage is another challenge for predicting temperature profiles within Yukon and northern British Columbia. Intensely cold, high-pressure cells may give rise to conditions in which cold air drains from high mountain areas to low valley bottoms. Near Fort Nelson, British Columbia, monitoring along an elevation gradient during one event showed a difference of 31 ºC between the warmest (highest) and coldest (lowest) sites (Harris, 1982). An accurate model of temperature in the region therefore requires an analysis of lapse rates on a month-to-month basis.

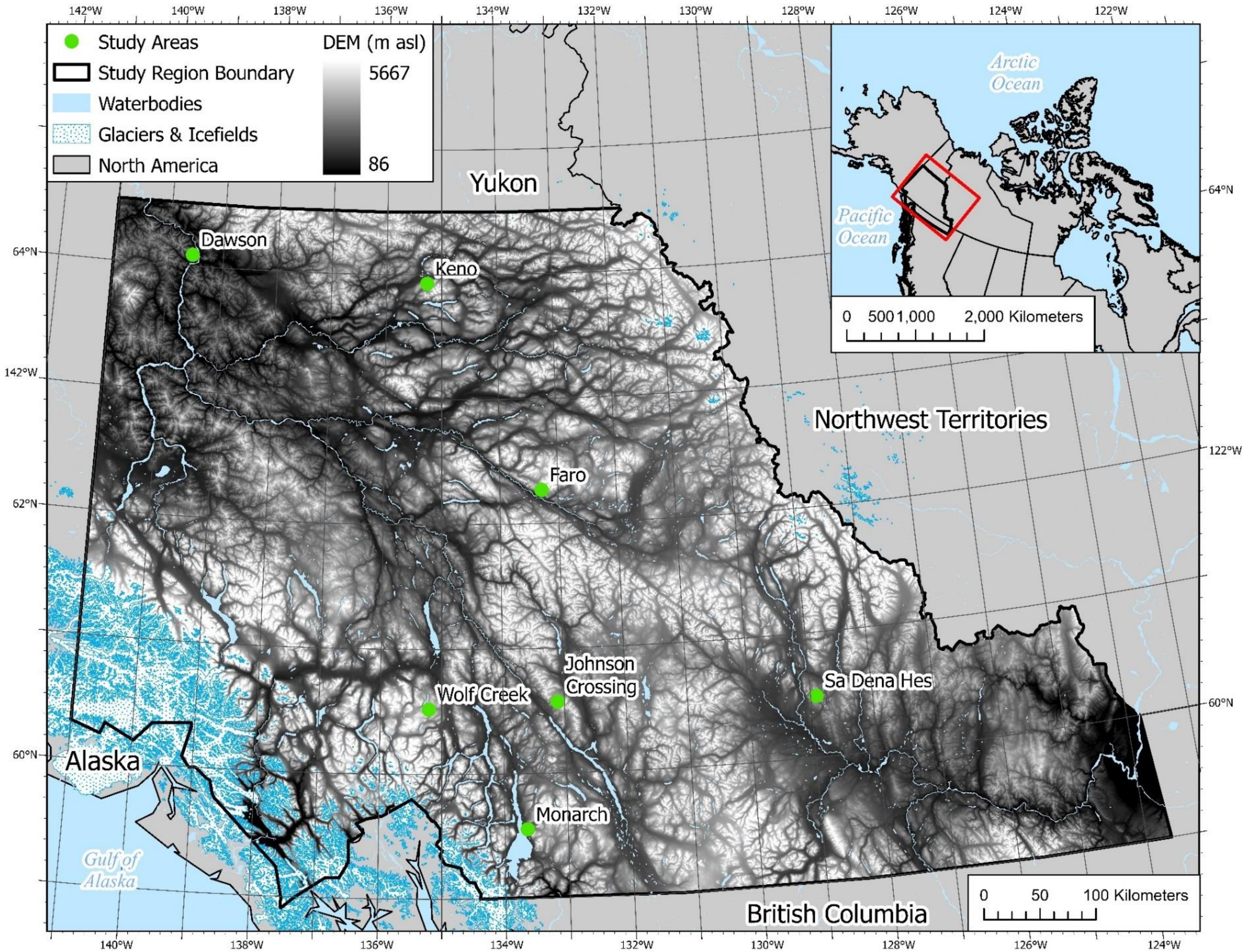

Figure 1-1. Topographic map of study area located in northern British Columbia and southern Yukon (ArcGIS Pro, 2020, Government of Canada, 2016; ESRI Data and Maps, 2021; Government of Canada, 2019a; ArcGIS Pro, 2020).

Another factor affecting the climate patterns of southern Yukon and northern British Columbia is the degree of continentality (Bonnaventure & Lewkowicz, 2013). A higher degree of continentality (DOC) occurs where there is a larger difference in mean temperature from the coldest month to the warmest month. Areas that are located closer to the ocean have smaller differences in temperature between the warmest and coldest months (Bonnaventure & Lewkowicz, 2013). The further inland the area, the greater the degree of continentality and the greater the annual temperature range.

Understanding lapse rates in the study area is important because air temperature is critical to ecological processes and the distribution of permafrost. Lewkowicz *et al.* (2012) derived a mean annual air temperature (MAAT) map for this study area at a 30 x 30 m resolution using short-term data and the strong relationship between degree of continentality and annual lapse rates below tree line (*Figure 1-2*). This map shows temperature ranging from >5 °C in maritime areas to <-10 °C in high, unglaciated mountains (Lewkowicz *et al.*, 2012). However, no recent maps of monthly temperatures exist for the study area. More detailed monthly analyses based on longer records and modelled monthly temperature lapse rates would allow for improved spatial modelling of MMAT profiles. A detailed analysis of annual temperature patterns would also allow for freezing and thawing degree day maps to be created.

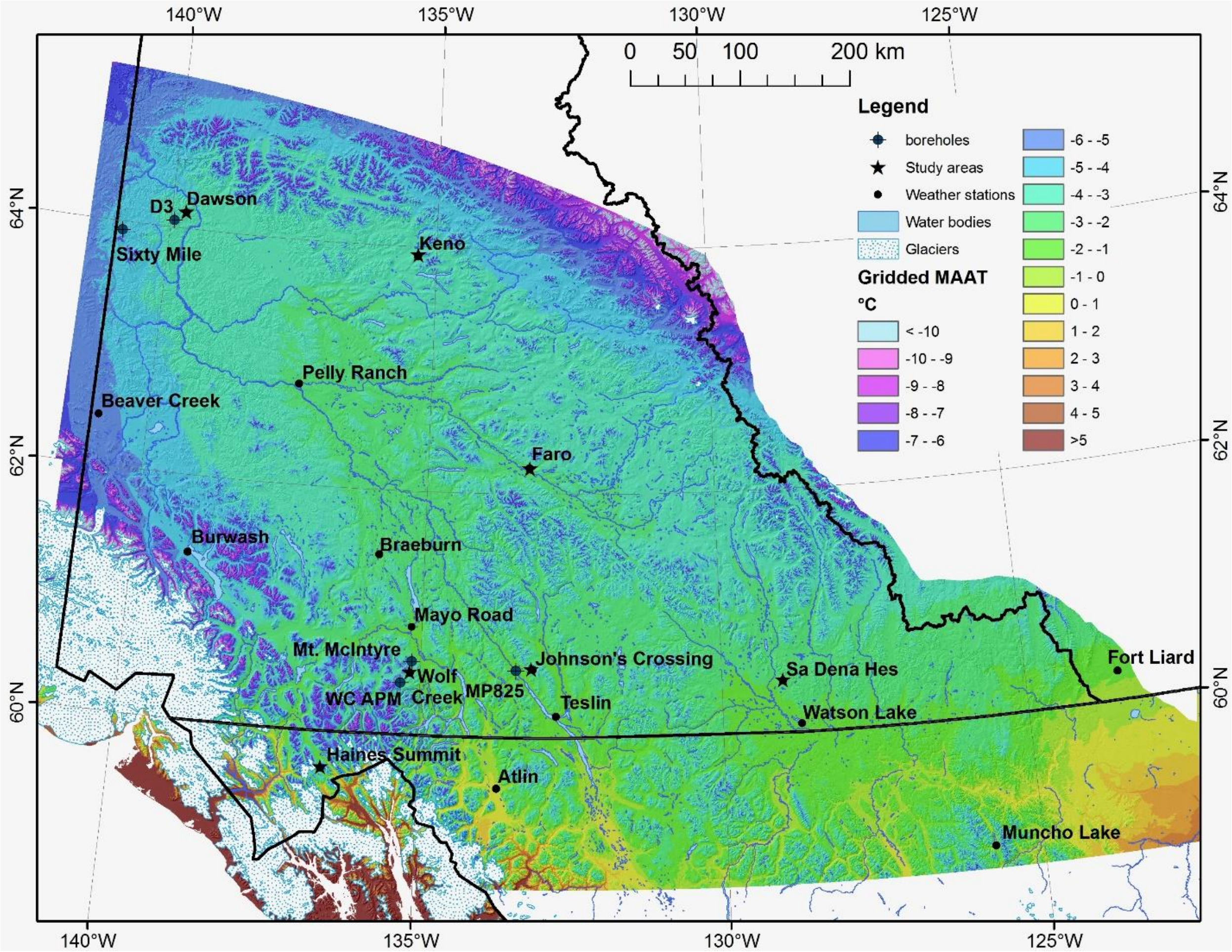

Figure 1-2. Mean annual air temperature predicted across the study region of northern British Columbia (59–60° N) and the southern half of the Yukon (60–65° N) (Lewkowicz et al., 2012).

1.2 Research Goals and Objectives

The objective of this thesis is to develop a better understanding of climate in the mountainous terrain of the southern Yukon and northern British Columbia. The research question is:

What is the relationship between climate indices developed using data from government climate stations and (1) monthly air temperature lapse rates, and (2) freezing and thawing degree-days?

This is answered by modelling MMAT across the region based on measured lapse rates and by modeling annual freezing and thawing degree days.

Data are available from seven areas that represent clusters of air temperature monitoring sites at varied elevations within the study region, as well as from single sites scattered across the region that are used for validation. The spatially clustered data are used to calculate monthly lapse rates and freezing and thawing degree days.

The following steps were taken to answer the research question:

1) Compilation of a dataset of mean daily and monthly temperatures for all field sites and for government climate stations.
2) Creation of monthly linear models of air temperature and elevation for each area.
3) Use of the linear models from the second step together with degree of continentality of the area to create MMAT maps for the entire study region.
4) Compilation of a dataset of total freezing degree days (FDD) and thawing degree days (TDD) for all field sites and for government climate stations.
5) Creation of linear models of TDD and FDD and elevation for each area.
6) Use of the linear models from the fifth step together with degree of continentality of the area to create TDD and FDD maps for the entire study region.

The research is significant as climate, and especially air temperature, is important to many other fields of study. The MMAT maps provide more detail regarding temperature than those currently available (e.g., Wahl *et al.*, 1987; Lewkowicz *et al.*, 2012). As an example of their potential utility, the MMAT maps could be used to investigate the impact of changing climate conditions on the range of a species (Rowland *et al.*, 2016; IPCC, 2019).

FDD and TDD maps do not currently exist for this region. Their development allows for temperature at the top of permafrost (TTOP) modelling which requires FDD and TDD as inputs (Bevington & Lewkowicz, 2015; Way & Lewkowicz, 2016).

1.3 Background

1.3.1 Climate of southern Yukon and northern British Columbia

The study region ranges from 59 ºN to 64.5 ºN and has a subarctic continental climate with characteristically warm summers up to 15 °C and cold winters with average monthly temperatures between -20 and −30 °C (Rowland *et al.*, 2016; Wahl *et al.*, 1987). Average annual air temperatures range from -14 °C to 2 °C, with a mainly north-south trend, except for the high elevation cold area within the St. Elias and Coast Mountain ice fields (Wahl *et al.*, 1987). However, extremes in temperature have shown a range of 99.3 °C, with a measured high of 36.5 °C in 2004 in Mayo and a low of -62.8 °C in 1947 in Snag (Government of Canada, 2019b; Wahl *et al.*, 1987).

Precipitation within the region is non-uniform in distribution, largely due to local topography. Northeast sides of mountain chains can receive as little as 250 – 300 mm of rain annually whereas southern coastal areas can receive up to 2000 – 3500 mm annually (Wahl *et al.*, 1987). The variability in precipitation is a result of orographic lifting, stripping moisture from the warm maritime air masses as they move inland (Rowland *et al.*, 2016). Precipitation is highest between June and December with less falling from January to May (Wahl *et al.*, 1987). Much of the St. Elias and Coast Mountain ranges in southwestern Yukon and northwestern British Columbia are currently glaciated (Wahl *et al.*, 1987). The study area also experiences high winds that cause snow drift and displacement, resulting in an uneven snowpack depth which can influence the presence of permafrost at a site (Bonnaventure & Lewkowicz, 2012).

Climate change in the study region will result in increases in temperature, changes in annual precipitation, thawing of permafrost, and glacial melt (Rowland *et al.*, 2016; Bush & Lemmens, 2019; IPCC, 2019). With these changes come challenges for infrastructure, alterations to species ranges, changed river flow patterns, and increased numbers of forest fires that may negatively impact air quality (Government of Yukon, 2018). Over the past 50 years, Yukon has seen a 2 °C increase in temperature and a 6% increase in precipitation, whereas the average global temperature has only increased 0.74 °C in the past century (Government of Yukon, 2018; IPCC, 2012). Although the Yukon and British Columbia governments have put in place mitigation strategies to reduce greenhouse gas emissions, the global oceanic and atmospheric transport systems mean that the world as a whole will need to drastically reduce greenhouse gas emissions to mitigate the changes occurring in this sub-arctic climate zone (Government of Yukon, 2009). Gaining a better understanding of the current climate in the area, the central goal of this thesis, is a first step in developing a better understanding of future climate change.

1.3.2 Modelling MMAT through lapse rates in complex terrains

There is a considerable literature on air temperature trends with elevation in complex topography. A study in southeastern Australia in a plateau to valley scarp transition looked at various factors influencing lapse rates including elevation, aspect, slope, and vegetation (Laughlin, 1982). The study found that temperature inversions were uncommon in the area but did occasionally occur with extreme weather conditions (Laughlin, 1982).

Rolland (2003) examined lapse rates in the Italian and Austrian Alps. The goal was to determine seasonal and spatial differences in lapse rates in the mountain ranges. Differences in lapse rates among the alpine areas were linked to differences in the height of the mountains and their corresponding valley depths (2003). Lapse rates were much lower than the global annual average lapse rate of -6.5 °C/km with many of them being close to -1 °C/km (Rolland, 2003). The strongest lapse rates were observed in summer and the weakest in the winter months (Rolland, 2003).

Kattel *et al.* (2012) undertook a similar study in the Himalayas focusing on the lapse rate on a southern slope in the complex terrain. This location had an uneven distribution of precipitation similar to the Yukon study region as a result of orographic lifting (Bonnaventure & Lewkowicz, 2013). The study found that there were no inverted lapse rates but that there were seasonal variations that resulted in weaker than average lapse rates (Kattel *et al.*, 2013).

Seasonal variations in lapse rates are a common occurrence in the complex topography found in high mountain regions. Wahl *et al.* (1987) used available climate data for Yukon based on 30-year normals from 1951 to 1980. The analyses included MMAT maps for the territory, but these are lacking the detail that a small grid cell analysis and a better understanding of monthly lapse rates could provide (*Figure 1-3* & *Figure 1-4*) (Wahl *et al.*, 1987). These maps also appeared without updates in Scudder (1997).

Bonnaventure & Lewkowicz (2013) developed a broad distribution model of lapse rates in Yukon and northern British Columbia, indicating a latitudinal gradient in lapse rate strength. Annual lapse rates in the area were shown to be weaker than the global average across the entire area and were slightly positive in central Yukon (Bonnaventure & Lewkowicz, 2013). MMAT for January and July for sites in the Dawson and Wolf Creek areas were also plotted against elevation and revealed inverted lapse rates in January but normal lapse rates in June (Lewkowicz *et al.*, 2012).

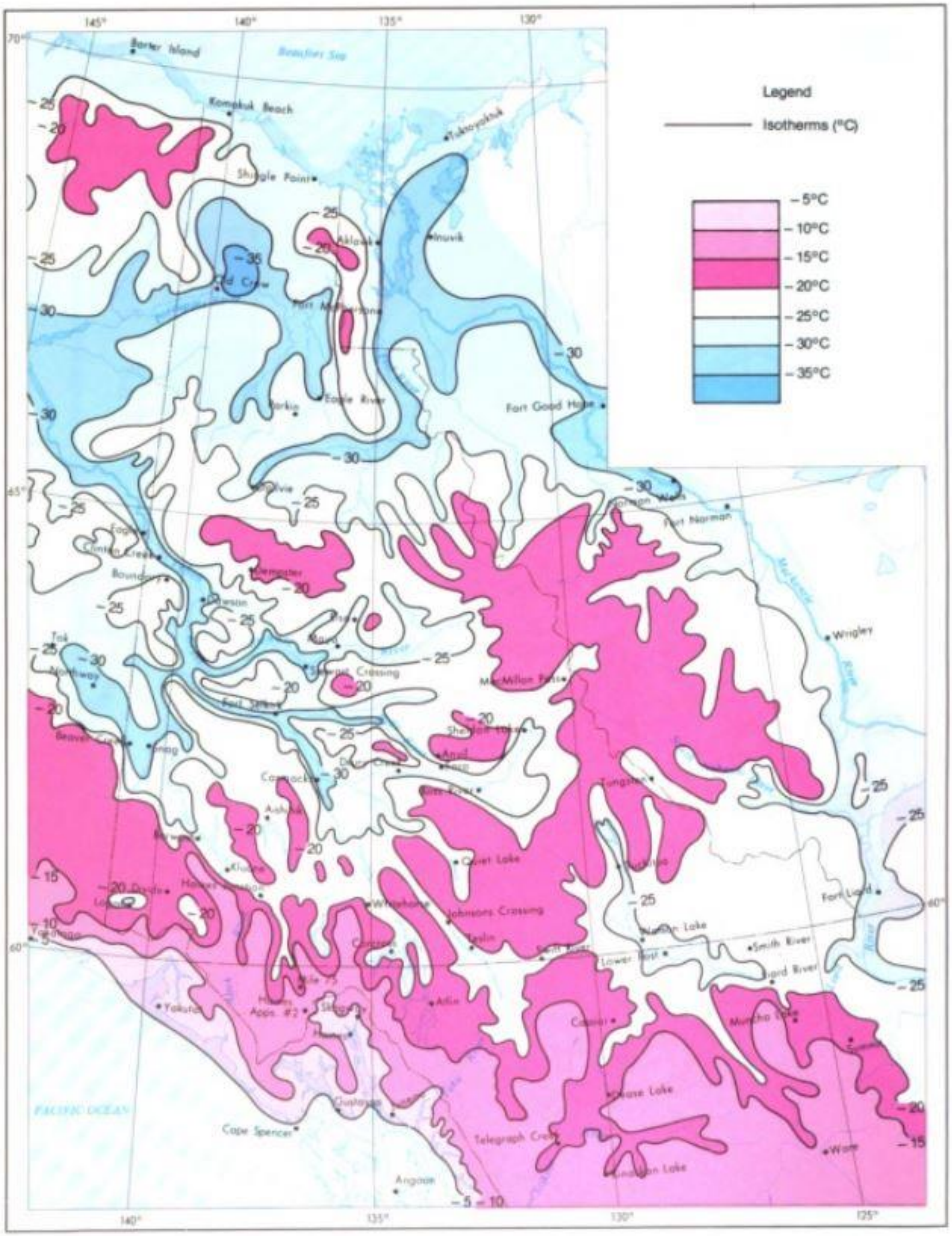

Figure 1-3. January mean daily temperature (Wahl et al., 1987).

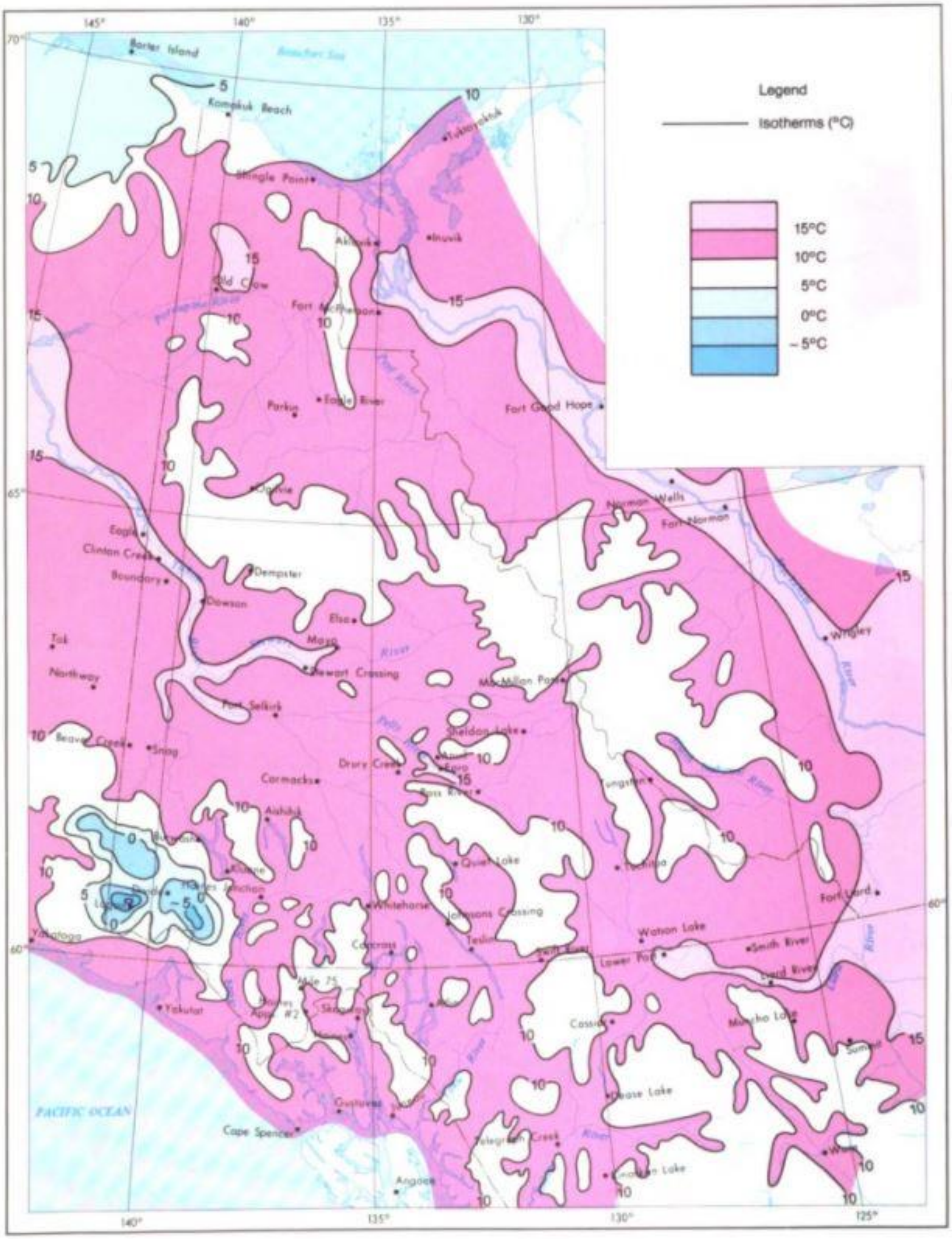

Figure 1-4. July mean daily temperature (Wahl et al., 1987).

1.3.3 FDD and TDD in TTOP modelling

Air temperatures can be used to develop freezing and thawing degree day indices (FDD and TDD, respectively) through the summation of temperatures above or below 0 °C over the course of a year. FDD and TDD are calculated in this thesis based on a blended year average from air temperature data collected from 2001 – 2019.

FDD and TDD values can be used to predict ground surface temperatures and ultimately the temperature at the top of permafrost (TTOP) (Smith and Riseborough, 2002). F/TDD from air temperature data account for a portion of the n-factor value required for calculating the TTOP. The n-factor is the ratio of FDD and TDD for the air and the ground surface and is calculated by dividing F/TDD_s by F/TDD_a (Karunaratne & Burn, 2004). However, since ground surface temperatures are more spatially variable than air temperatures and are also influenced by the snowpack (Bonnaventure & Lewkowicz, 2012), the F/TDD_s are not developed in this thesis.

1.4 Thesis structure

This thesis consists of five chapters. The first chapter outlines the background and objectives of the thesis. The second chapter describes the regional setting of the study region as well as the Environment and Climate Change Canada sites and study area specific information. Chapters 3 and 4 have been prepared as articles for submission to peer-reviewed journals. The third chapter explores mean monthly air temperature focusing on the spatial modelling of air temperatures across the study region as well as the mean annual air temperature map calculated from the mean monthly air temperatures. The fourth chapter explores freezing and thawing degree days focusing on the spatial modelling of these values across the study region as well as the mean annual air temperature map calculated from the models. A comparison of the two mean annual air temperatures maps is also given in chapter 4. The fifth chapter comprises a summary of findings as well as conclusions based on the modelled MMAT, MAAT, FDD, and TDD values.

CHAPTER 2: STUDY REGION AND AREAS

2.1 Regional setting and permafrost distribution

The study area encompasses almost 500,000 km^2 of the southern Yukon and northern British Columbia from 59° to 64.5° N and from 124° to 141° W within the territory, with data collection regions around Wolf Creek, Johnson's Crossing, Dawson, Keno, Faro, Sa Dena Hes and Monarch Mountain (Atlin) (*Figure 2-1*). The data collection sites within each region were set up by Antoni Lewkowicz and monitored over the years by him and his graduate students. Alex Bevington (Government of British Columbia) provided some of the more recent data for the Monarch Mountain sites. Air, surface, and ground temperature data from multiple sites at each of the locations were collected between 2001 and 2019 at a bi-hourly interval for a total of approximately 780 station years. The majority of the study area (79%) is located below the modelled treeline as are the majority of the weather stations (*Figure 2-2*).

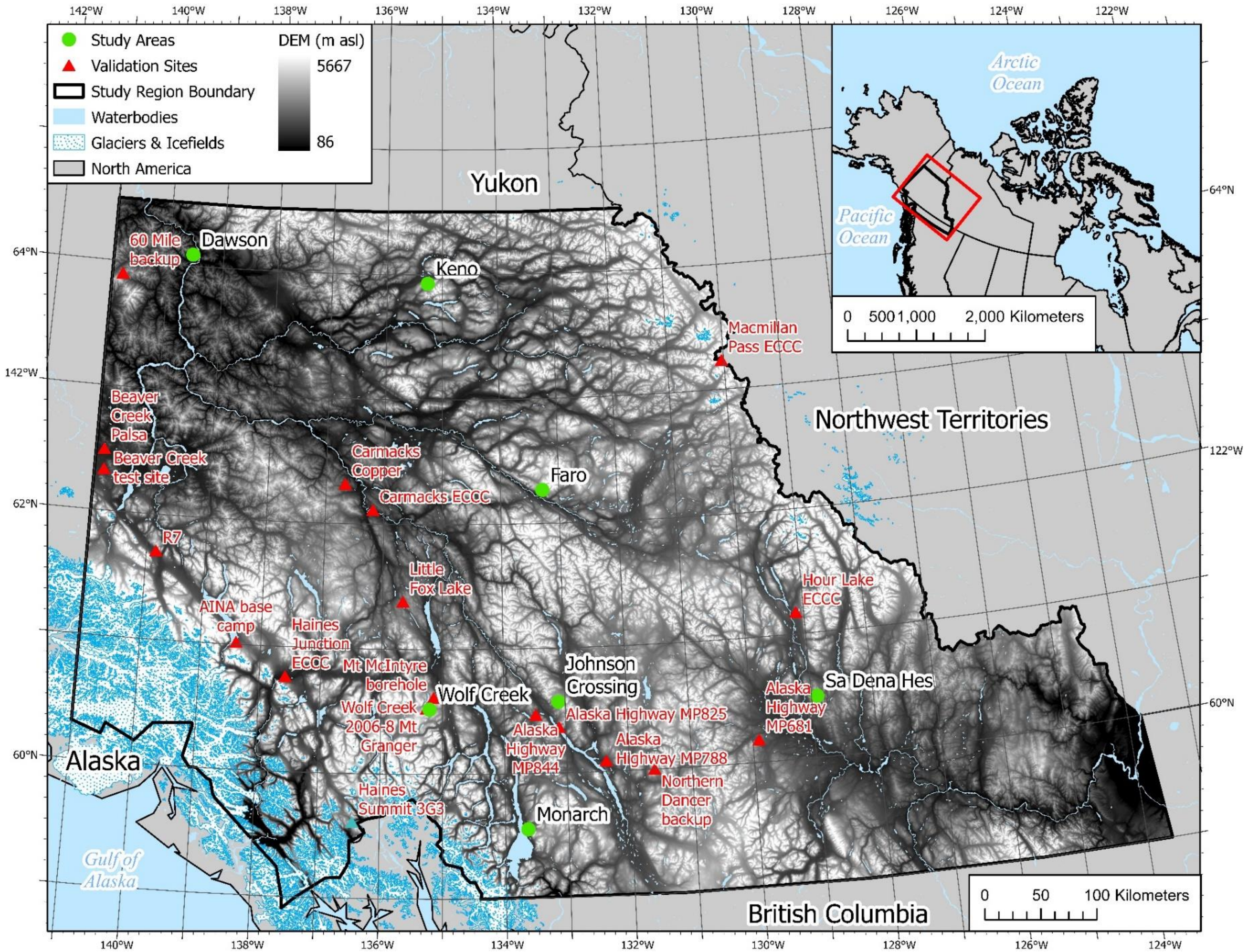

Figure 2-1. Study regions and validation sites in study area of southern Yukon and northern British Columbia, Canada. Study region locations are based on geographic centres of the individual sites within a study region (Government of Canada, 2016; ESRI Data and Maps, 2021; Government of Canada, 2018; ArcGIS Pro, 2020).

The bedrock is primarily sedimentary and metamorphic in origin with some volcanic and intrusive rocks in the southern portion of Yukon and northern British Columbia (Scudder, 1997). The entirety of the study area is underlain by permafrost ranging from isolated patches (southern Yukon) to continuous (northern Yukon) (*Figure 2-3)* (Bonnaventure & Lewkowicz, 2012). There is an extensive icefield within the St. Elias and Coast Mountains in the southwestern part of the study area (*Figure 2-3*), the result of very cold temperatures within these high mountains as well as high annual precipitation (Bonnaventure & Lewkowicz, 2012; Wahl *et al.*, 1987).

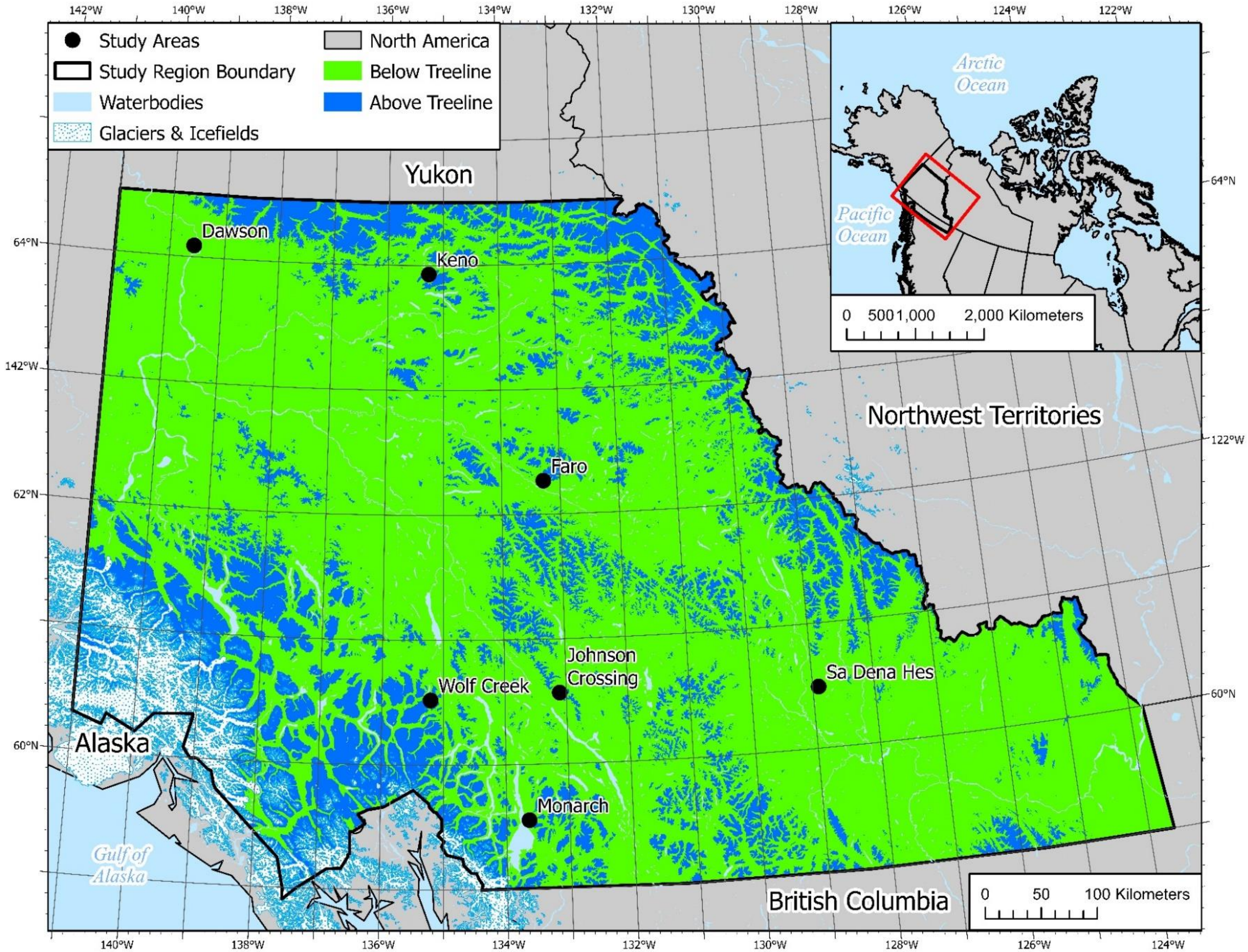

Figure 2-2. Area above and below treeline within the study area. 79% of the study area is located below treeline, 21% is located above treeline. These values exclude areas covered by glaciers or ice fields, where the model was not used to predict temperatures. The seven study areas used in creating the model are shown. Map based on treeline model and DEM from Chapter 3.

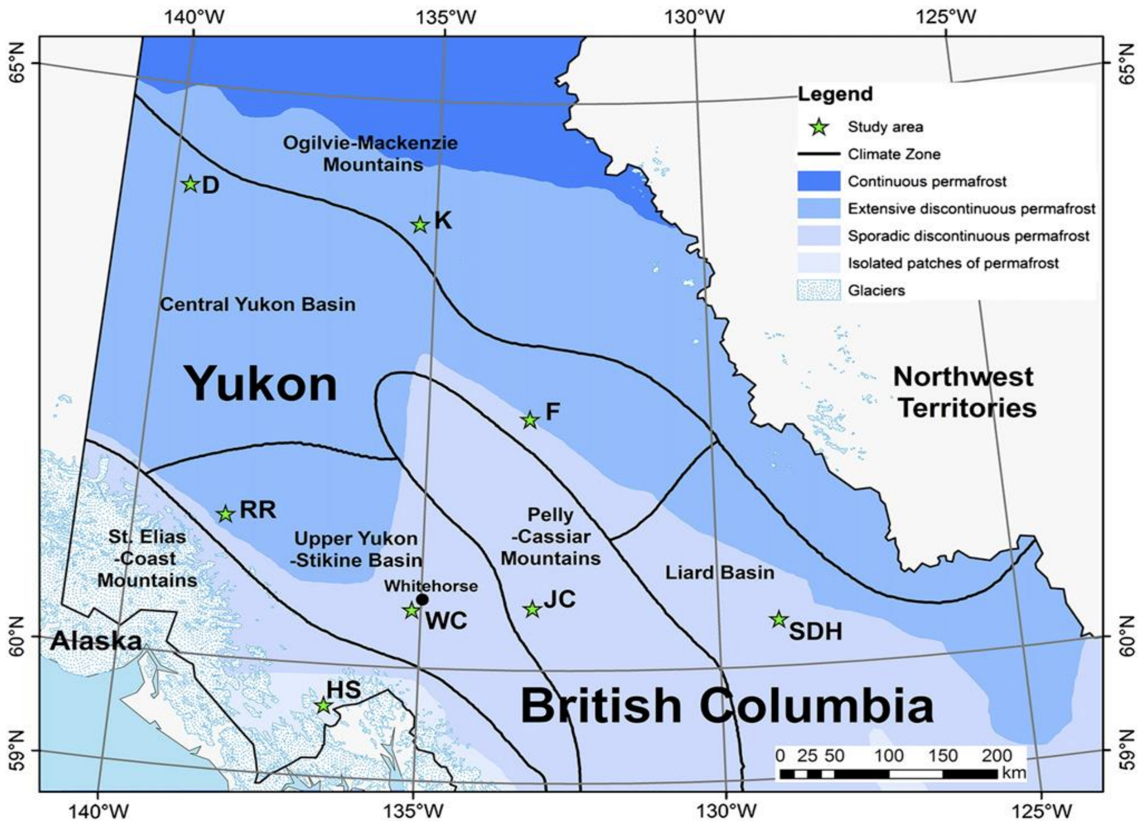

Figure 2-3. Map of the study region showing the locations of the Johnson's Crossing (JC), Sa Dena Hes (SDH), Faro (F), Keno (K) and Dawson (D) study areas in relation to permafrost zones (Heginbottom et al., 1995) and climatic regions (Wahl et al., 1987) (Bonnaventure & Lewkowicz, 2012).

2.2 Environment and Climate Change Canada sites & homogenization

Air temperature and precipitation data from Environment and Climate Change Canada (ECCC) stations were used to calibrate the spatial models. Where possible, homogenized ECCC data were used to ensure long term temporal comparability. The closest homogenized ECCC station to the centre of a region was used for that region (*Table 2-1*).

Homogenization of ECCC station data is a multi-part process that involves joining data for sites in close proximity, correcting biases created by changes in how time was observed, detecting non-climate related shifts in monthly data collection, and adjusting monthly temperature for non-climate related shifts (Vincent *et al.*, 2012). Sometimes ECCC stations are relocated or shut down and new stations started nearby, often within a 20 km radius of the previous station. These stations were combined to allow for longer historical data at each ECCC site (Vincent *et al.*, 2012).

Table 2-1. Study regions in Yukon and British Columbia paired with nearest homogenized Environment and Climate Change Canada weather stations (Government of Canada, 2017; Government of Canada, 2018).

Study area	Corresponding ECCC station	Distance to ECCC station (km)
Johnson's Crossing	Teslin (Aut)	49
Wolf Creek	Whitehorse	22
Sa Dena Hes	Watson Lake (Aut)	42
Faro	Faro (Aut)	8
Dawson	Dawson	22
Keno	Mayo	46
Monarch	Atlin	4

Seven study areas with multiple sites varying in elevation were monitored from 2006 to 2019 as indicated in *Table 2-2*. These sites varied in vegetation type but were all located below treeline. These sites were the basis of the MMAT, FDD and TDD models across the study region. The data and trends from these sites informed the model inputs for areas below treeline. Although some sites above treeline were monitored, they were insufficient to create spatially variable models of MMAT, FDD, and TDD above treeline. Areas above treeline were modelled using a lapse rate of -6 °C/km for all months of the year, as justified in Chapter 3.

2.3 Study area specific information

Table 2-2. Study area information for number of usable sites within each area, minimum and maximum elevation of sites within the area, general vegetation cover, and the start date of data collection.

Study area	# of Sites	Minimum elevation (m asl)	Maximum elevation (m asl)	Lat/Long (WGS84)	Vegetation cover	Data collection range
Johnson's Crossing	11	896	1356	60.57°, -133.11°	Combination of coniferous forest, birch, and willow trees. Variable groundcover of small shrubs/grass/mosses.	2006 – 2018
Wolf Creek	22	630	1457	60.52°, -135.22°	Mainly conifers at low elevations, then birch, spruce, and willow. Variable moss/lichen/grass groundcover.	2006 – 2017
Sa Dena Hes	11	821	1300	60.49°, -128.90°	Mixed but mainly coniferous forest. Thick moss/lichen/grass groundcover.	2006 – 2009
Faro	11	644	1340	62.27°, -133.28°	Mainly open spruce forest with some birch and willow. Thick moss/lichens/grass groundcover.	2006 – 2009
Dawson	12	331	1119	64.09°, -139.56°	Mainly open aspen, spruce, willow, and birch forest. Moss/lichen/herb groundcover of varying thickness.	2007 – 2019
Keno	11	709	1478	63.93°, -135.26°	Mainly open spruce/birch/fir/willow forest. Variable groundcover of moss/lichen/grass.	2006 – 2018
Monarch	5	705	1283	59.55°, -133.64°	Open mixed forest types at lower elevations.	2010 – 2019

CHAPTER 3: MEAN MONTHLY AIR TEMPERATURE MODELLING IN SOUTHERN YUKON AND NORTHERN BRITISH COLUMBIA USING LAPSE RATES AND DEGREE OF CONTINENTALITY

3.1 Abstract

Mean monthly and mean annual air temperatures across the southern Yukon as well as a portion of British Columbia (59 °N to 64.5 °N) were modelled based on measurements at 83 monitoring sites operating for up to 14 years. The placement of these sites at elevations of 330-1480 m asl enabled surface lapse rate modelling on a regional scale that was correlated with degree of continentality in most months. Elevation, degree of continentality, and 30-year climate normals were used to create models of mean monthly air temperature (MMAT) for each month of the year as well as a mean annual air temperature (MAAT) map for the region. The highest MMAT values in the warmest and coldest months of the year, July and January, exceeded those in previous analyses, as did the range of January values. MAAT values were similar to previous models of temperature with MAAT mainly between -6 °C and 0 °C (Lewkowicz *et al.*, 2012). The 10 °C July isotherm generally occurred at elevations above the mapped treeline elevation which may be an indication of climate change occurring faster than ecological change. These new maps can be used to help understand species range change, underlying permafrost conditions, and climate patterns over time.

3.2 Introduction

Air temperatures in Arctic and subarctic regions are rising as a result of climate change (IPCC, 2019). The average annual temperature in Canada increased by 1.7 °C from 1948 to 2016 but northern Canada saw a 2.3 °C increase (Bush & Lemmen, 2019). Changing air temperatures affect the physical environment in many ways, including the ecology, by altering the distribution of plants and the ranges of animals. Rising air temperatures cause changes to the cryosphere, melting sea and glacial ice and thawing permafrost (Melvin *et al.*, 2016). Extra water from melted ice and thawing ice-rich permafrost can alter the hydrology of an area. Thawing of ice-rich permafrost or the addition of extra moisture to soil through ice melt can cause surface destabilization, resulting in detachment slides and thaw slumps, features that have become increasingly common in the past two decades (Lewkowicz & Way, 2019). Buildings and other infrastructure (e.g., roads, pipelines and railways) previously constructed on soil underlain by permafrost can be destabilized due to climate change (Larson *et al.*, 2008; Melvin *et al.*, 2016; IPCC, 2019).

The degradation of permafrost is a costly economic as well as social concern in all northern countries (Larsen *et al.*, 2008). Air temperatures are related to permafrost temperatures and rate of degradation (Bonnaventure & Lewkowicz, 2012). Developing a better understanding of climate in northern regions will impact the ability of governments and communities to understand how temperatures are changing on a larger scale and potentially, to identify areas where greater adaptive measures are required.

The focus of this paper is on developing maps of monthly air temperatures for the southern half of the Yukon Territory and the adjacent northern tier of British Columbia. Previous temperature maps for this area are outdated (Wahl *et al.*, 1982; Scudder, 1997), on a different time scale, or based on short data collection periods (Lewkowicz *et al.*, 2012). Updated monthly temperatures are needed to improve our understanding of air temperature change on a regional or local scale as climate change continues to impact the study region. Although government weather stations have been shown to be accurate when compared to independent temperature measurements at a synoptic scale on a daily and annual basis (Chaput & Gajewski, 2014), most are located in valley bottoms. The average elevation of government weather stations within the study region that have 30-year climate normals is 619 m asl (Government of Canada, 2022b) while the average elevation of the region is 1085 m asl (excluding areas covered by icefields or glaciers) and the maximum elevation is 5667 m asl (Government of Canada, 2019a). Long-term temperature data from government weather stations may not accurately represent temperatures at higher elevations, due to inverted or weaker than average lapse rates in the study region (Bonnaventure *et al.*, 2012; Lewkowicz *et al.*, 2012). This phenomenon is a result of a lack of vertical mixing of air between high mountain peaks and valley bottoms, as well as low amounts of insolation, most notably during the winter (Kattel *et al.*, 2013; Rolland, 2003).

The objective of this study is to provide spatial models of MMAT across the complex mountainous terrain of the study region in an effort to gain a better understanding of temperature trends with variable monthly lapse rates. Mean monthly air temperature models across the elevation gradients in the study region were created from hourly or bi-hourly air temperature data collected at 83 individual sites in seven study areas. Understanding temperature profiles within the study region will allow for further research in areas including ecology, hydrology, permafrost, as well as climate analyses.

3.3 Methods

The development of the spatial models of mean monthly air temperature required five main steps: (1) Digital Elevation Model (DEM) preparation, (2) treeline modelling, (3) data processing, (4) spatial modelling, and (5) MMAT model validation (*Figure 3-1*). Details of each step are given below. The components of the methods overview are numbered and are referenced throughout the methods as the input, output, or tool is described.

3.3.1 Methods overview

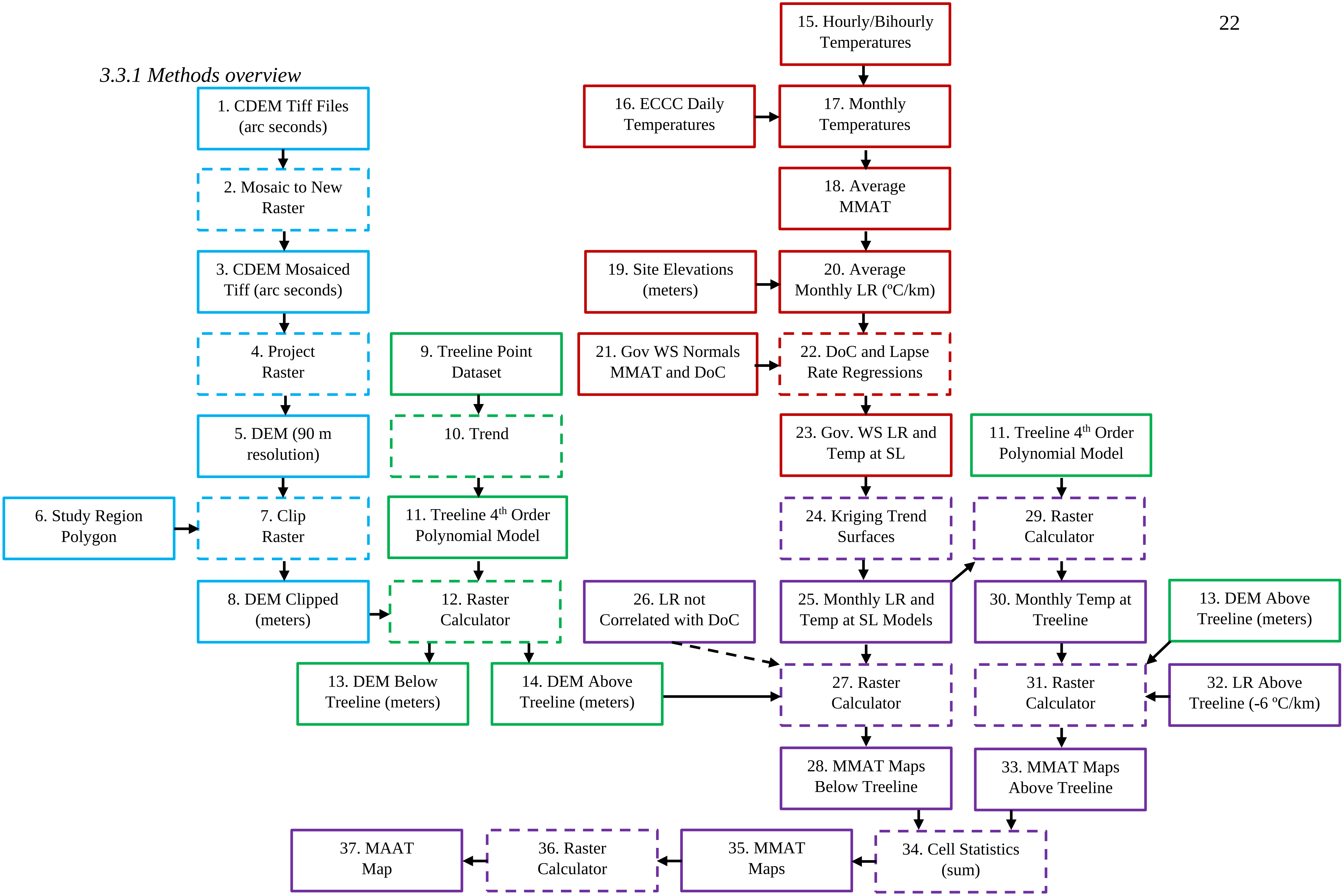

Figure 3-1. Mean monthly air temperature methods overview. Solid boxes correspond to inputs or outputs. Dashed boxes correspond to ArcGIS Pro tools or Excel calculations.Blue boxes outline the steps of the DEM preparation, green outlines the steps to create a treeline model, red outlines the data processing, and purple outlines the MMAT modelling process.

3.3.2 Digital Elevation Model (DEM) preparation

A DEM was needed to apply a spatial model of lapse rates across the study region. The process shown within the blue boxes in *Figure 3-1* are explained in more detail in this section.

The Canada Digital Elevation Model (CDEM) was used. Individual raster tiles that were relevant to the study area were determined by referencing the National Topographic System of Canada (Government of Canada, 2021a). The DEM tiles were accessed from Government of Canada (2019a) as tiff files and imported into ArcGIS Pro (*Figure 3-1*, 1). Although the DEM could have been downloaded as one file for Canada, the resolution of this national model was much lower. For this reason, tiles needed to be downloaded individually.

All DEM tiff tiles were added to ArcGIS Pro, and the Mosaic to New Raster Data Management tool was used to create one continuous DEM file (*Figure 3-1*, 2). As a tiff file, data is stored in a Geographic Coordinate System (GCS) in a semi-round format that references the location on Earth. When running the Mosaic to New Raster tool, the GCS was set to North American Datum 1983 (NAD83) based on the Canadian Digital Elevation Model Product Specifications in order to ensure no distortion of the tiff files (Government of Canada, 2019a). The cell size and pixel type were kept the same from the raster properties of the tiff files (*Figure 3-1*, 3).

To be compatible with other datasets that were created, the DEM needed to be displayed using a projected coordinate system (*Figure 3-1*, 4). The projected coordinate system used was UTM Zone 8N which converted the units of the raster from arc seconds (radians) to meters. The Project Raster Data Management tool was used to convert from the geographic coordinate system (NAD83) to the projected coordinate system (UTM Zone 8N). The cell size was set to 90 x 90 m using the default nearest neighbour resampling technique (*Figure 3-1*, 5).

The projected raster was then clipped to the exact size and shape of the study area using the Clip Raster Data Management tool based on a polygon outline of the study region (*Figure 3-1*, 6 & 7). The coordinate system was preserved by setting the output coordinate system in Environments to UTM Zone 8N. The Processing Extent was set to the study area boundary file. The resulting DEM raster file was used to set environments for all further raster creations and calculations to ensure consistency (*Figure 3-1*, 8).

3.3.3 Treeline model

A treeline elevation file provided by Dr. Philip Bonnaventure (University of Lethbridge) that was updated from the treeline dataset used in Lewkowicz and Bonnaventure (2011), was used to define the treeline. This section of the methods is shown in green in *Figure 3-1*. The dataset was provided as a point dataset and was converted into a raster by fitting a fourth order polynomial trend surface to the data using the Trend 3D Analyst tool (*Figure 3-1*, 9, 10, & 11). A fourth order polynomial was previously used to model treeline in the study region (Lewkowicz *et al.*, 2012) and showed the lowest error in comparison to other polynomials as well as simple kriging trend surfaces available through ArcGIS Pro. The output cell size was set to 90 m. The Environments were all set to the DEM raster specifications.

The treeline trend surface was used to divide the DEM into areas above and below treeline. This was done using the Raster Calculator Spatial Analyst tool. The elevation values up to treeline were found by using the equation DEM <= Treeline (*Figure 3-1*, 8 & 12). The resulting binary raster showed all cells below treeline with a value of 1 and all cells above treeline with a value of zero. To determine the elevation of cells below treeline only, the new above treeline binary raster was multiplied by the DEM file using the Raster Calculator (*Figure 3-1*, 13). Any cells in the DEM below or at treeline were multiplied by 1 and resulted in the same value. Any cells in the DEM above treeline were multiplied by zero and resulted in a zero value. Since there were no zero values in the original DEM, any cells with a value of zero were removed from the raster using the Set Null Spatial Analyst Tool with the conditional clause that any cell with a value of 0 was to be set to a NoData value in the raster. This process was repeated using the equation DEM > Treeline in the Raster Calculator to create a DEM that only contained the elevation of cells above treeline based on the elevation difference from the treeline instead of sea level (*Figure 3-1*, 14).

3.3.4 Data processing

The data processing section is shown in red in *Figure 3-1*. Datasets were assembled from hourly or bi-hourly measurements made at screen height (1.6 m) with Onset Hobo Pro data-loggers (various models; accuracy ±0.2 °C) at 83 sites within the seven study areas (*Figure 3-2*) from 2006 to 2019 (*Figure 3-1*, 15). The original BoxCar or HoboWare files were exported to Excel. The data was visually checked for anomalies that would indicate issues, such as missing data, extreme values, or incorrect readings. After a visual check and removing any data that was anomalous, daily average temperatures were calculated using functions built into Excel. If a day was missing more than 6 hours of measurements it was considered incomplete and the daily average temperature value was not calculated.

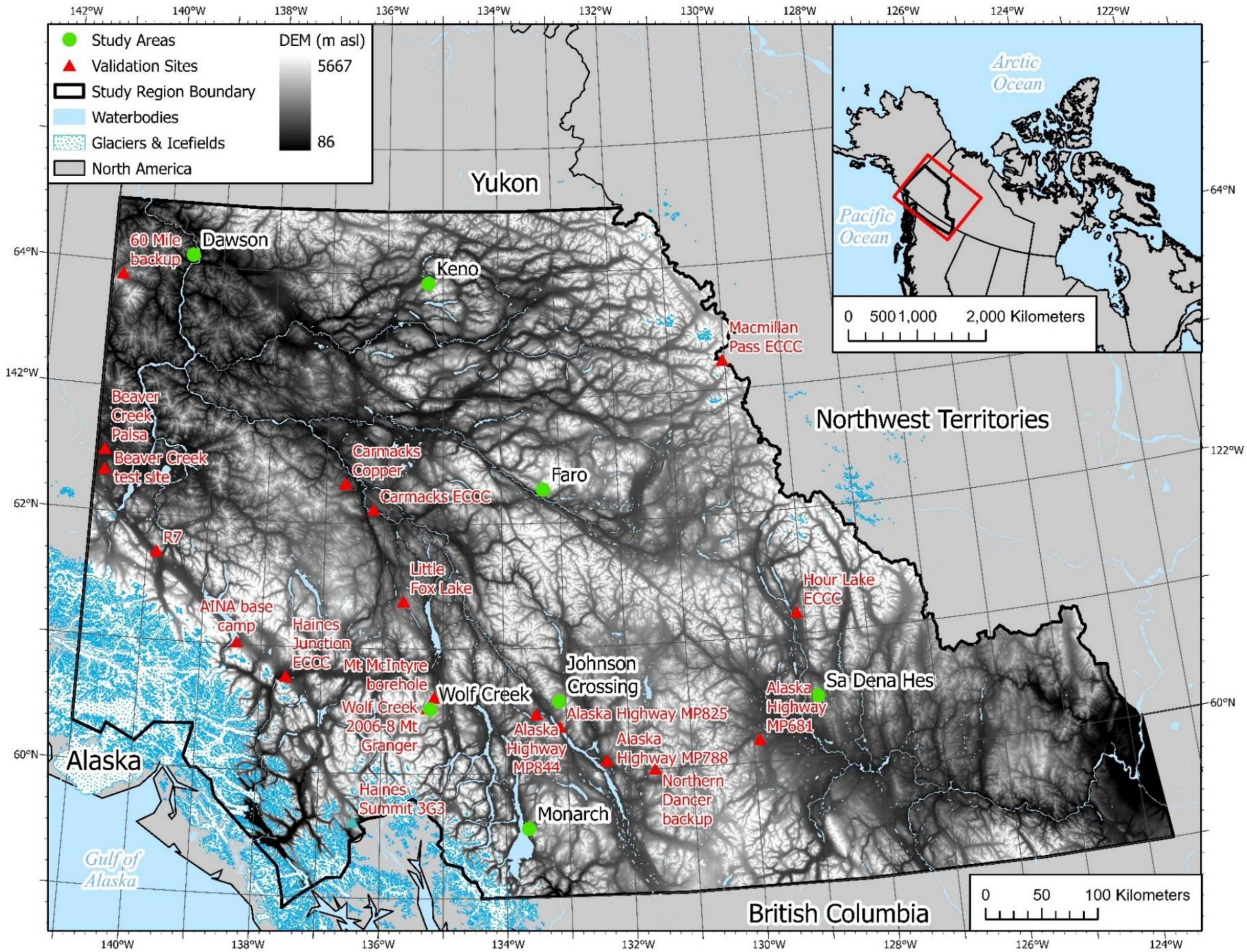

Figure 3-2. Study regions and validation sites in study area of southern Yukon and northern British Columbia, Canada. Study region locations are based on geographic centres of the individual sites within a study region (Government of Canada, 2016; ESRI Data and Maps, 2021; Government of Canada, 2018; ArcGIS Pro, 2020).

Mean monthly temperatures were calculated from the daily averages. MMAT was calculated for each site and each month that the monitoring station was active (*Figure 3-1*, 17). If a month was missing more than 7 days of data, it was excluded from further analysis. MMATs for 20 individual stations not in clusters were also calculated to test the accuracy of the spatial models (validation sites in *Figure 3-2*). A breakdown of the amount of data missing from excluded months can be found in Appendix A.

The average monthly temperature for the nearest homogenized ECCC station, when applicable, was used to anchor the model to lower elevations (*Figure 3-1*, 16). Since ECCC sites are located within populated areas, usually valley bottoms, they were used to ensure the linear regressions of lapse rates were accurate at lower elevations. ECCC weather stations provided greater temporal continuity than some of the field site dataloggers and only six of 84 linear regressions of observed MMAT and degree of continentality did not include ECCC station data. Linear regressions in Microsoft Excel can produce inaccurate values, however linear regressions were tested in R for each set of linear regressions with no difference found in the level of significance of any part of the models or in the values of y-intercept or slope.

Annual surface lapse rates were found to be significantly correlated with degree of continentality in Lewkowicz and Bonnaventure (2011). Degree of continentality is calculated by finding the difference in mean temperature for the warmest and coldest months of the year. This relationship was assessed for monthly lapse rates using data from the seven study areas. Regressions were tested at the 0.1 significance level.

All sites below treeline within a given area were used to create a linear model of the MMAT against elevation for each month of each year, resulting in multiple linear models of the lapse rate for each month (*Figure 3-1*, 18, 19, & 20). This was done by regressing the MMAT for a given year at all monitoring sites within a given area against the elevation of each site. The regressions were run in Excel using the Data Analysis tool and tested for overall regression significance as well as the significance of the slope. An informal check of the difference in regression slopes when including and excluding the closest ECCC station was done, and no major differences were found between the two options. This indicated that including the low elevation ECCC site in the model did not exert an inordinate control on the linear relationship.

An average of the slope and y-intercept of the statistically significant monthly linear models were then used as the estimate of the lapse rate for that area. For example, 12 years of data are available for January in the Keno area, so there were 12 linear monthly models of lapse rate that could potentially be used to create an average lapse rate for January. However, the linear regression as a whole as well as the slope were not statistically significant in 2016, so it was excluded and the average lapse rate in January in the Keno region was based on the other 11 slopes.

If the elevation range of the active stations was less than 400 m in a particular month, that month was excluded. This was done to ensure that the temperature change along the elevation gradient could be attributed to more than instrumental inaccuracies. This range criterion was chosen to maximize the number of years of record while limiting the impact of logger measurement error and the influence of local topography and microclimates on lapse rates.

A total of 51 ECCC and U.S. National Centers for Environmental Information (NCEI) stations with 30-year climate normals (1981-2010) were used to build the spatial models of MMAT (*Figure 3-3*). The 30-year normal MMAT values for each month were retrieved (Government of Canada, 2019c; NCEI, n.d.) and imported into Excel. There were six months of missing values in the 30-year normals, affecting 3 of the 27 ECCC stations. No NCEI stations had missing data. The missing values were infilled by calculating the average change in MMAT for all other ECCC stations from the previous month to the missing month and from the missing month to the following month. The average of these two changes was then used with the previous month's value to infill the missing MMAT. For example, the Stewart Crossing ECCC station was missing MMAT for May and the following calculations were used to estimate the missing value.

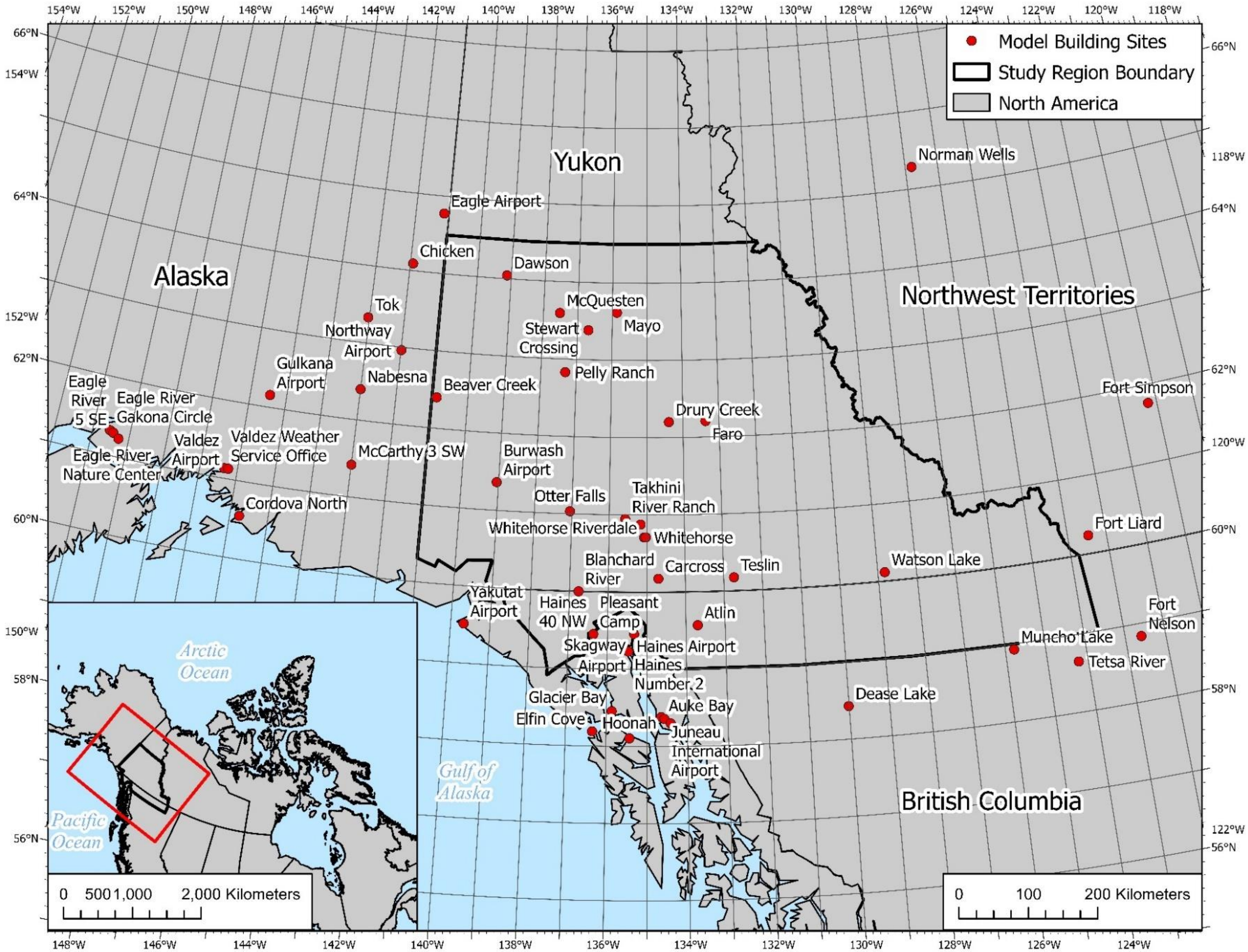

Figure 3-3. Government weather stations (Appendix C, Table C-1 and C-2) within the study region as well as surrounding areas used to build the models of mean annual air temperature based on calculated lapse rates and temperatures at sea level and treeline. (Government of Canada, 2016; Government of Canada, 2019c; ESRI Data and Maps, 2021; NCEI, n.d.).

$$Average\ MMAT\ change\ from\ April\ to\ May\ =\ 6.9\ ºC$$
$$Average\ MMAT\ change\ from\ May\ to\ June\ =\ 5.4\ ºC$$
$$April\ MMAT\ =\ 1.5\ ºC$$
$$June\ MMAT\ =\ 14.6\ ºC$$

$$Predicted\ May\ MMAT\ using\ April\ to\ May\ change\ = 1.5\ ºC\ +\ 6.9\ ºC$$
$$Predicted\ May\ MMAT\ using\ April\ to\ May\ change\ = 8.4\ ºC$$

$$Predicted\ May\ MMAT\ using\ May\ to\ June\ change = 14.6\ ºC - 5.4\ ºC$$
$$Predicted\ May\ MMAT\ using\ May\ to\ June\ change = 9.2\ ºC$$

$$Average\ predicted\ May\ MMAT = \frac{8.4\ ºC + 9.2ºC}{2}$$
$$Average\ predicted\ May\ MMAT = 8.8\ ºC$$

If two consecutive months had missing data, only the average change in MMAT from the previous or following month was used. For example, the Drury Creek ECCC station was missing MMAT for both May and June and the following calculations were used to determine the missing value for May. The same process was used to determine the missing June MMAT, substituting the average MMAT change from April to May with the average MMAT change from June to July.

$$Average\ MMAT\ change\ from\ April\ to\ May\ =\ 6.9\ ºC$$
$$April\ MMAT\ =\ 1.7\ ºC$$
$$Predicted\ May\ MMAT\ =\ 1.7\ ºC\ +\ 6.9\ ºC$$
$$Predicted\ May\ MMAT\ =\ 8.6\ ºC$$

The degree of continentality (DoC) for each of the government weather stations was calculated from the difference in January and July MMAT from the 30-year climate normals (1981-2010). A linear equation was used with the following variables to create the spatial model of lapse rates across the study area (*Figure 3-1*, 21).

$$Lapse\ Rate = (DoC\ Regression\ Slope) * (DoC) + (DoC\ Regression\ Intercept)$$

Lapse rates below treeline for each of the 51 government climate stations (*Appendix C, Table C-1 and C-2*) were calculated using the linear regression between lapse rate and degree of continentality in the months that the relationship was found to be statistically significant (*Figure 3-1*, 22). An example of this for the Drury Creek ECCC station in January is shown below.

$$Degree\ of\ Continentality\ Regression\ Slope\ =\ 0.65\frac{\frac{ºC}{km}}{ºC} =\ 0.65\ km^{-1}$$

$$Degree\ of\ Continentality\ Regression\ Intercept = \ -14.77\ \frac{ºC}{km}$$

$$Degree\ of\ Continentality\ of\ Drury\ Creek =\ 35.1\ ºC$$

$$Lapse\ Rate = DoC\ Regression\ Slope(DoC) + DoC\ Regression\ Intercept$$

$$Lapse\ Rate = (0.65\ km^{-1}\ ) * (35.1\ ºC) - 14.77\ \frac{ºC}{km}$$

$$Lapse\ Rate = 8.0\ ºC/km$$

If there was no statistically significant relationship between lapse rate and degree of continentality for the month, the average of the lapse rates from the seven study areas was used across the entire study region. This was the case, for example, in May, when the lapse rate for the region was uniformly -5.2 ºC/km.

The projected temperature at 0 m asl was calculated using lapse rates for each month at each of the 51 government weather stations as well as the 30-year normal MMAT and elevation (*Figure 3-1*, 23). This provided the sea level values for the spatial model of MMAT that could then be raised up to treeline with the lapse rate and Digital Elevation Model. An example of this calculation using the Drury Creek ECCC station in January is shown below. The 30-year normal MMAT for the Drury Creek ECCC station is known as well as the elevation of the station. Using these values and the previously calculated lapse rate for January, the linear equation can be rearranged to calculate the temperature at sea level, by solving for the Y intercept.

$MMAT = -21.1\ ºC$

$January\ Lapse\ Rate = 8.0\ \frac{ºC}{km}$

$Elevation = 0.609\ km$

$MMAT = (Lapse\ Rate) * (Elevation) + (Temperature\ at\ Sea\ Level)$

$Temperature\ at\ Sea\ Level = (-Lapse\ Rate) * (Elevation) + MMAT$

$Temperature\ at\ Sea\ Level = (-8.0\ \frac{ºC}{km}) * (0.609\ km) - 21.1\ ºC$

$Temperature\ at\ Sea\ Level = -26.0\ ºC$

3.3.5 Spatial modelling of MMAT

Spatial modelling of MMAT is shown in purple boxes in *Figure 3-1* and will be expanded upon in this section. Lapse rates below treeline and temperature at sea level calculated previously for each of the 51 government weather stations along with their geographic coordinates and elevation data for each site were saved in five csv files sorted by UTM zones: 6N, 7N, 8N, 9N, and 10N (Government of Canada, 2021b). These files were then imported into ArcGIS Pro as XY tables. The tables were then converted to points using the XY Table to Points Data Management tool and by defining the coordinate system as the appropriate UTM zone. The points were then merged so they could be used as one dataset using the Merge Data Management tool. The output coordinate system was set as UTM Zone 8N since it was most central and covered much of the study area.

The Geostatistical Wizard was used to explore Kriging methods for monthly lapse rates and temperatures at sea level using the government weather station data from within and surrounding the study region (*Figure 3-1*, 24). Weather stations outside of the study area were included to minimize edge effects in the spatial models. Through trial-and-error comparison of standard error and root mean square error, the best fit Kriging type for the data was found to be Stable Optimized Kriging for lapse rates and Stable Kriging for temperatures at sea level using default ArcGIS Pro parameters (*Figure 3-1*, 25). The trend surfaces were run for the lapse rates below treeline for each month of the year that there was a statistically significant relationship with degree of continentality. No trend surface was created for months where the relationship was not statistically significant because a constant value was used in later calculations (*Figure 3-1*, 26).

Stable Kriging was used to create monthly trend surfaces of temperature at sea level based on the projected values from the lapse rate below treeline.

Lapse rates and temperatures as sea level trend surfaces were converted to raster formats with the GA Layer to Rasters Geostatistical Analyst tool using the DEM file for above and below treeline, where appropriate, to define the Environments. MMAT profiles for the study Region were then calculated below treeline using the linear equation as shown:

$$MMAT = (LR\_BTL\_TrendSurface) * (DEM\_BTL) + (SeaLevelTemp\_TrendSurface)$$

MMAT profiles for the study region above treeline were calculated using a lapse rate of -6 ºC/km at all locations and in all months. This value was chosen following the calculation of average annual lapse rates for two pairs of sites, each pair containing one site as close to treeline as possible, and the other site at the highest overall elevation, usually a mountaintop. The calculated lapse rates were -6.0 ºC/km between Mt. McIntyre (1569 m asl) and Mt. Granger (2077 m asl) and -4.5 ºC/km between Dawson 8 (1119 m asl) and 60-Mile backup (1450 m asl). Given the limited data and the global average lapse rate of -6.5 ºC/km, a value of -6 ºC/km was chosen. Observed lapse rates below treeline in the summer months, when air temperature inversions are generally absent, were not as strong as -6.5 ºC/km, further supporting the decision to use a weaker lapse rate than the global average above treeline. To calculate the temperature above treeline, the temperature at treeline for each month first needed to be calculated using the lapse rate below treeline, temperature at sea level trend surfaces, and the treeline elevation raster (*Figure 3-1*, 11, 25, 29, & 30):

$$TempAtTreeline = (LR\_BTL\_TrendSurface) * (TreelineDEM) + (SeaLevelTemp\_TrendSurface)$$

The MMAT above treeline was then calculated using the Raster Calculator based on the lapse rate of -6 ºC/km, the DEM above treeline, and the temperature at treeline (*Figure 3-1*, 13, 30, 31, 32, & 33):

$$Temp\_ATL = (-6.0\ \frac{ºC}{km}) * (DEM\_ATL) + (TempAtTreeline)$$

MMAT above and below treeline were then combined into one raster using the Sum function of the Cell Statistics Spatial Analyst Tool (*Figure 3-1*, 34 & 35). All environments were set to the DEM raster.

Given the difference in surface conditions, it was decided that the MMAT projections should not be extended over icefields and glaciers. To exclude these areas, a glacier and ice fields shapefile (Government of Canada, 2022a) was imported in ArcGIS Pro and converted to a raster using the Polygon to Raster Conversion Tool with the environments set to the DEM file specifications. This resulted in values of 1 where glaciers and ice fields existed and NoData values everywhere else. To create a mask within the study area, the Reclassify Spatial Analyst Tool was used to change NoData values to 1 and previous values of 1 to NoData. The reclassified ice and glacier raster was used to mask each MMAT map with the Extract by Mask Spatial Analyst Tool.

Finally, a MAAT map was created with the Raster Calculator by finding the sum of all MMAT maps and dividing by 12 (*Figure 3-1*, 36 & 37).

3.3.6 MMAT model validation

To test the accuracy of the MMAT models, the MMAT for 20 sites across the study area, both above and below treeline, were imported into ArcGIS Pro as XY Tables. A minimum of three years of record was required for each validation site to offset the potential impact of including a particularly warm or cold year. Six sites were located above treeline, 14 below treeline, and none had been used in developing the models. The tables were converted into points following the same XY Table to Point process used previously. The observed MMAT for each month as well as the MAAT were calculated from measured values for each of the validation points using the same process as was used for the model input data. The modelled MMAT for each month as well as the MAAT for each of the 20 validation points were extracted from the appropriate rasters using the Identify function of ArcGIS Pro. These values were added into an Excel spreadsheet alongside the measured values at each site.

Linear regressions were run on each measured and modelled dataset pair. For example, a linear regression using January MMAT Measured values was regressed against January MMAT modelled values. This process was done for each month of the year as well as the MAAT values. The root mean square error was also calculated for the measured and modelled MMAT and MAAT values of the validation sites.

3.4 Results

The results below (1) examine the seasonal and spatial variation in monthly lapse rates for the seven study areas, (2) present the MMAT maps, (3) evaluate the MMAT model using independent site measurements, and (4) are summarized as a map of MAAT.

3.4.1 Monthly lapse rates

The annual variation in lapse rate values for all seven study areas is shown in *Figure 3-4*. All sites had positive lapse rates in the winter months, December through February, with the exception of Monarch in December. There was nearly no altitudinal change in temperature at the Monarch study area in that month as the lapse rate was -0.3 ºC/km. The largest inversions occurred at Sa Dena Hes, with lapse rates reaching 14.2 ºC/km.

There was a larger variation in average lapse rates between sites in the winter months compared to the warmer months of the year (April through October). For example, while the January lapse rate for Sa Dena Hes averaged 14.2 ºC/km, the January lapse rate for Monarch was only 1.8 ºC/km, giving a 12.4 ºC/km difference between the two study areas. Conversely, the July lapse rate was -6.0 ºC/km at Sa Dena Hes and -4.8 ºC/km at Monarch, showing a much smaller difference in lapse rates of only 1.2 ºC/km. Thus, there was greater homogeneity in lapse rates across the study region in summer than in winter. Spatially, summer lapse rates were consistently weaker at Dawson than in the other six study areas, with inversions in lapse rates during the summer in some years. The most negative summer lapse rate was at Wolf Creek with a value of -7.0 ºC/km which is even stronger than the global annual average of -6.5 ºC/km.

Inversions in lapse rates occurred for a maximum of five months (Dawson and Sa Dena Hes), and for a minimum of two months (Monarch) (*Figure 3-4*). The degree of continentality of the study area (*Figure 3-4*) was directly correlated with the seasonal duration of mean inverted lapse rates. The lower the degree of continentality, the fewer months with inverted lapse rates and the reverse for a higher the degree of continentality.

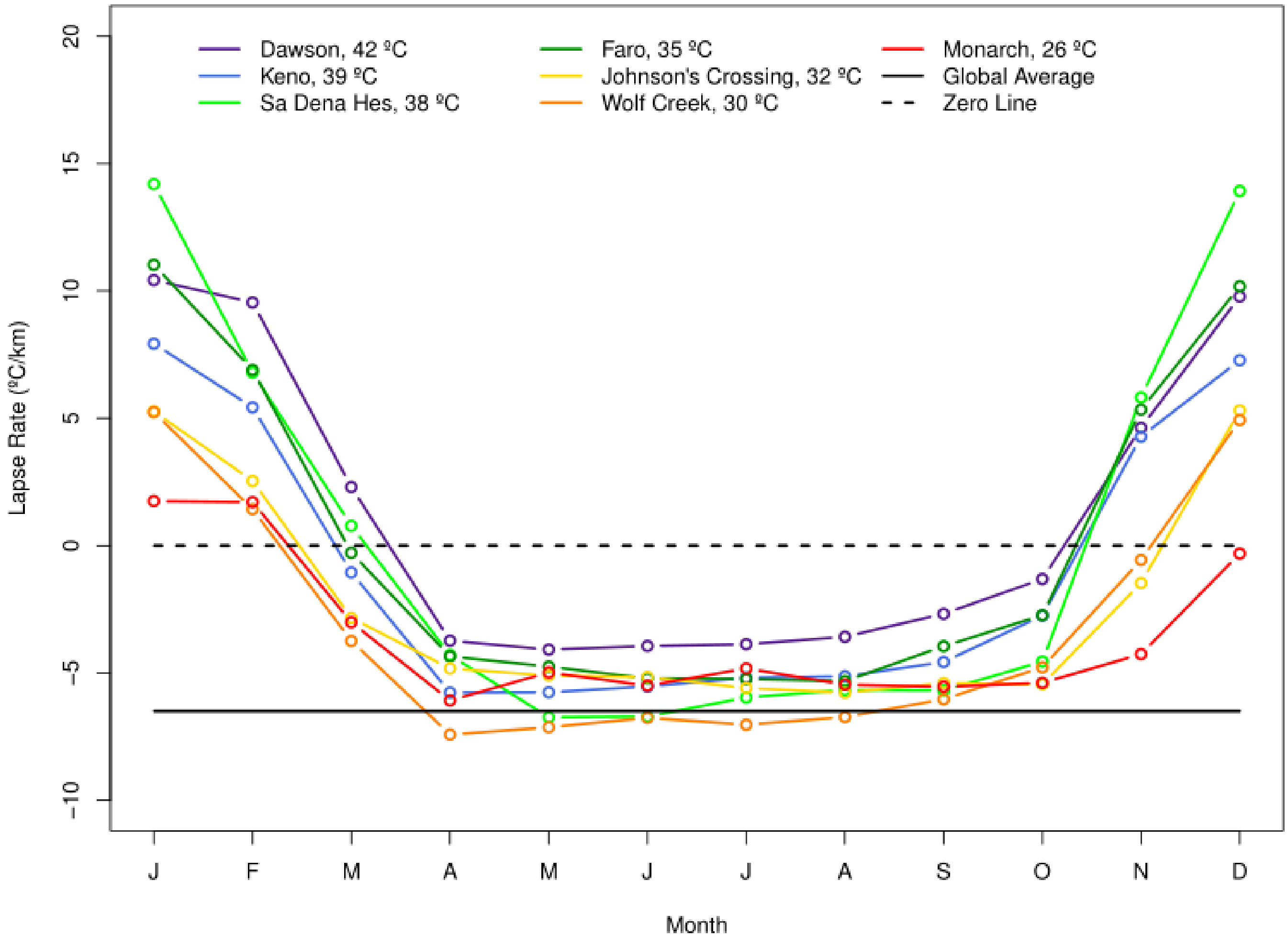

Figure 3-4. Monthly lapse rates at the seven study areas used to create models of MMAT. The Zero line is the threshold for inverted lapse rates. The global average annual lapse rate of -6.5°C/km is also shown. The degree of continentality for each study area is given in the legend. Specific monthly lapse rate values can be found in Appendix B.

3.4.2 Mean monthly and seasonal air temperature

Modelled mean monthly air temperatures across the study region show a smooth cycle over the year (*Figure 3-5*). Average MMAT across the study region was lowest in January and highest in July, as was expected, while a minimum monthly value of -43.7 °C and a maximum of 17.3 °C, were predicted for the same months, respectively. Most modelled temperatures through the year fell between -21 °C and 15 °C. April through September showed the least amount of variation between the average and maximum MMAT in the study region with an average difference of 5.5 ºC, whereas the colder months, October through March showed a larger difference with an average of 10.5 ºC. The average annual difference between average and maximum MMAT was 8 ºC. The difference between the minimum and average MMAT however, was much larger. This results from small areas with very cold temperatures such as mountain peaks and areas near the icefields. The average difference between the minimum and average MMAT for the study region was 27.7 ºC, decreasing slightly to 26.2 °C in the colder months from October to March.

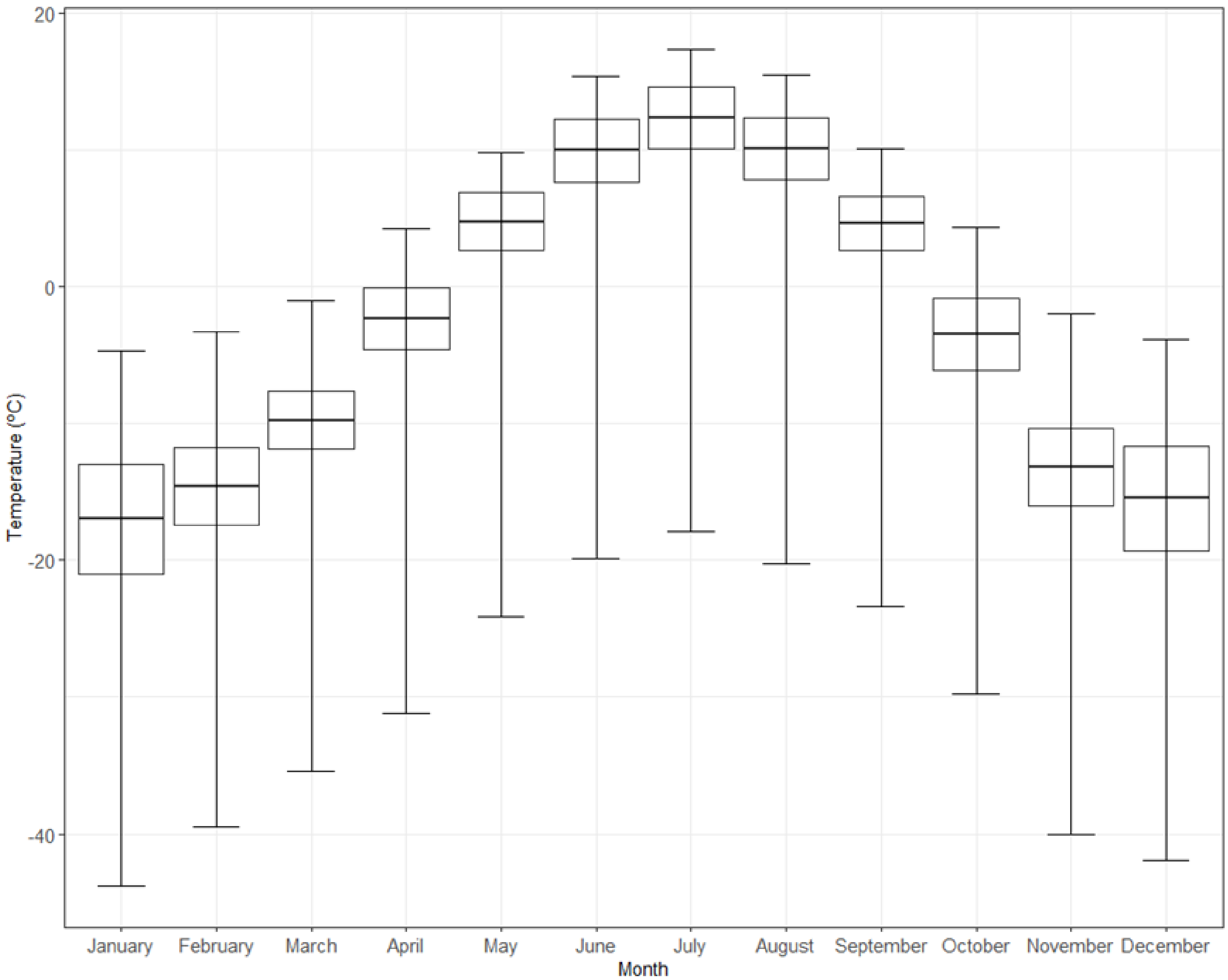

Figure 3-5. Annual cycle of MMAT across the study region. Maximum and minimum values are the warmest and coldest modelled MMAT grid cells, respectively, in a given month, while the average is the mean of all the grid cells.Mean MMAT is shown as the horizontal line within the boxes ± one SD on either side. The lines extending from the box represent the maximum and minimum MMAT value for the month across the entirety of the study region.

Discussion of the results focuses on monthly conditions grouped by the four seasons: winter (December, January and February) (*Figures 3-6 to 3-9*), spring (March, April and May) (*Figures 3-10 to 3-13*), summer (June, July and August) (*Figures 3-14 to 3-17*), and autumn (September, October, November) (*Figures 3-18 to 3-21*). For simplicity, all temperatures below -30 °C are symbolized with a single colour on the maps.

Winter has inverted lapse rates in all three months except near the coast in December. Therefore, low temperatures are found at low elevations and higher temperatures occur near treeline before the inversion reverses (*Figure 3-6*). Temperatures are lowest in January and warmest in February. What is likely an anomalously warm area resulting from edge effects, is present in the northeast of the region in January, due to kriging in an area with few nearby stations.

The widest range in modelled MMAT occurred for December through February, reaching almost 50 °C across the study region (*Figure 3-7, 3-8, & 3-9*). This heterogeneity contrasted with the high degree of homogeneity for the remaining 9 months of the year.

There is a clear example of the impact of lapse rate inversions below treeline in December southwest of Dawson (*Figure 3-7*). Temperatures within the -24.9 °C to -20 °C range occur at lower elevations, with temperatures of -19.9 °C to -15 °C at higher elevations that are still below treeline. As elevation increases above treeline and lapse rates normalize, temperatures decrease again to the -24.9 °C to -20 °C range. Visually, the darker blues (colder temperatures) are both within the boundaries of lighter blues (warmer temperatures) as well as surrounding the lighter blue areas. This trend of colder to warmer and back to colder temperatures profile actually starts in this area in November (see Figure 3-21 below).

The degree of continentality appears to influence temperature patterns in the winter months due to the impact of the lapse rate inversions. Latitude is also partially influential on the temperature profiles in the winter months with a north-south temperature gradient in MMAT more visible in February (*Figure 3-9*) than in the other winter months.

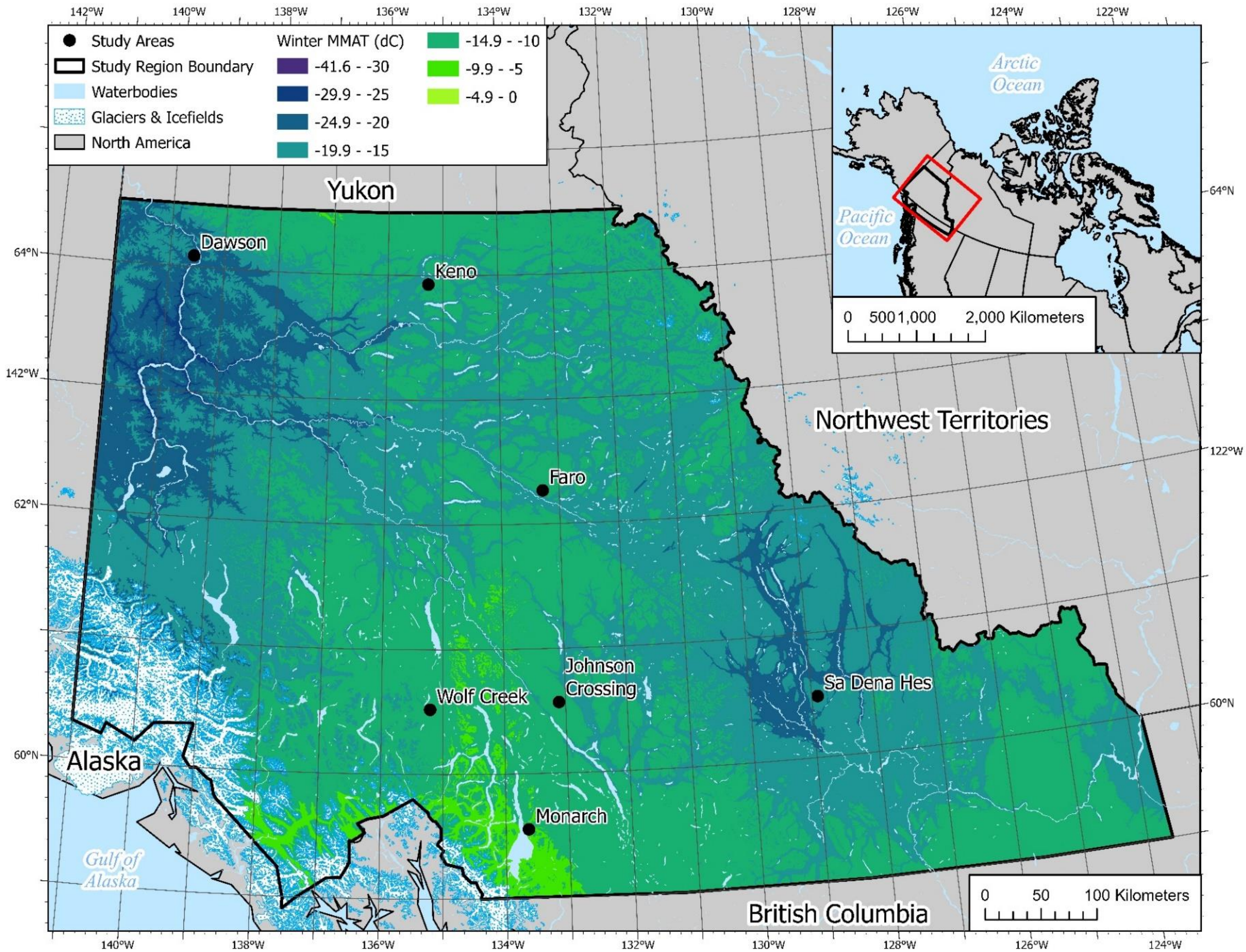

Figure 3-6. Modelled winter (December – February) mean air temperature across study region in northern British Columbia and southern Yukon, from 50 – 64.5° N. The seven study areas used in building the model are shown. Whitehorse (not shown) is located approximately 10 km northeast of Wolf Creek.

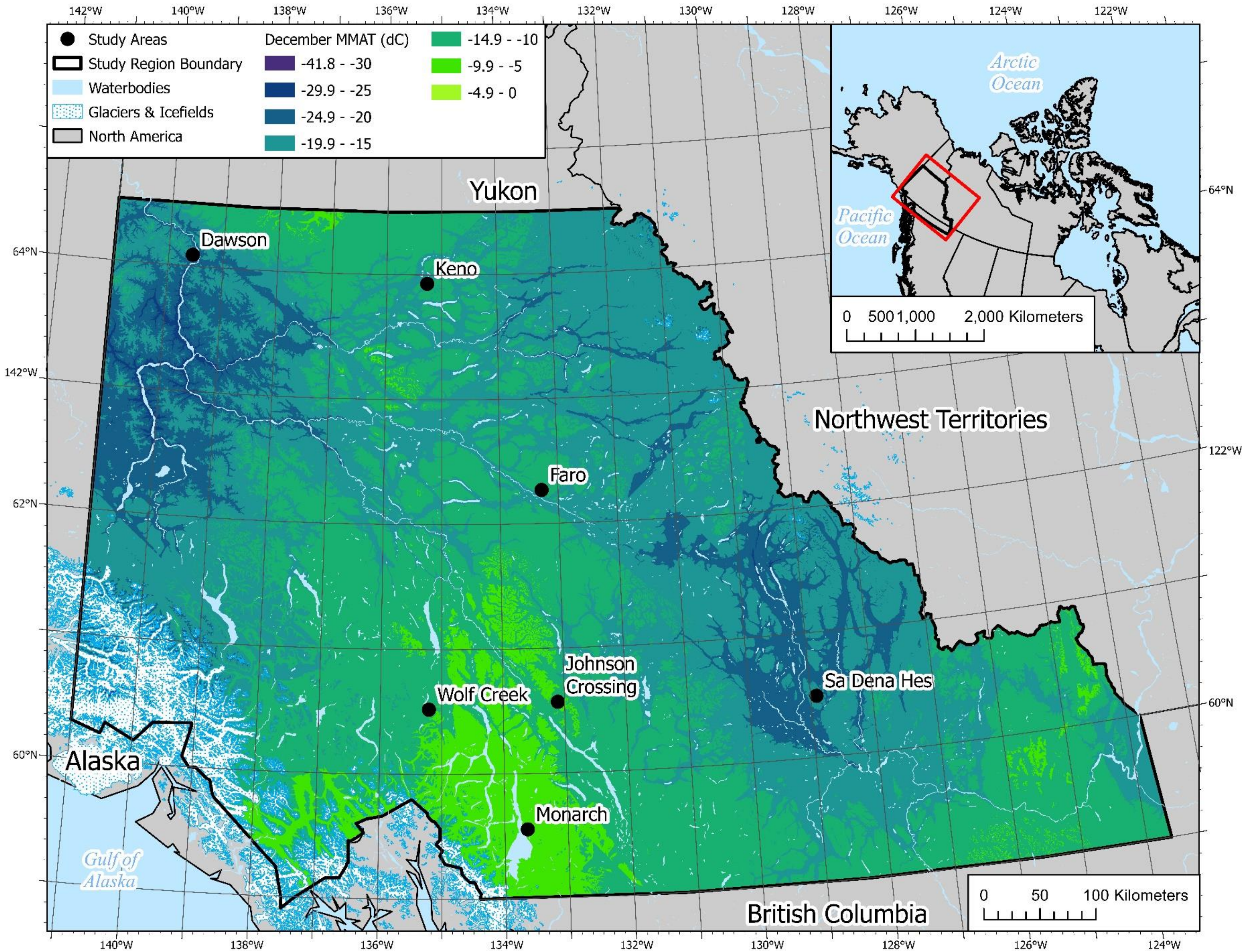

Figure 3-7. Predicted December mean air temperature (MMAT) values across study region in northern British Columbia and Southern Yukon, from 59 – 64.5° N. The seven study areas used in building the model are shown. Whitehorse (not shown) is located approximately 10 km northeast of Wolf Creek. Average MMAT across the study region was calculated to be -15.5 °C.

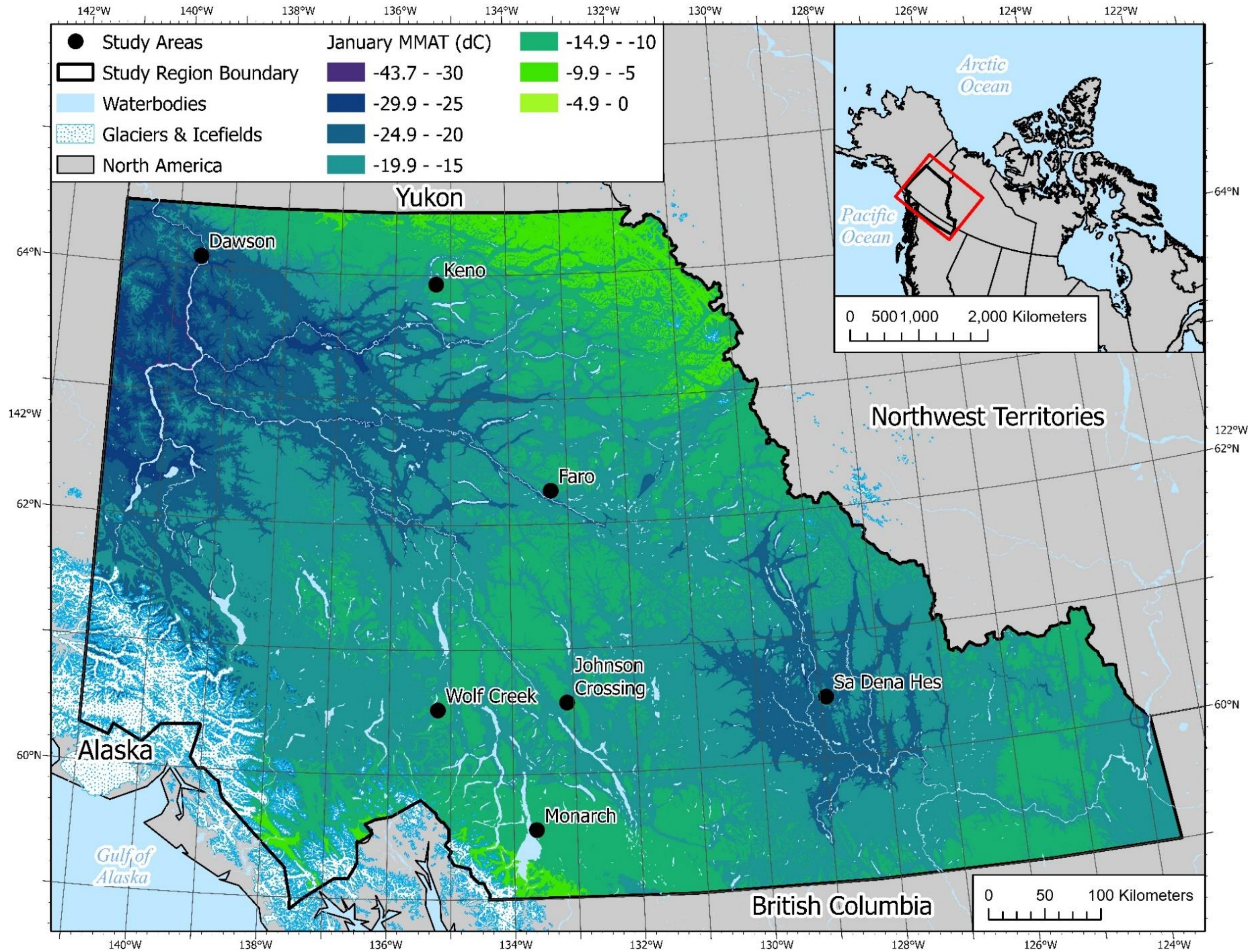

Figure 3-8. Predicted mean January air temperature (MMAT) values across study region in northern British Columbia and Southern Yukon, from 59 – 64.5° N. The seven study areas used in building the model are shown. Whitehorse (not shown) is located approximately 10 km northeast of Wolf Creek. Average MMAT across the study region was calculated to be -17 °C.

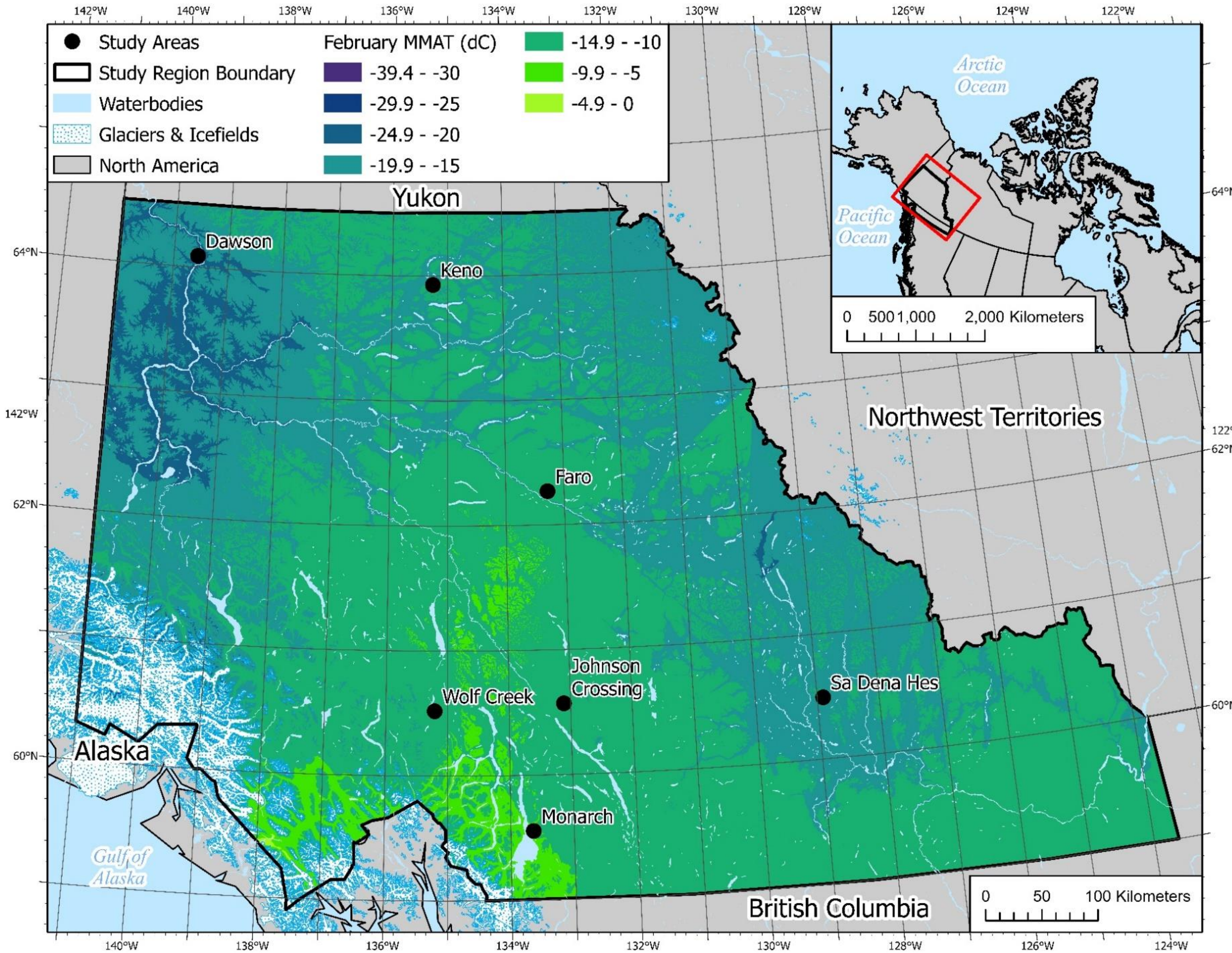

Figure 3-9. Predicted mean February air temperature (MMAT) values across study region in northern British Columbia and Southern Yukon, from 59 – 64.5° N. The seven study areas used in building the model are shown. Whitehorse (not shown) is located approximately 10 km northeast of Wolf Creek. Average MMAT across the study region was calculated to be -14.6 °C.

Spring shows a high degree of homogeneity across the study region (*Figure 3-10*). The majority of the study region consists of temperatures from -10 °C to -5 °C. This pattern is consistent from March through to May, but the average temperature increases significantly from -9.8 °C in March (*Figure 3-11*) to 4.8 °C in May (*Figure 3-13*).

The period from March through to May involves the end of inverted lapse rates and a transition to normal lapse rates. In March (*Figure 3-11*), lapse rates are close to 0 °C/km with Dawson and Sa Dena Hes study areas having slightly inverted lapse rates and the remaining five study areas showing weaker than average but negative lapse rates (see *Figure 3-4*). Lapse rates closer to 0 °C/km result in a homogenous temperature profile with elevation having little impact on the values. The combined effect of degree of continentality as well as latitude is more obvious in March with colder temperatures persisting at higher latitudes as well as further inland, whereas the central, lower latitudinal areas have warmed to the -9.9 °C to -5 °C range (*Figure 3-11*).

The effect of degree of continentality decreases through April and May, with elevation becoming the dominant influence on temperature (*Figures 3-12 & 3-13*). Lower elevation valley bottoms are noticeably warmer than high elevation areas in both April (*Figure 3-12*) and May (*Figure 3-13*).

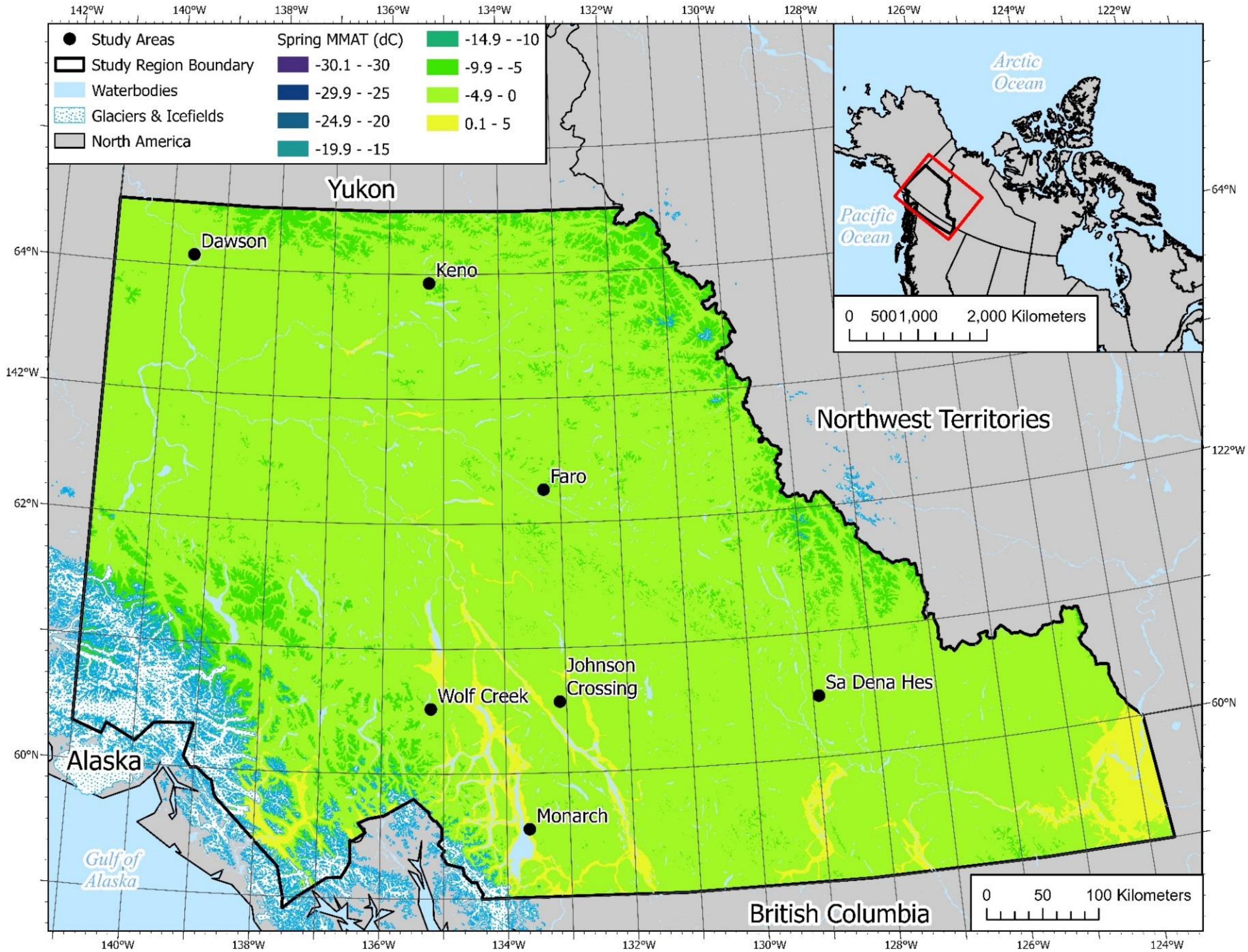

Figure 3-10. Modelled spring (March - May) mean air temperature across study region in northern British Columbia and Southern Yukon, from 59 – 64.5° N. The seven study areas used in building the model are shown. Whitehorse (not shown) is located approximately 10 km northeast of Wolf Creek.

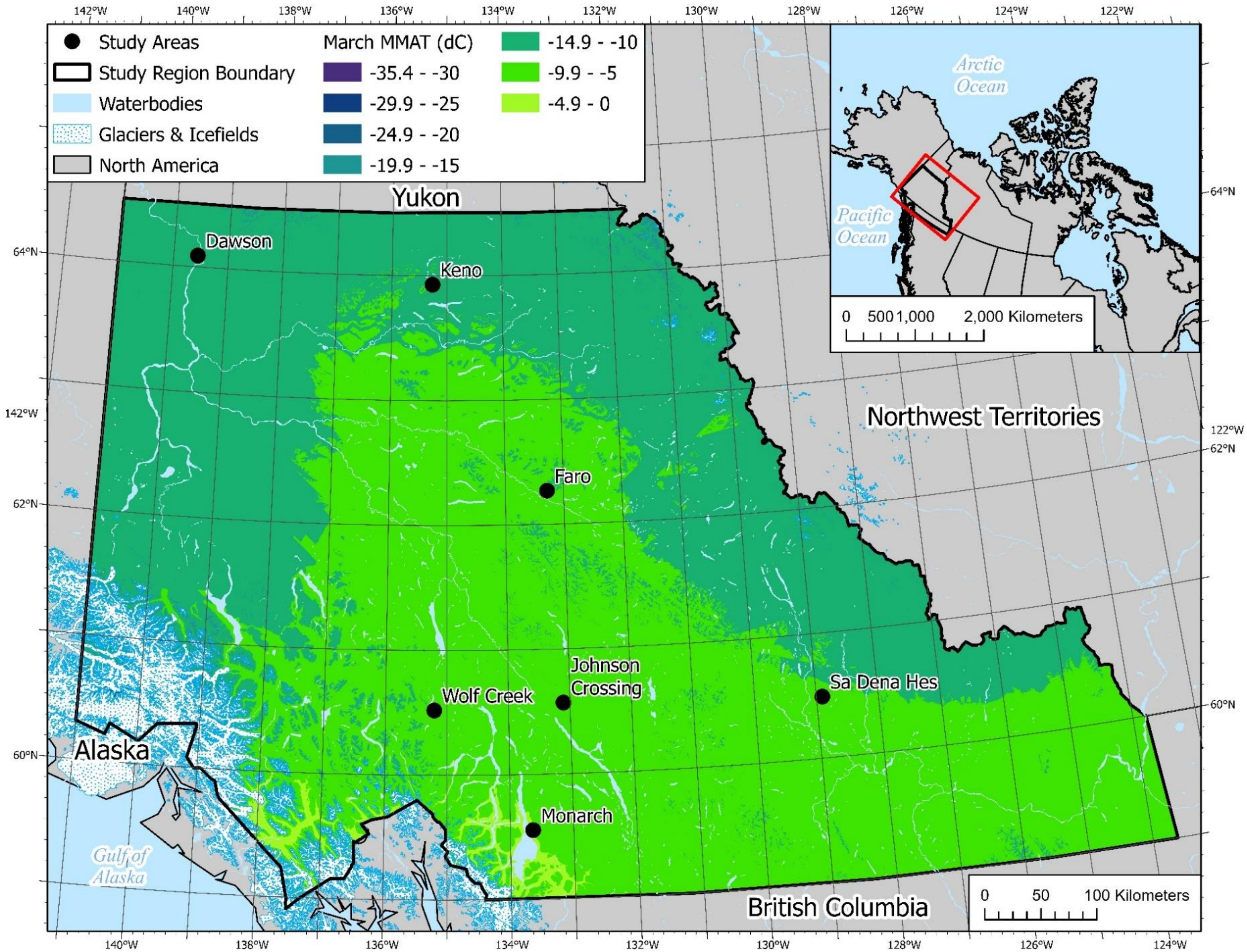

Figure 3-11. Predicted mean March air temperature (MMAT) values across study region in northern British Columbia and Southern Yukon, from 59 – 64.5° N. The seven study area used in building the model are shown. Whitehorse (not shown) is located approximately 10 km northeast of Wolf Creek. Average MMAT across the study region was calculated to be -9.8 °C.

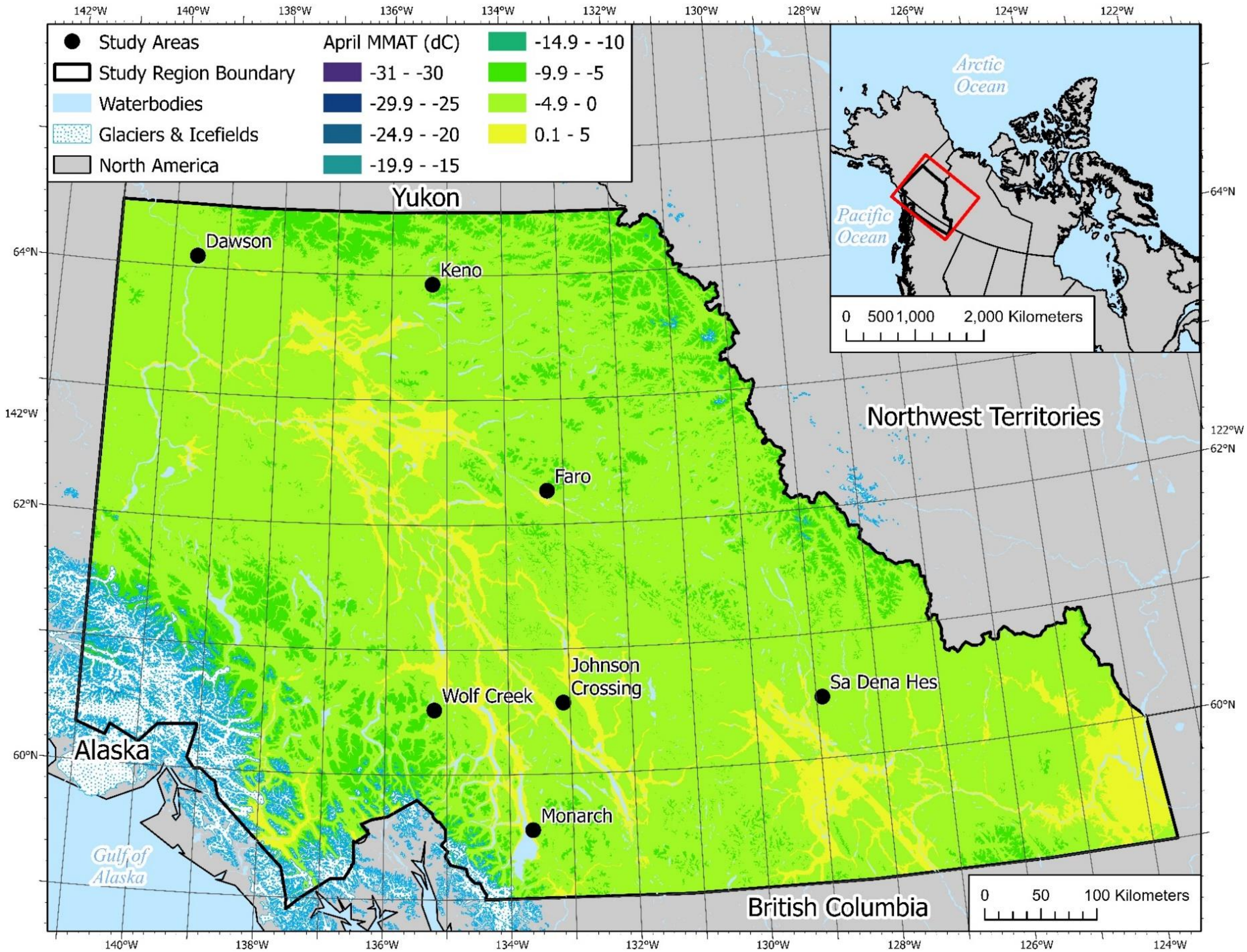

Figure 3-12. Predicted mean April air temperature (MMAT) values across study region in northern British Columbia and Southern Yukon, from 59 – 64.5° N. The seven study areas used in building the model are shown. Whitehorse (not shown) is located approximately 10 km northeast of Wolf Creek. Average MMAT across the study region was calculated to be -2.4 °C.

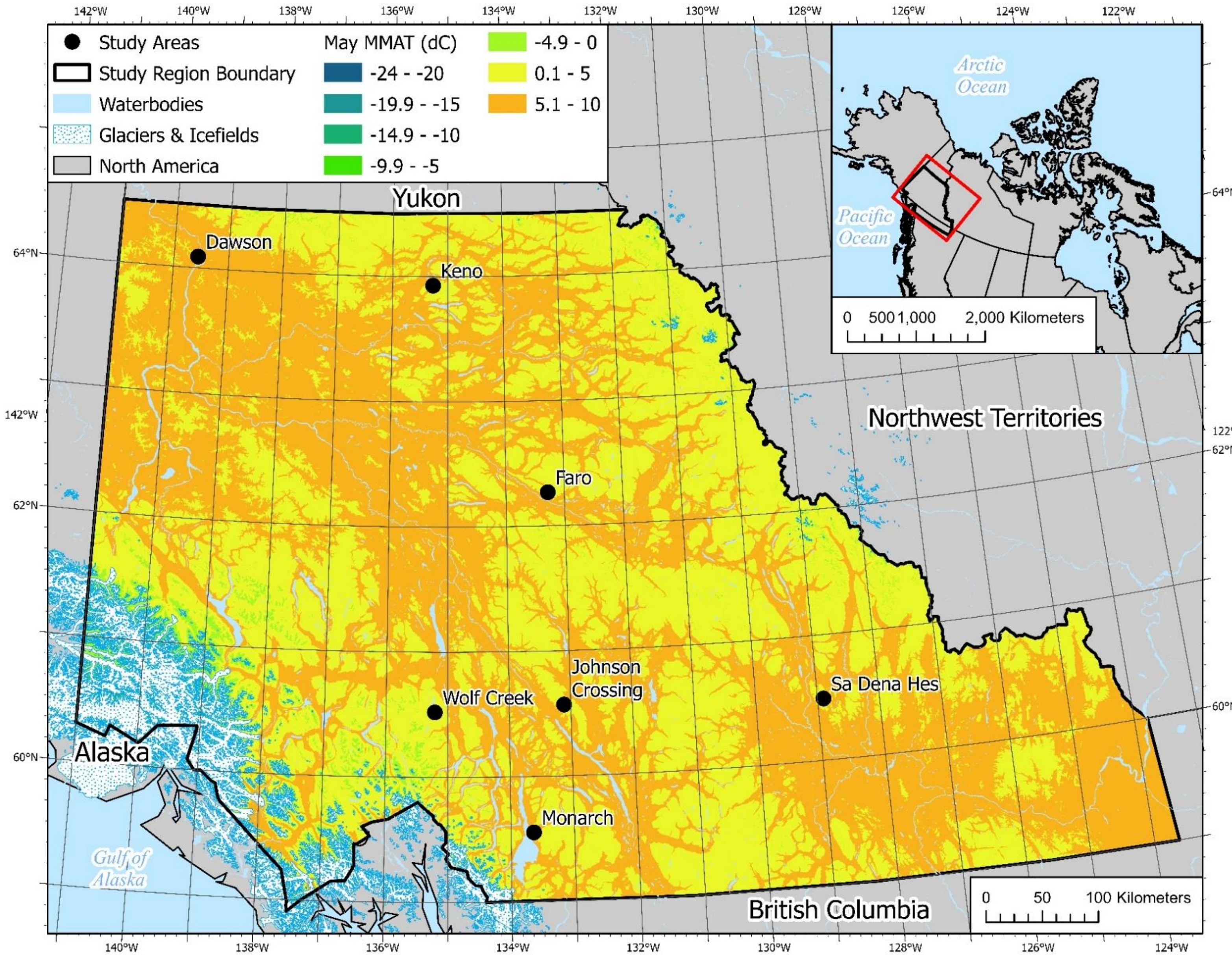

Figure 3-13. Predicted mean May air temperature (MMAT) values across study region in northern British Columbia and Southern Yukon, from 59 – 64.5° N. The seven study areas used in building the model are shown. Whitehorse (not shown) is located approximately 10 km northeast of Wolf Creek. Average MMAT across the study region was calculated to be 4.8 °C.

Summer showed relatively low spatial variation in temperature across the study region with most MMAT values being within a 15 °C range (*Figure 3-14*). Normal, although weak, lapse rates (*Figure 3*-4) result in warmer valley bottoms and colder temperatures at higher elevations (*Figure 3-15, 3-16, 3-17*). Both elevation and latitude play a role in the MMAT gradients for the summer months, more so than with the transition months of March through May. However, the most influential variable is elevation. The higher temperatures in the northeast of the study region are evidence of the strength of elevation influence.

The warmest MMAT temperatures occur in July with maximum temperatures reaching 17.3 °C at low elevations (*Figure 3-15*) before beginning to drop as the summer ends and fall begins. The degree of continentality does not have a significant relationship with lapse rates across the study region in the summer months, with the main influence being elevation.

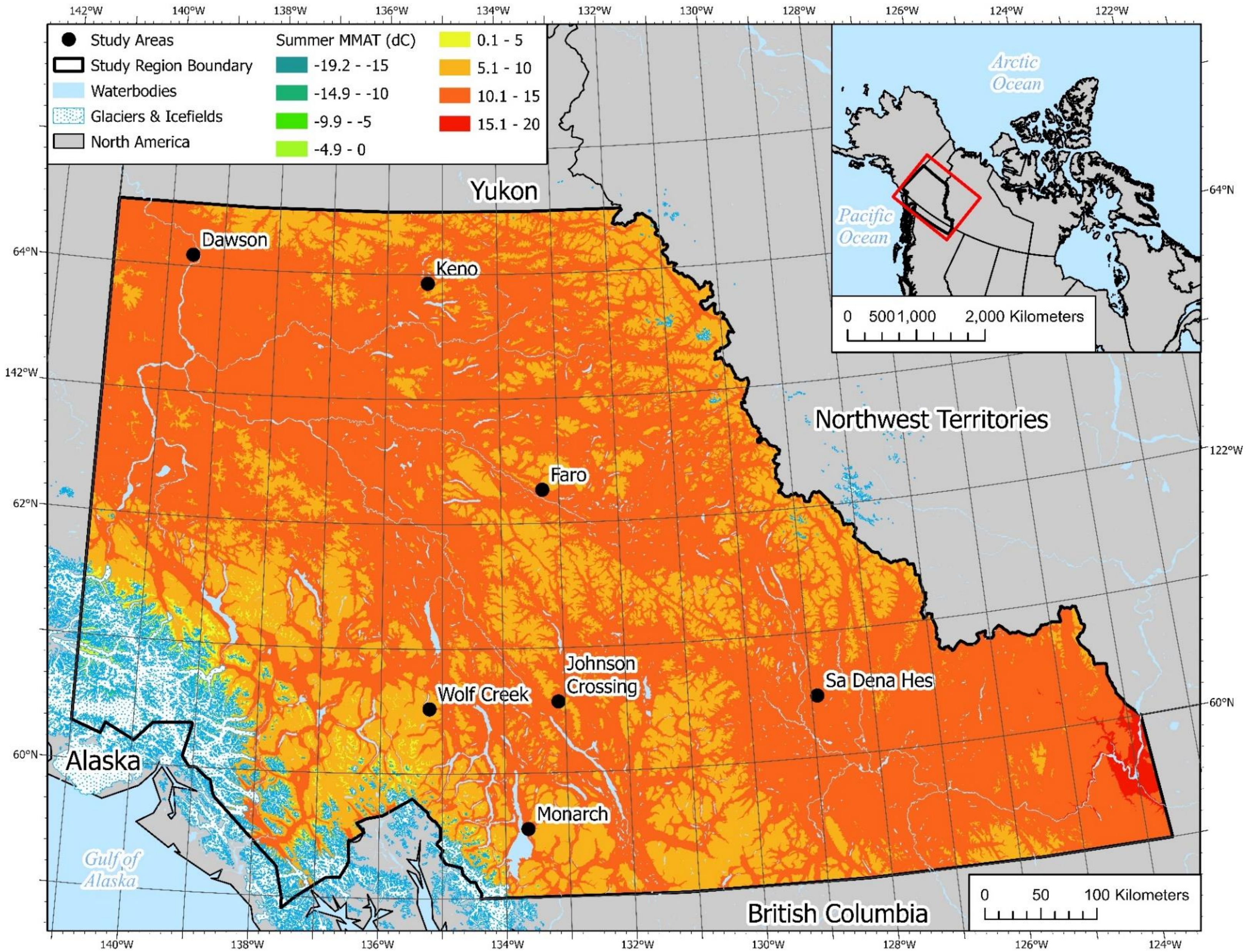

Figure 3-14. Modelled summer (June – August) mean air temperature across study region in northern British Columbia and Southern Yukon, from 59 – 64.5° N. The seven study areas used in building the model are shown. Whitehorse (not shown) is located approximately 10 km northeast of Wolf Creek.

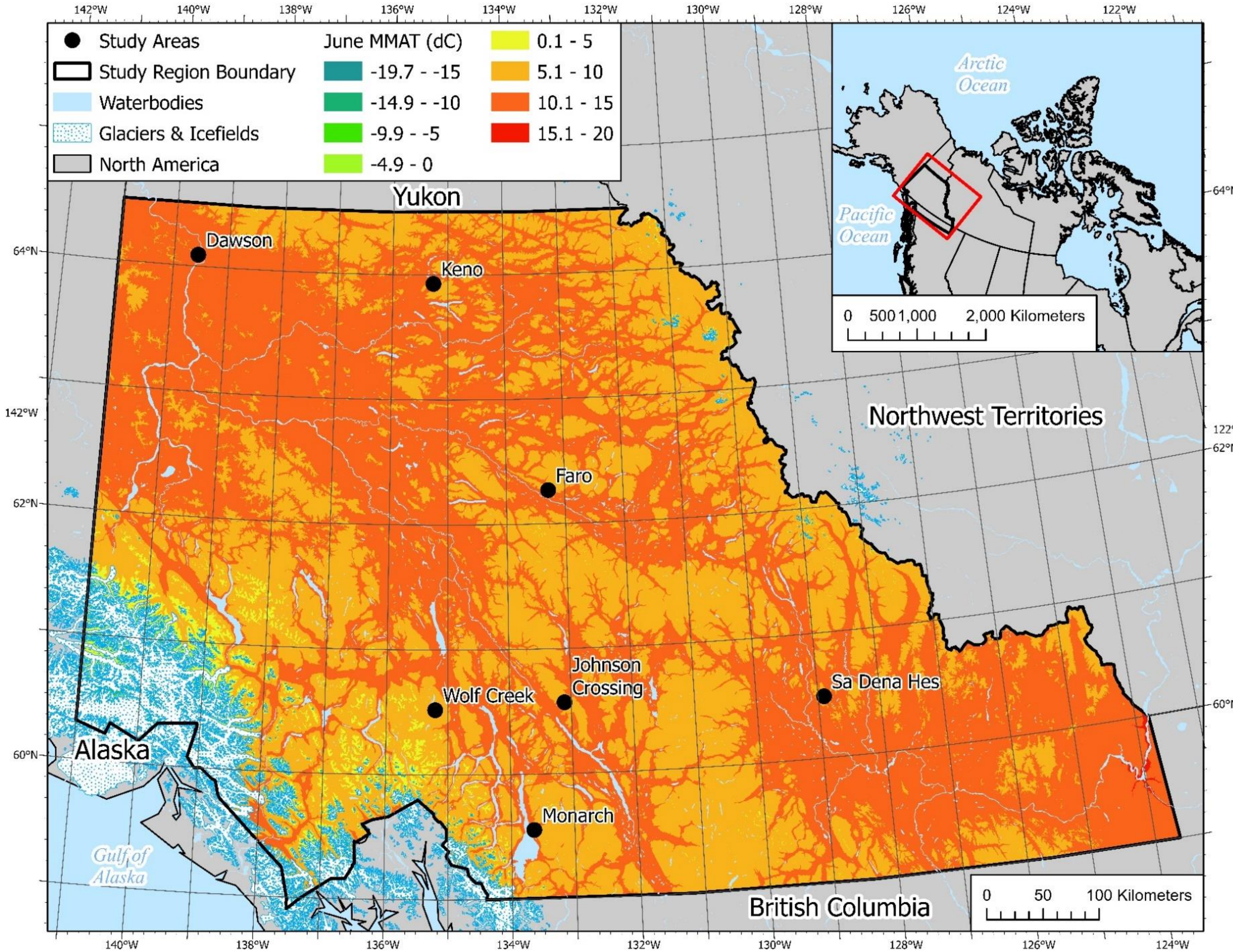

Figure 3-15. Predicted mean June air temperature (MMAT) values across study region in northern British Columbia and Southern Yukon, from 59 – 64.5° N. The seven study areas used in building the model are shown. Whitehorse (not shown) is located approximately 10 km northeast of Wolf Creek. Average MMAT across the study region was calculated to be 7 °C.

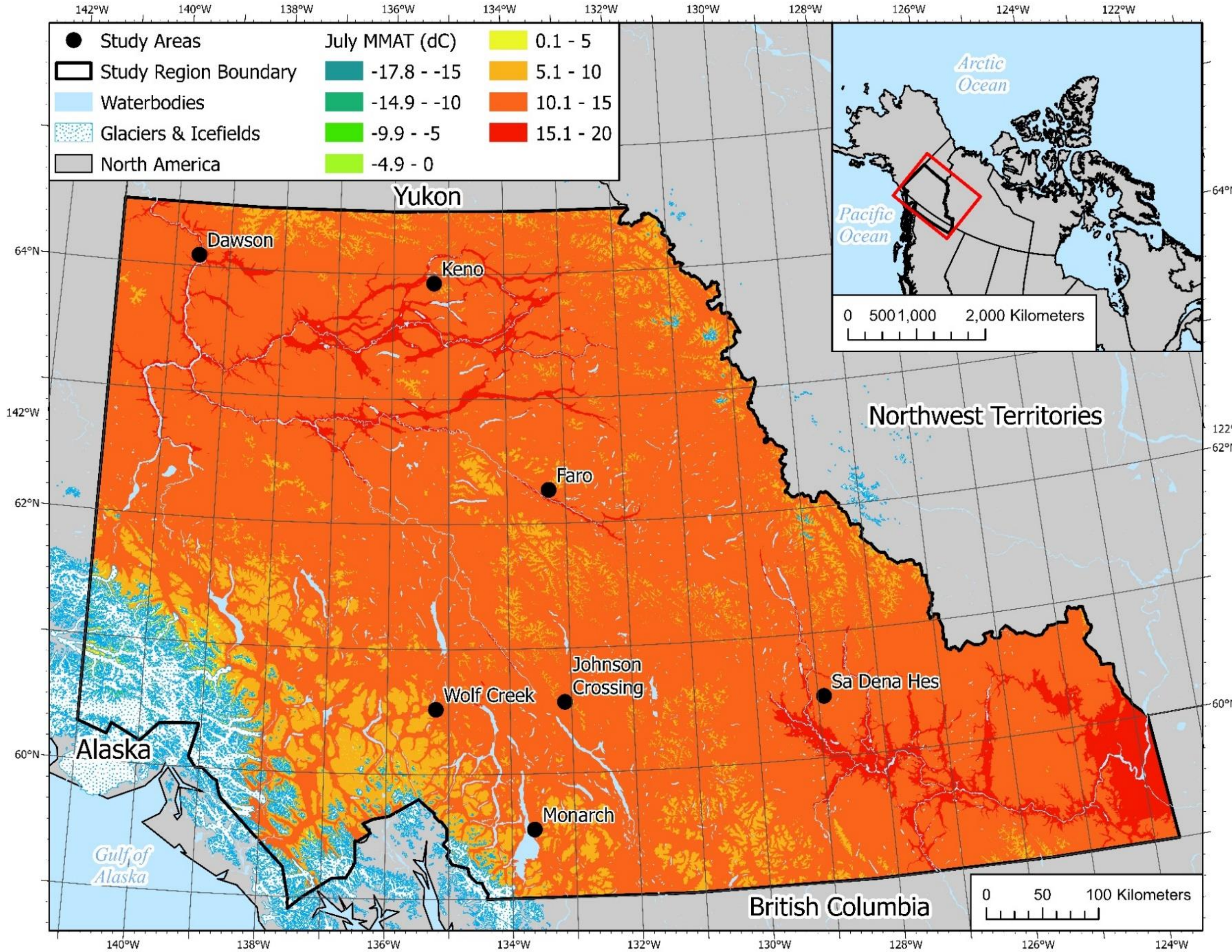

Figure 3-16. Predicted mean July air temperature (MMAT) values across study region in northern British Columbia and Southern Yukon, from 59 – 64.5° N. The seven study areas used in building the model are shown. Whitehorse (not shown) is located approximately 10 km northeast of Wolf Creek. Average MMAT across the study region was calculated to be 12.4 °C.

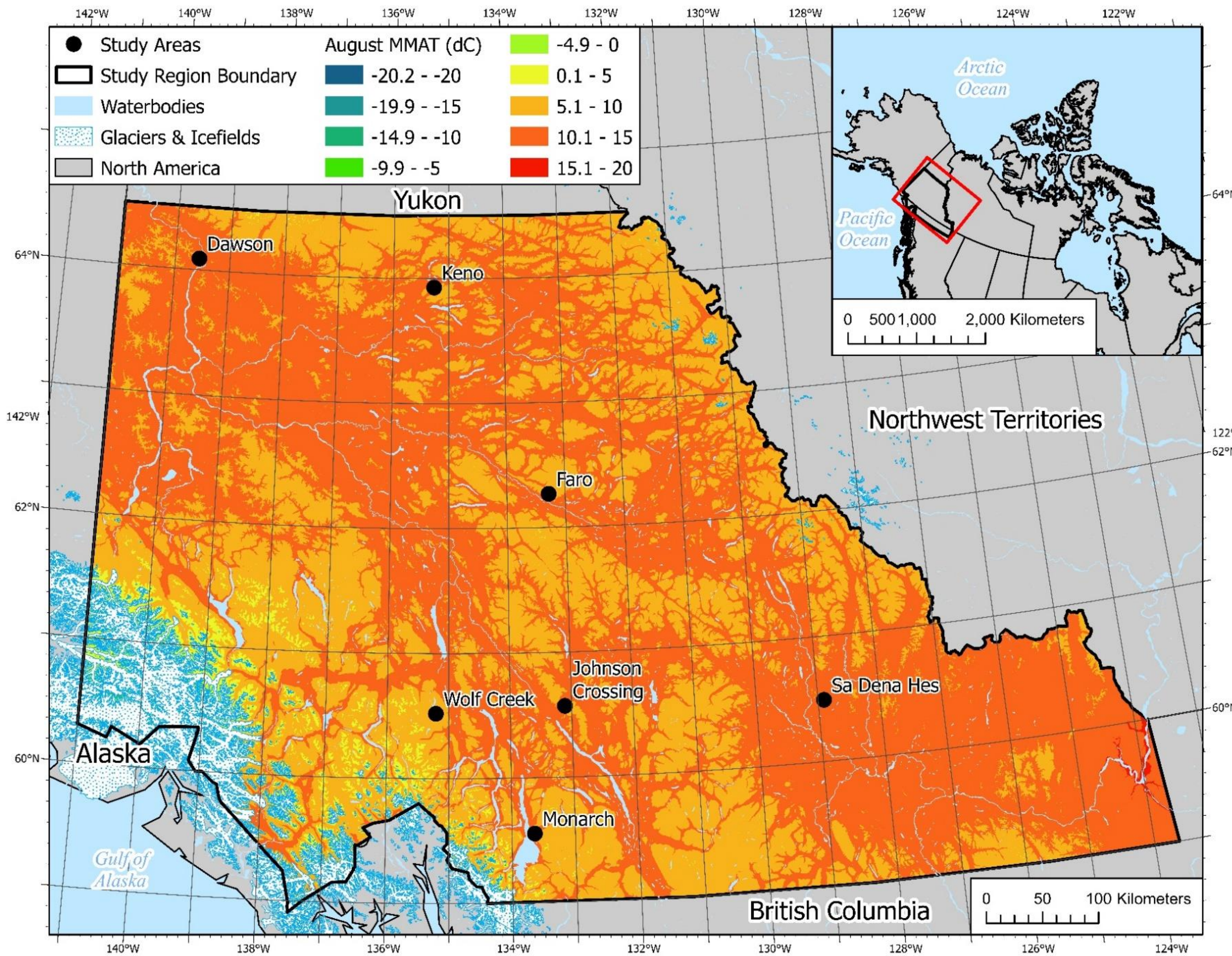

Figure 3-17. Predicted mean August air temperature (MMAT) values across study region in northern British Columbia and Southern Yukon, from 59 – 64.5° N. The seven study areas used in building the model are shown. Whitehorse (not shown) is located approximately 10 km northeast of Wolf Creek. Average MMAT across the study region was calculated to be 10.1 °C.

Autumn is the start of cooling in the region with average seasonal temperatures falling below 0 °C in most areas (*Figure 3-18*). The cooling temperatures transgress from north to south across the study region (*Figures 3-18, 3-19, 3-20*) as well as downward towards the valley bottoms.

As autumn progresses, the influence of continentality increases. In both September (*Figure 3-19*) and October (*Figure 3-20*), latitude and altitude play large roles in determining the temperature. Warmer areas are found further south and persist further north in valley bottoms, while the surrounding higher elevation areas exhibit lower temperatures. In November (*Figure 3-21*), the influence of continentality starts to become evident. While warmer temperatures persist in the southern part of the study region with temperatures between -9.9 °C – -5 °C, colder temperatures of -24.9 °C – -20 °C are present along valley bottoms south of Dawson while warmer temperatures between -19.9 °C – -15 °C and -14.9 °C – -10 °C cover the surrounding higher elevations.

The development of these cold valley bottoms can be seen in November even with the large degree of homogeneity in MMAT persisting across the study region (*Figure 3-21*). The cold valley bottoms continue through to February (*Figure 3-11*), corresponding to the greatest inversions in lapse rates across the study region (*Figure 3-4*).

Elevated temperatures exist in the valleys of northwest B.C. from October (*Figure 3-19*) to March (*Figure 3-12*). This is a result of warmer air from the Gulf of Alaska moving inland, creating weaker inversions in lapse rate than the rest of the study region during the cold months (see Monarch in *Figure 3-4*).

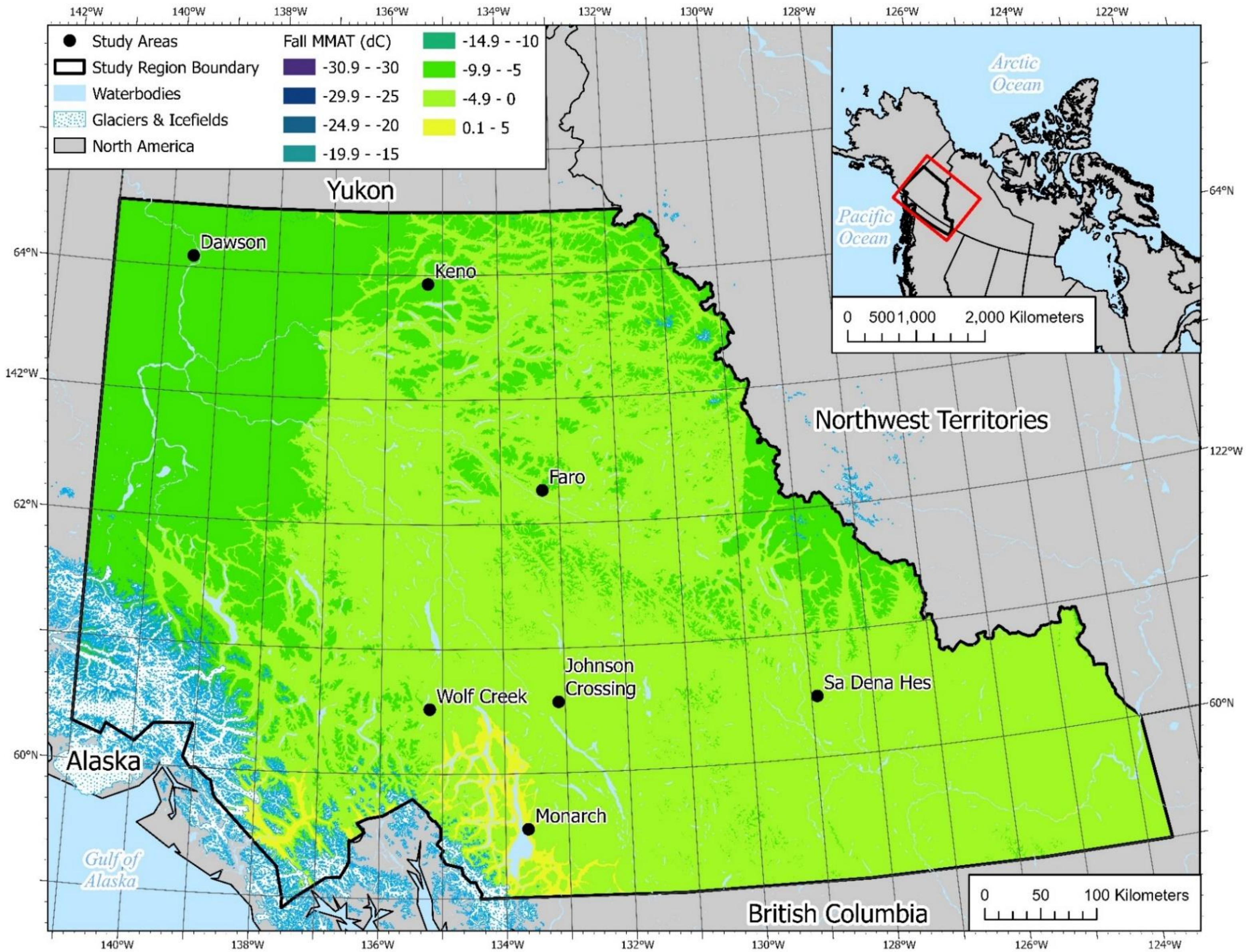

Figure 3-18. Modelled autumn (September – November) mean air temperature across study region in northern British Columbia and Southern Yukon, from 59 – 64.5° N. The seven study areas used in building the model are shown. Whitehorse (not shown) is located approximately 10 km northeast of Wolf Creek.

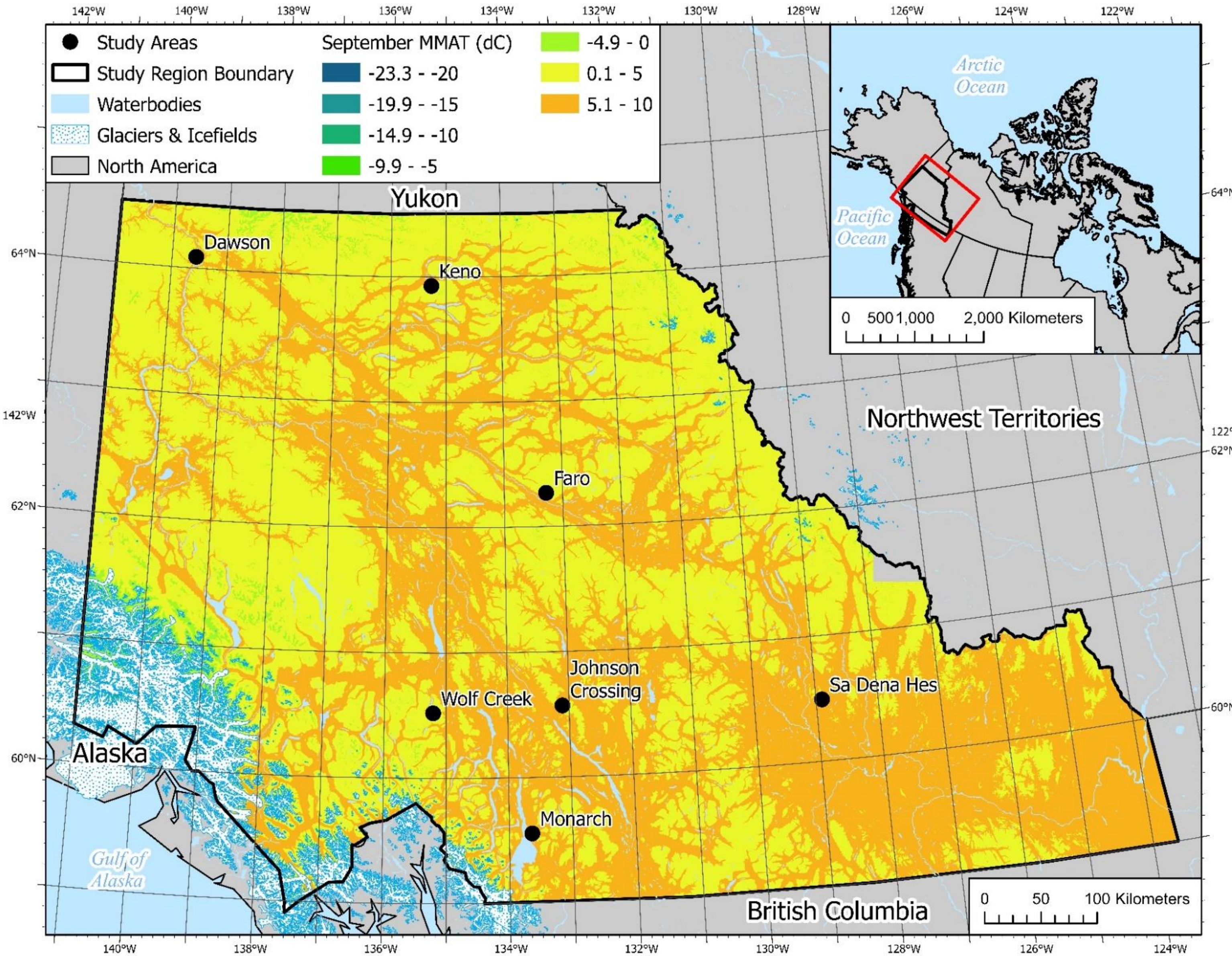

Figure 3-19. Predicted mean September air temperature (MMAT) values across study region in northern British Columbia and Southern Yukon, from 59 – 64.5° N. The seven study areas used in building the model are shown. Whitehorse (not shown) is located approximately 10 km northeast of Wolf Creek. Average MMAT across the study region was calculated to be 4.6 °C.

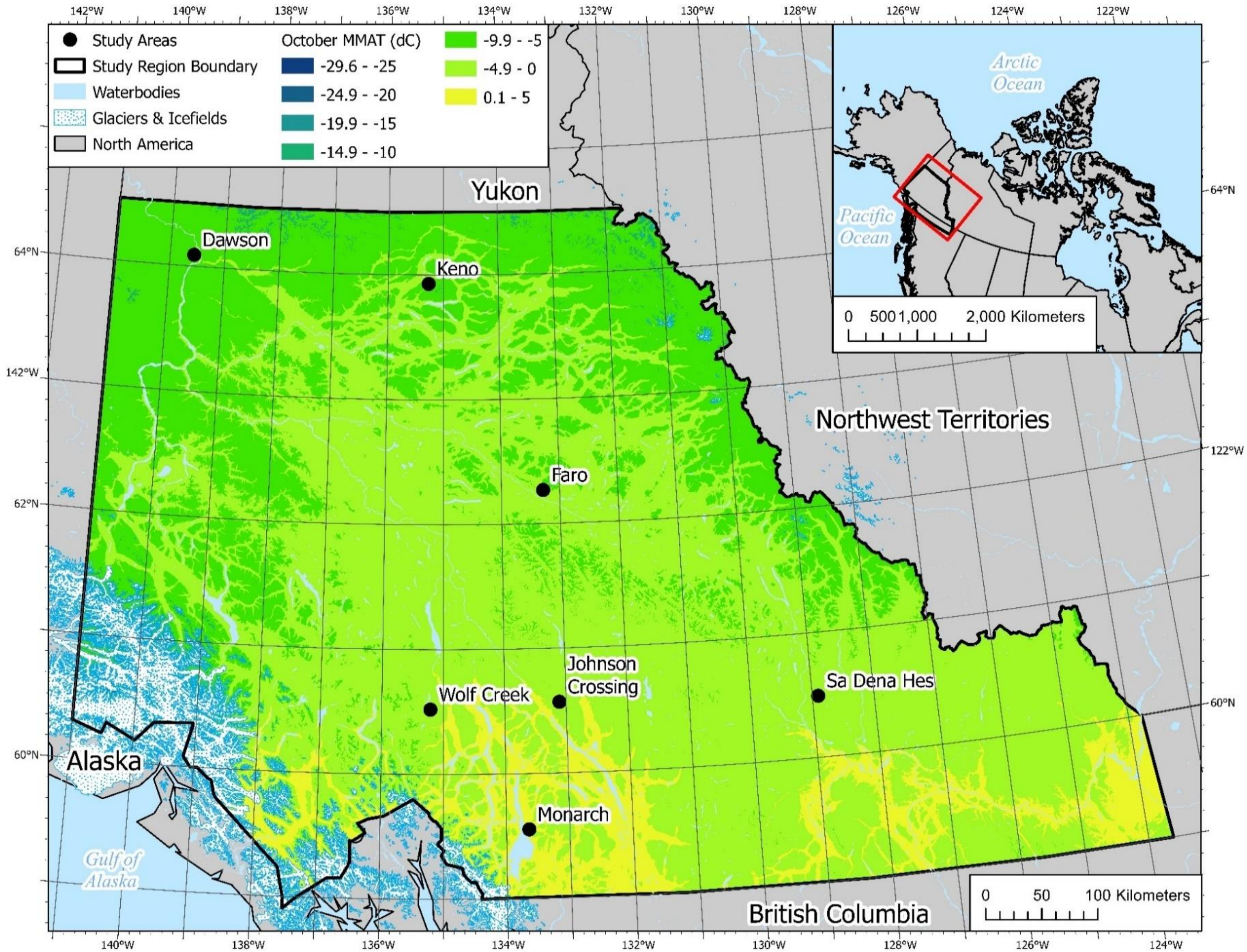

Figure 3-20. Predicted mean October air temperature (MMAT) values across study region in northern British Columbia and Southern Yukon, from 59 – 64.5° N. The seven study areas used in building the model are shown. Whitehorse (not shown) is located approximately 10 km northeast of Wolf Creek. Average MMAT across the study region was calculated to be -3.5 °C.

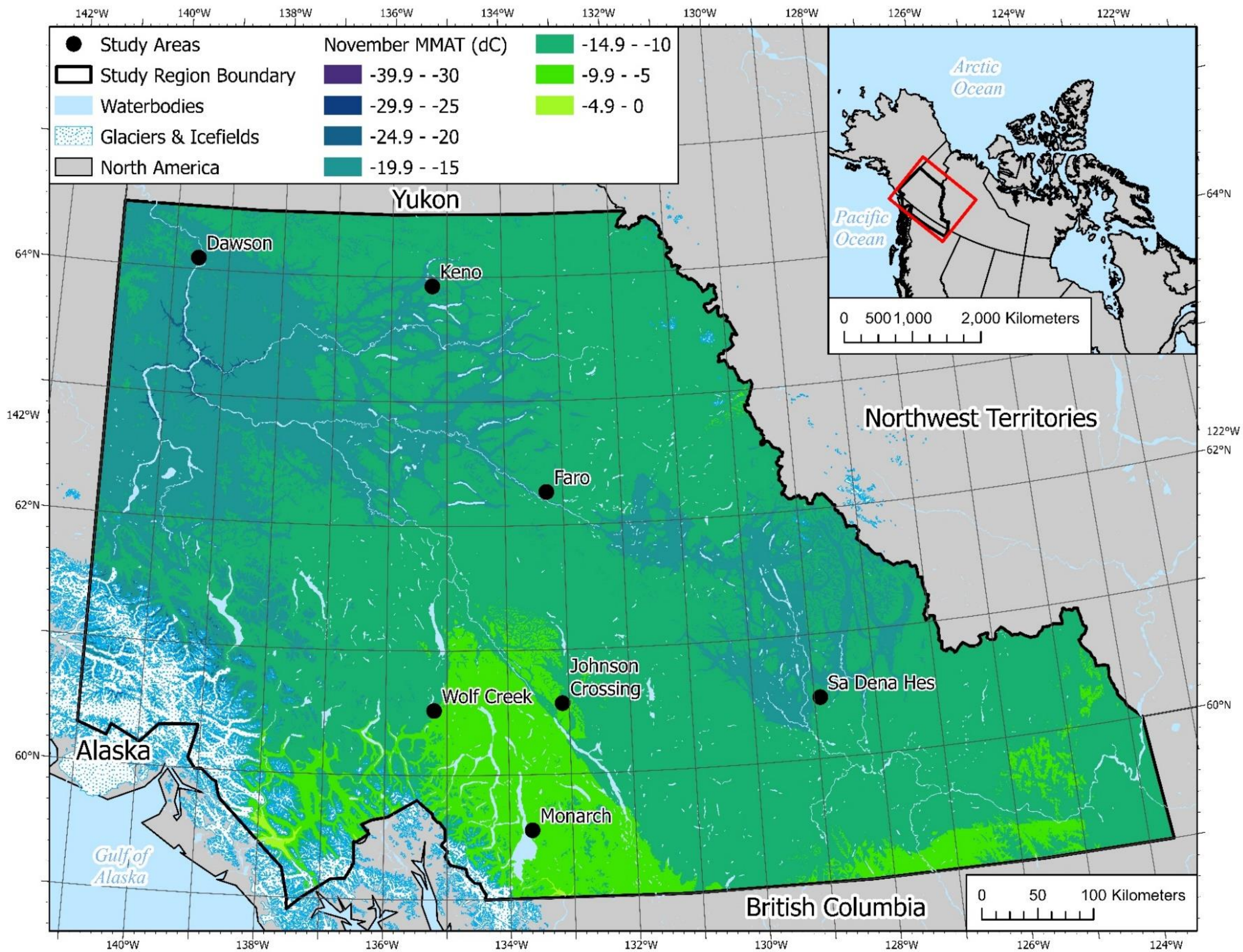

Figure 3-21. Predicted mean November air temperature (MMAT) values across study region in northern British Columbia and Southern Yukon, from 59 – 64.5° N. The seven study areas used in building the model are shown. Whitehorse (not shown) is located approximately 10 km northeast of Wolf Creek. Average MMAT across the study region was calculated to be -13.2 °C.

3.4.3 Evaluation of the MMAT models

The accuracy of all the MMAT models was tested by comparing model predictions to measurements at 20 sites across the study region (see *Figure 3-2 and Appendix D, Table D-1*). Results can be examined in relation to the RMSE and the slope of the best-fit regression line between observed and predicted MMATs (*Table 3-3*).

The models showed highest accuracy levels in the summer with RMSE values <1.0 °C (*Table 3-3*). Conversely, the largest RMSE was for January, but this was heavily influenced by two sites located near the boundaries of the study region. The higher RMSE values in the winter are also due in part to the greater overall range in MMAT values, allowing for more variation between measured and modelled temperatures. All the regression slope coefficients in *Table 3-3* were statistically significant at p=0.1. Ideally, coefficients should equal unity, but with the exception of October, all slopes are < 1, meaning measured values are generally higher than modelled values. The relationship between measured and modelled MMAT was weakest from December to March, corresponding to the months with larger RMSE values.

Table 3-1. Root Mean Square Error and regression slope coefficients for modelled vs. observed MMAT values at 20 validation sites.

Month	RMSE	Regression Slope Coefficient
January	4.43	0.66
February	2.39	0.63
March	2.19	0.67
April	1.07	0.82
May	1.81	0.95
June	0.71	0.88
July	0.95	0.82
August	0.88	0.91
September	0.90	0.91
October	1.41	1.19
November	2.02	0.80
December	2.84	0.77
MAAT	1.18	0.97

Four sites from below treeline (*Figure 3-23)* and four sites from above treeline (*Figure 3-24)* were chosen to highlight these comparisons. RMSE was low for AINA Base Camp and Beaver Creek Palsa with values of 0.92 and 1.33 respectively. One month was modelled poorly for each site with a model deviation of -3.6 °C at Beaver Creek Palsa in January and 2.4 °C at AINA Base Camp in March.

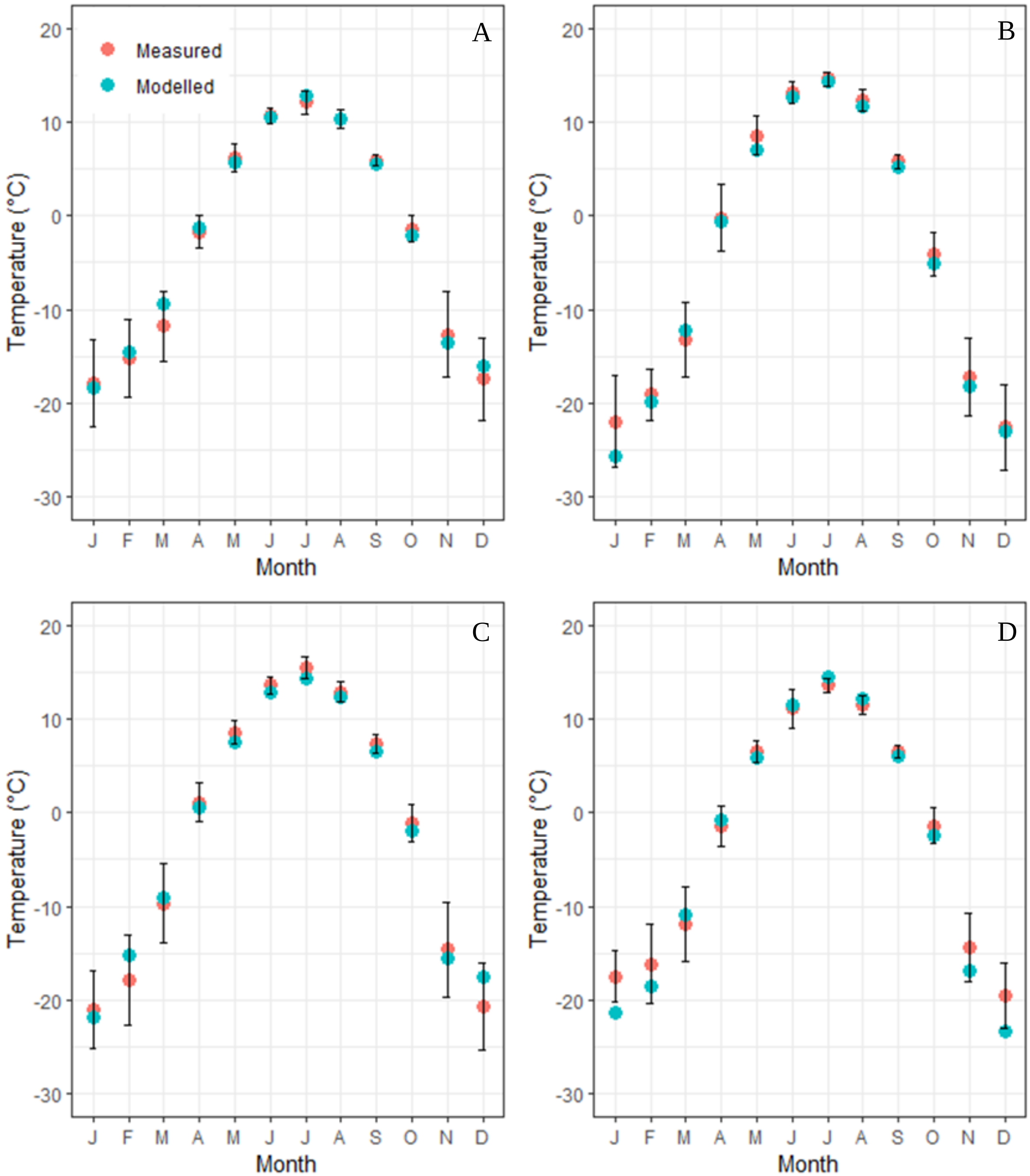

Figure 3-22. Modelled and measured MMAT values for four validation sites located below treeline. A – AINA Base Camp (UO site) (RMSE 0.92), B – Beaver Creek Palsa (UO site) (RMSE 1.33), C – Carmacks (ECCC site) (RMSE 1.43), D – Hour Lake (ECCC site) (RMSE 1.98). Measured values are an average of a minimum of three years of data. Bars represent the SD of measured MMAT temperatures during the collection period.

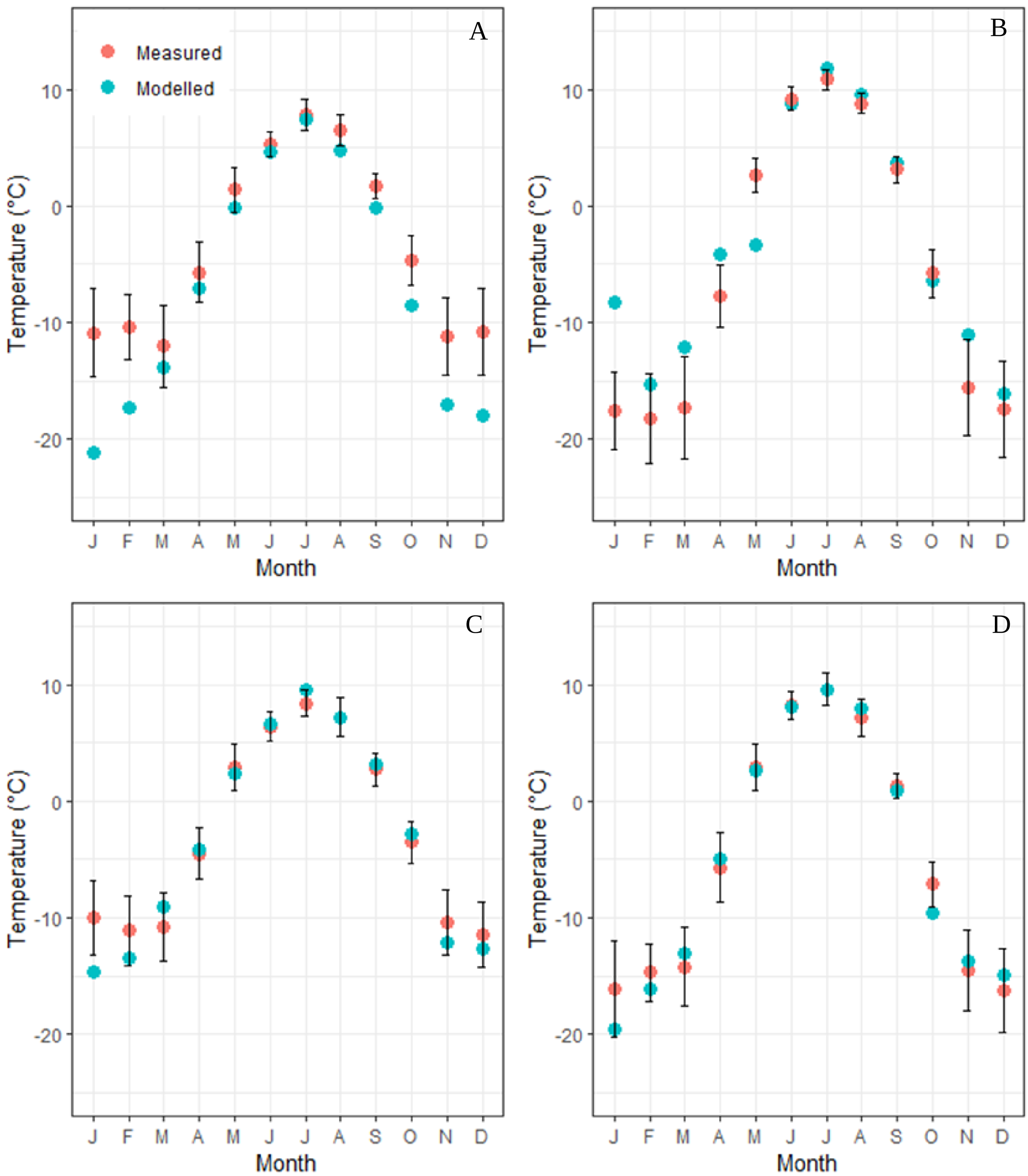

Figure 3-23. Modelled and measured MMAT values for four validation sites located above treeline. A – Alpine Burwash Backup (UO site) (RMSE 4.69), B – Macmillan Pass (ECCC site) (RMSE 4.03), C – Northern Dancer Backup (UO site) (RMSE 1.76), D – 60 Mile Backup (UO site) (RMSE 1.45). Measured values were averages of a minimum of three years of data. Bars represent the SD of measured MMAT temperatures during the collection period.

Of the four sites below treeline, AINA Base Camp and Beaver Creek Palsa were modelled well (RMSE of 0.92 and 1.33 respectively) with only one month for each predicting poorly: March for AINA Base Camp and January for Beaver Creek Palsa (*Figure 3-22A, Figure 3-22B*). However, in both instances, the modelled values are within one standard deviation of measured MMAT values. Carmacks validation site showed strong similarities between the modelled and measured values of MMAT throughout the year with only March and December showing slightly greater differences, again within one standard deviation of measured MMAT values. Hour Lake ECCC was predicted the most poorly of these four validation sites with discrepancies between modelled and measured temperatures being most noticeable from November through February when the modelled temperature was consistently lower than the measured temperatures. December and January were outside of one standard deviation from measured MMAT values. However, the other months do not show a clear trend of the model predicting lower than measured temperatures (*Figure 3-22D*).

Four sites above treeline with varying levels of model validation strength are shown in *Figure 3-23*. RMSE was relatively low for Northern Dancer Backup and 60 Mile Backup with values of 1.76 and 1.45 respectively. January was modelled poorly for each site with a model deviation of -3.6 °C at 60 Mile Backup and -4.6 °C at Northern Dancer Backup. The differences between modelled and measured values are greater on average than for the sites below treeline. The model tended towards lower than measured temperatures in the winter for sites above treeline. This suggests that the lapse rate above treeline may not be as strong as the lapse rate of -6 °C/km used in the model. The exception to this is Macmillan Pass where the below treeline values are high due to edge effects of the model domain which affect the above treeline values too and makes them too warm.

Alpine Burwash Backup, Northern Dancer Backup, and 60 Mile Backup all showed fairly accurate modelled MMAT from April through September, but much greater deviations from measured values from October through March (*Figure 3-23A, Figure 3-23C, Figure 3-23D*). Modelled MMAT values are more than one standard deviation of measured MMAT values from November through February at Alpine Burwash Backup. This temporal pattern of greater difference between measured and modelled MMAT values is similar to the sites below treeline. Macmillan Pass, which is located at the northeastern edge of the study region, showed large discrepancies between measured and modelled temperatures from November through May, and especially in January with an absolute difference of 9.3 °C (*Figure 3-23B*), with modelled temperatures almost always warmer than the measured ones. These deviations indicate that the model may not perform as well near the boundaries of the study region and especially in winter.

The remainder of the measured and modelled MMAT at the 20 validation sites are presented in Appendix D, *Table D-2 and D-3*.

3.4.4 Mean Annual Air Temperature

Modelled MAAT for the study region was calculated as the average of the twelve MMAT maps. The resulting map shows a range of values from -30.5 °C to 4 °C (*Figure 3-25*). The warmest locations are near the Gulf of Alaska as well as in the southeast portion of the study region. Colder areas are found further inland, as a result of an increasing degree of continentality. A general south-north gradient is present with temperatures of -2 °C – 0 °C in the southernmost part of the study region, progressing to -2 °C – -4 °C in the central part, and then to temperatures < -4 °C in the northwest. Temperatures in the northeast portion of the study region are not as low as in the northwest but this may be an artefact of the limited data in this area and the generally warmer than measured predictions in winter (e.g., for Macmillan Pass, *Figure 3-23B*). As expected, the lowest MAAT values occur at very high elevations surrounding the glaciers and ice fields in the southwest part of the study region.

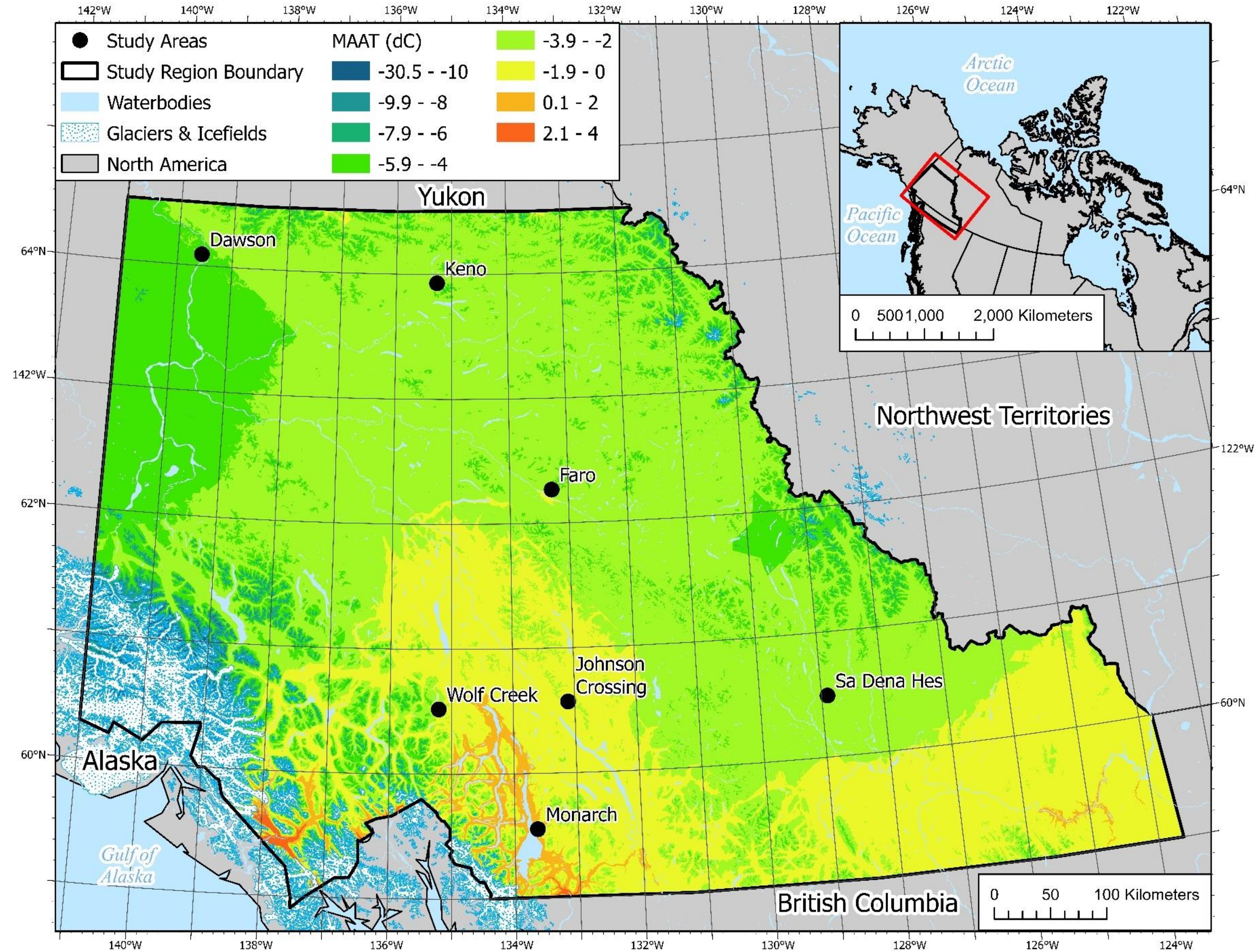

Figure 3-24. Modelled mean annual air temperature (MAAT) values calculated as the average of all MMAT maps. Whitehorse (not shown) is located approximately 10 km northeast of Wolf Creek. Average MAAT across the study region was calculated to be -2.8 °C.

3.5 Discussion

3.5.1 Factors affecting model validity

The validation showed better performance of the model in some parts of the study region than in others. Edge effects of the model were most noticeable near Macmillan Pass ECCC station along the northeast border of the study region and Alpine Burwash Backup near the glaciers and icefields in the southwestern part of the study region. The edge effects at Macmillan Pass were likely a result of the lack of data in the surrounding area, for both the lapse rate modelling and for building the spatial model. Although government weather stations from outside the study region were used to create the models of MMAT, they were mainly at lower elevations and within Alaska (*Figure 3-3*), creating better modelled values in the southern and western parts of the study region and less accurate modelled values in the northeastern part of the study region.

Alpine Burwash Backup is located close to the glaciers and ice fields as well as near the edge of the study area. Glaciers and ice fields can create local climate patterns, especially lower temperatures than the surrounding areas (Wahl *et al.*, 1987). Alpine Burwash Backup, however, showed lower modelled than measured values throughout the year, but especially from October to February (*Figure 3-24*). This suggests that winter inversions below treeline are stronger than modelled or that the normal lapse rate above treeline is weaker than modelled. Another possible explanation for the discrepancies between measured and modelled values at these sites is a difference in lapse rate and temperature behaviour within clouds. Alpine Burwash Backup, Northern Dancer Backup, and Mount Granger are the three highest elevation validation sites at 1627, 1809, and 2077 m asl respectively. These sites are at high enough to be within cloud cover on many days of the year.

In general, the MMAT models performed better in the warmer months when temperatures are more uniform across the study region. This can be attributed to a limited range of temperatures, resulting in smaller differences between measured and modelled values. The difference in model performance between warmer and colder months can also be attributed to greater spatial variability in lapse rates across the study region in the winter months, as well as microclimate variability. Cold air drainage can have a significant impact on temperatures at a study site. Individual validation sites are also susceptible to winter weather conditions causing rime accumulation on temperature shields. Rime is a buildup of ice that can block accurate measurements of temperatures. Since sites are visited mainly in the spring through fall months for easier access, the likelihood of witnessing rime buildup on a temperature shield is low and can mainly be detected through analyzing daily temperature patterns. Sites with rime buildup may show reduced diurnal variation in temperatures.

Although efforts were made to eliminate inaccurate field data, it is possible that some errors in the vast dataset were not recognized. This could have resulted in negative impacts on the model. However, such issues are thought to be of minor significance given that a minimum of three years of data were available for each site.

Factors such as elevation, latitude, and longitude of validation sites did not appear to have any relationship to the difference between measured and modelled temperatures. Overall, the differences were likely a result of model inputs being unequally distributed across the study region and surroundings as well as varying periods of data collection for input and validation data. A more consistent record of data for both model building and validation would have been preferable but was prevented by a combination of site setup dates as well as temperature logger failures.

3.5.2 Comparison with other temperature profile maps

Wahl *et al.* (1987) created the current MMAT maps for the Yukon Territory, developing contour maps based on government weather station data. The models used 75 sites with 30-year climate normals, 38 of which were located within Yukon and the remainder within Alaska, British Columbia, and Northwest Territories. Of the 38 sites within Yukon, 32 had mostly complete 30-year normals data and 6 had limited information. Although the government weather stations are mostly at lower elevations, lapse rate inversions were incorporated into these maps (Wahl *et al.*, 1987) but the method used was not specified. Here, comparisons are made between the January, July and MAAT maps from Wahl *et al.* (1987) and those from the current modelling.

The January MMAT map in Wahl *et al.* (1987) had a maximum temperature of -5 °C, whereas the new modelled MMAT map shows a maximum January MMAT value of 0 °C (*Figure 3-25*). The overall range of the maps also differs, with a range in isotherms from -5 °C to -35 °C (Wahl *et al.*, 1987) compared to the range of the newly modelled MMAT from 0 °C to -43.7 °C. The most noticeable difference is the significantly colder prediction of temperatures surrounding the glaciers and ice fields in the southwest. The temperatures over the ice fields themselves were not monitored during the collection period and therefore this area was excluded from the models of MMAT. However, surrounding temperatures were the lowest in the region (*Figure 3-25B*). The low winter temperatures surrounding Sa Dena Hes are also evident in the 1987 MMAT maps from November through February (Wahl *et al.*, 1987).

The nature of the printed isolines used by Wahl *et al.* (1987) limits the amount of detail that can be shown on those maps. In contrast, the new raster models show detailed spatial variation, especially across elevation gradients in the same region. The pattern is similar, such as in the northwest part of the study area (*Figure 3-25B*), but the details are absent in Wahl *et al.* (1987).

July MMAT maps showed temperatures largely within the range of 5 °C to 20 °C with very similar patterns in temperature to Wahl *et al.* (1987) (*Figure 3-26*). The valley bottoms are warmer than higher elevations in July, indicating normal lapse rate behaviour. The homogeneity of the MMAT across the study area persists from March through October in both MMAT models. General trends of warm valley bottoms and colder high elevation areas continue throughout these months with the coldest temperatures centered on and around the glaciers and ice fields. A notable difference between the MMAT maps above and the maps created by Wahl *et al*. is the cooler MMAT values predicted by the latter in the northeastern portion of the study area. Through the evaluation of Macmillan Pass ECCC validation site, it was clear the models of MMAT did not predict well in that area. The 1987 MMAT maps, therefore, may be a more accurate representation of temperature in that part of the study area.

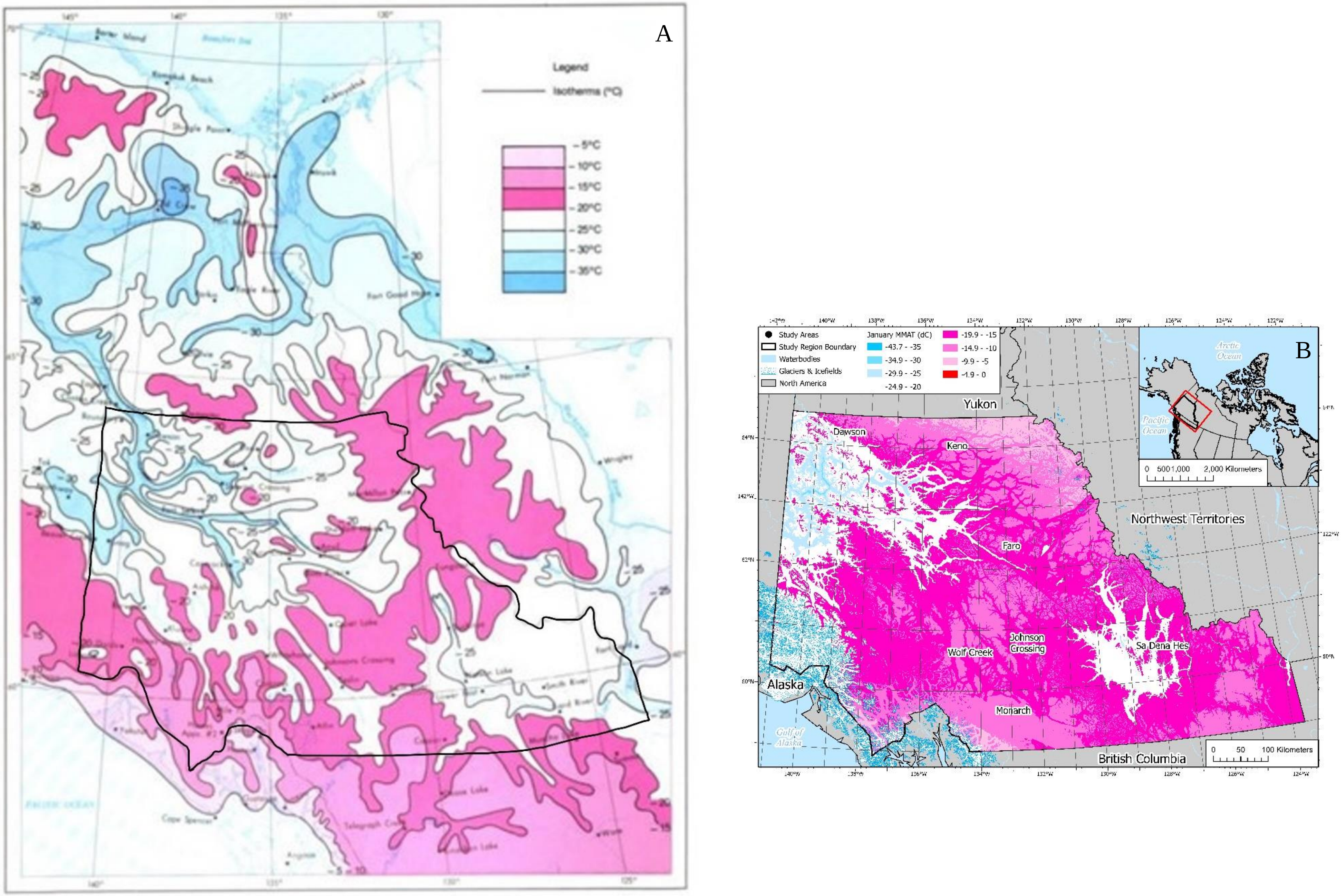

Figure 3-25. January MMAT values for Yukon Territory. Isotherm map (A) created by Wahl et al. (1987). (B) Gridded 90 x 90 m cell map created using modelled lapse rates below treeline and standard -6 °C/km lapse rate above treeline. Symbology has been matched as closely as possible for comparison to the map by Wahl et al. (1987). Red was used to indicate warmer temperatures than the top of the scale used by Wahl et al. (1987).

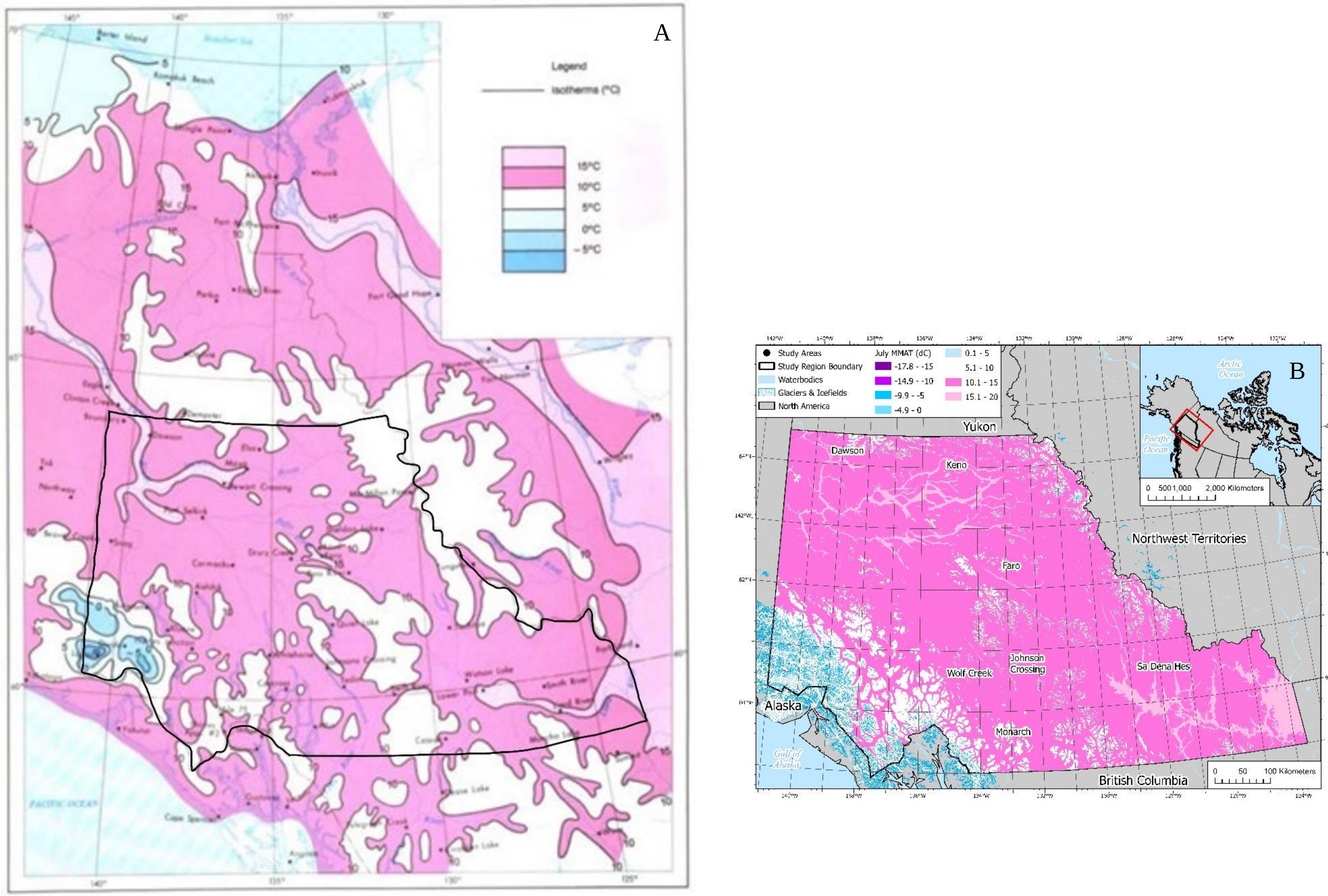

Figure 3-26. July MMAT values for Yukon Territory. Isotherm map (A) created by Wahl et al. (1987). Gridded 90 x 90 m cell map (B) created using modelled lapse rates below treeline and standard -6 °C/km lapse rate above treeline. Symbology has been matched as closely as possible for comparison to the map by Wahl et al. (1987). Purple was used to indicate colder temperatures than the end of the scale used by Wahl et al. (1987).

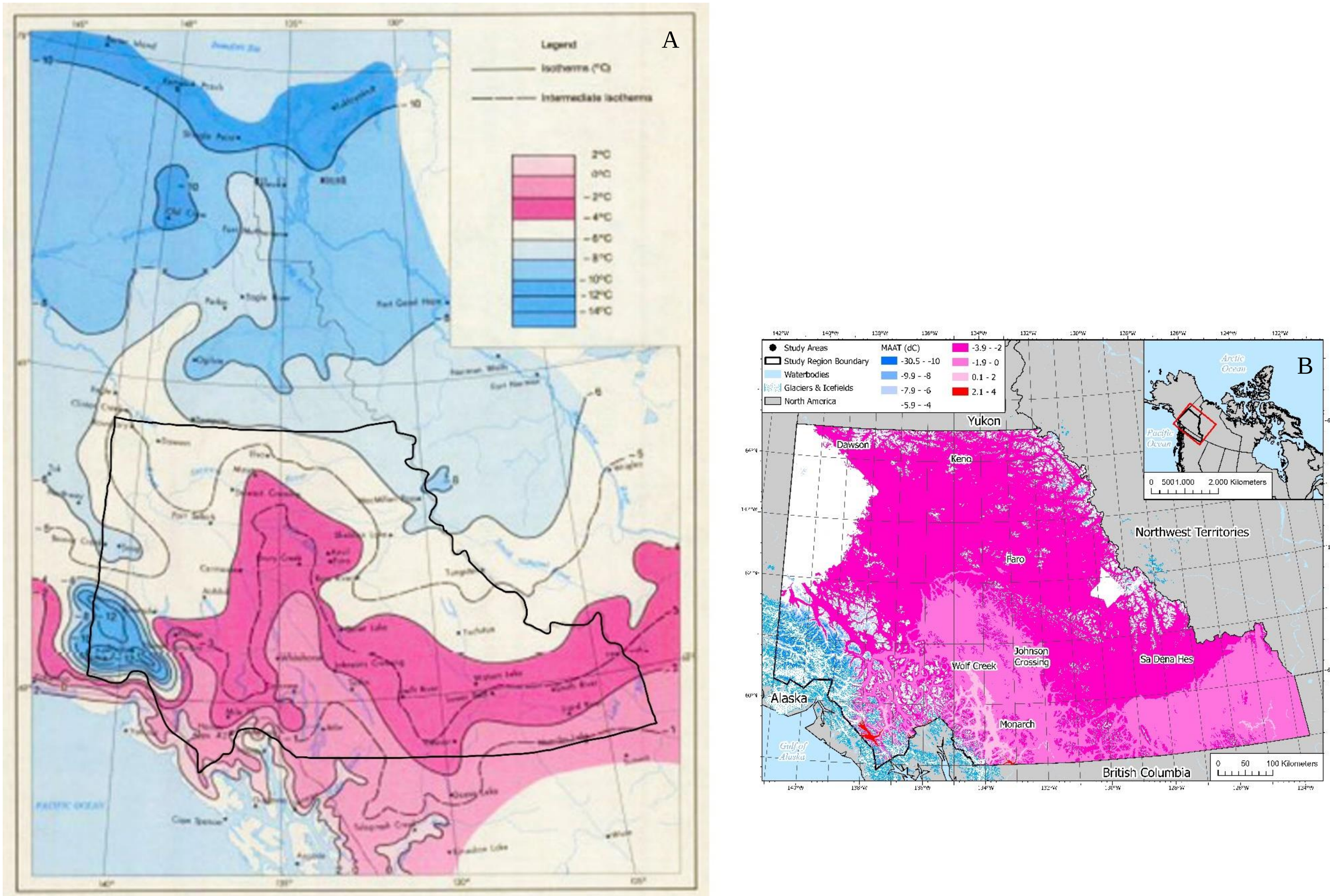

Figure 3-27. MAAT values for Yukon Territory. Isotherm map (A) created by Wahl et al. (1987). (B) Gridded 90 x 90 m cell map created using modelled lapse rates below treeline and standard -6 °C/km lapse rate above treeline. Symbology has been matched as closely as possible for comparison to the map by Wahl et al. (1987). Red was used to indicate warmer temperatures than the top of the scale used by Wahl et al. (1987).

The MAAT map created by Wahl *et al.* (1987) (*Figure 3-27A*), uses a symbology scale that was not copied exactly for *Figure 3-27B*, as the colder temperatures were combined into a single category. There were two reasons for this choice. First, the coldest temperatures exist mainly in the northern Yukon near the Beaufort Sea and in the ice fields in the southwest of the study region. These areas were not modelled in *Figure 3-27B*. Second, the symbology ranges were not easily distinguishable below -10 °C and their use would have made it difficult to identify the temperatures on the gridded map (*Figure 3*-27B).

The MAAT map created from the average of modelled MMAT values shows temperatures mainly between -5.9 °C and 0 °C (*Figure 3-27B*). The warmest areas, ranging between -1.9 °C to 0 °C, were located in the southern portion of the study region, extending further north close to the coast, highlighting the significance of continentality in determining temperatures. The majority of the study area had a MAAT of -3.9 °C to -2 °C (*Figure 3-27B*). The lowest extensive category on the map, -5.9 °C to -4 °C, is present at high elevations across the study region as well as in the northwest part of the study region surrounding and extending southwest of Dawson. The colder MAAT in the latter area can be attributed to weaker than average lapse rates, the degree of continentality, and the northernly location.

Contrary to the findings in *Figure 3-28B*, Lewkowicz *et al.* (2012) found the overall range in temperatures to be mainly between -7 °C and -1 °C (2012) (*Figure 3-28A*). The differences in the most common MAAT values across the study region is mostly attributed to different scale ranges for the two maps as well as different data collection periods. The data collection period used to create *Figure 3-28B* was significantly longer and included some recent warm years. The modelling method used between the two MMAT maps also varied, allowing for some variation in how temperatures were predicted across the study region. Regardless of methods and slight variations, both models of MAAT provide a good basis of recent air temperatures which will allow for comparisons in the future as temperatures in this part of Canada continue to change.

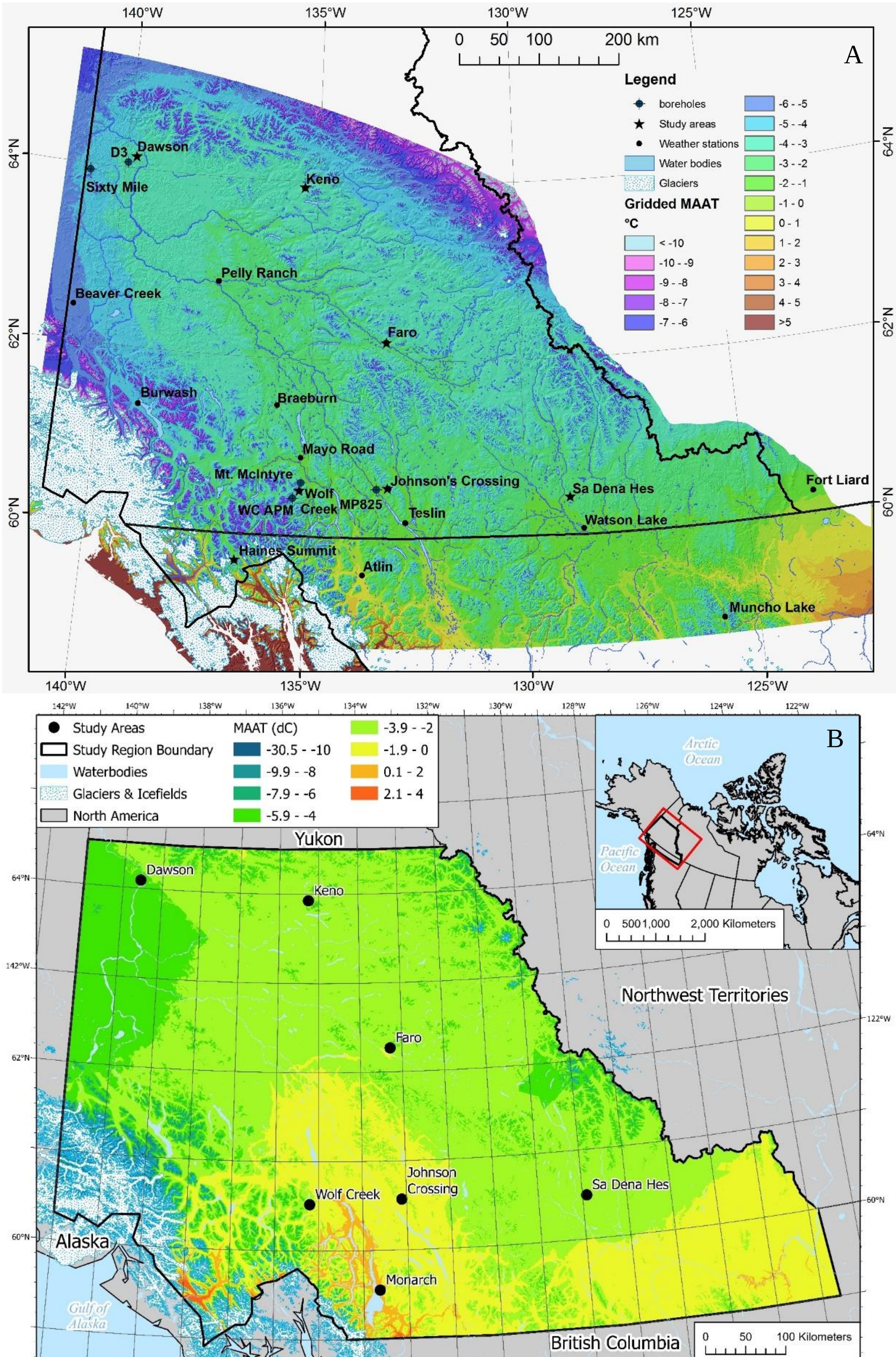

Figure 3-28. MAAT values for Yukon Territory. Gridded map (A) created by Lewkowicz et al. (2012). Gridded 90 x 90 m cell map (B) created using modelled lapse rates below treeline and standard -6 °C/km lapse rate above treeline.

3.5.3 Relationship between July MMAT and treeline

The 10 ºC isotherm in July is widely regarded as the limiting factor for tree growth (Daubenmire, 1954; D'Odorico *et al.*, 2013). The treeline, therefore, can represent an independent assessment of the July temperature model.

The July MMAT model showed 87.4% of the study region to be warmer than 10 ºC, of which 90.5% (79.1% of the region) was below treeline and 9.5% (8.3% of the region) was above treeline (*Table 3-1; Figure 3-29*). A very small proportion of the area (0.1%) below treeline was modelled as <10 ºC. The remaining 12.4% of the region was located above treeline and had modelled MMAT <10 °C.

Table 3-2. Areas with July MMAT above and below 10 ºC in relation to treeline.

Treeline	Temperature (°C)	Percent Area
Below Treeline	Above 10	79.10
	Below 10	0.13
Above Treeline	Above 10	8.33
	Below 10	12.44

Areas above treeline that also showed July temperatures >10 ºC were mainly located in the northern and eastern portions of the study region (*Figure 3-29C*). These could be indicative of model error if the relationship between treeline and temperature is exact. Of the cells that exceed 10 °C and are above treeline, more than three-quarters have modelled temperatures less than 11 °C (*Table 3-2*).

Table 3-3. Percent of area above treeline where modelled July MMAT exceeds 10°C at half degree intervals.

Temperature (°C)	Percent Area
10 - 10.49	47.8
10.5 - 10.99	29.9
11 - 11.49	15.2
11.5 - 11.99	6.0
>12	1.1

Assuming the treeline is mainly dependent on the July MMAT, the warmer temperatures for grid cells above the modelled treeline could be due to inaccuracies in (1) the MMAT modelling, (2) the treeline source data (developed from topographic maps and Google Earth images), (3) the trend surface fitted to treeline (a fourth order polynomial), or (4) to ecological change lagging behind climate change. In terms of the last point, the treeline maximum is the maximum limit for tree growth, meaning new growth takes time to catch up with the changing climate (Danby & Hik, 2007). Danby & Hik (2007) found that the strongest correlations were found using a 30-50 year forward average of tree growth. The relatively narrow band of temperatures that exceeded 10°C (mostly less than 1°C) but did not exhibit trees tends to support the idea that climate warming may be occurring faster than the ecological change that is needed to advance treelines to these higher elevations.

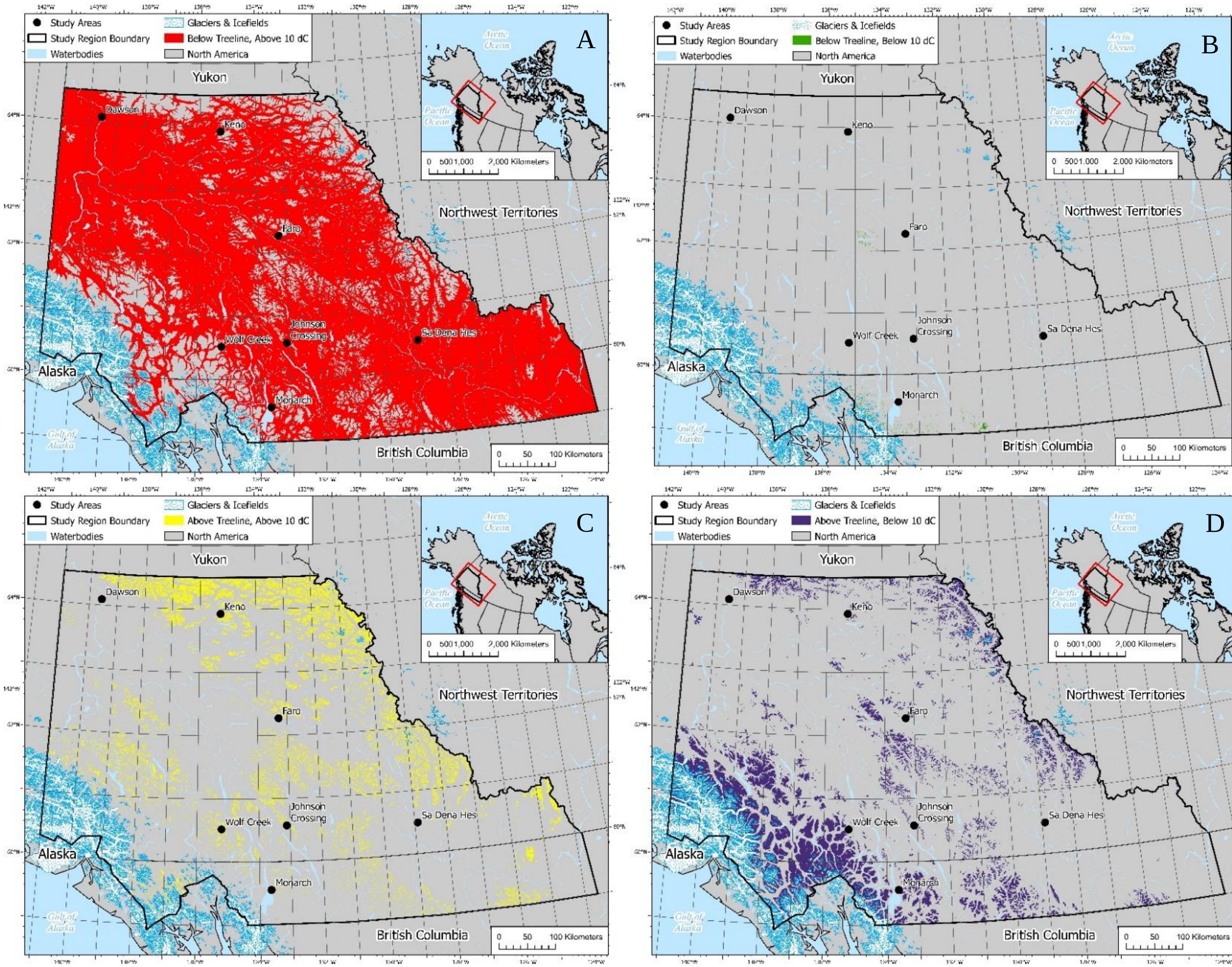

Figure 3-29. July MMAT values above and below treeline and the 10 °C threshold across study region in northern British Columbia and Southern Yukon, from 59 – 64.5° N. A – Below treeline and >10 °C, B – Below treeline and <10 °C, C – Above treeline and >10 °C, D – Above treeline and <10 °C. The seven study areas used in building the model are shown.

3.6 Conclusions

The updated MMAT temperature maps for the study region show similar spatial patterns to the MMAT maps created by Wahl *et al*. (1987) but more detail is provided using a raster model of MMAT rather than isolines. MMAT temperatures appear to have warmed slightly since the previous maps were created, but it is difficult to distinguish how much change has occurred due to the different methods used to create them. Validation data showed that the model performed best below treeline, indicating the lapse rates above treeline need further investigation to improve predictions for the highest elevations in the study region.

A July mean temperature of 10 °C approximated the altitudinal limit of trees in the region as expressed by a polynomial surface. However, while areas below treeline and <10 °C were virtually nonexistent, grid cells above treeline but with July temperatures >10 °C (predominantly between 10-11 °C) occupied 8 % of the region. One possibility for this imperfect accordance is that air temperatures have risen faster in recent decades than concomitant change in treeline elevation. This was also noted in treeline latitude and altitude changes as a function of increased temperatures studied in the St. Elias Mountain ranges (Danby & Hik, 2007).

The pattern of mean annual air temperatures is similar to those in previous studies (Wahl *et al.*, 1987; Lewkowicz *et al.*, 2012), but the current model shows more detail than previous models and is based on data collected over a longer period than the study by Lewkowicz *et al.* (2012).

3.7 References

Bonnaventure, P., & Lewkowicz, A. (2012). Permafrost probability modeling above and below treeline, Yukon, Canada. *Cold Regions Science and Technology, 79-80,* 92-106. DOI: 10.1016/j.coldregions.2012.03.004

Bush, E. & Lemmen, D.S., editors. (2019). Canada's Changing Climate Report; Government of Canada, Ottawa, ON. 444 p.

Chaput, M., & Gawjewski, K. (2014). Analysis of Daily Air Temperatures across a Topographically Complex Alpine Region of Southwestern Yukon, Canada. *Arctic*, *67*(4), 537–553. https://doi.org/10.14430/arctic4427

Daubenmire, R. (1954). ALPINE TIMBERLINES IN THE AMERICAS AND THEIR INTERPRETATION. *Butler University Botanical Studies*, *11*(8/17), 119–136.

Danby, R.K., & Hik, D.S. (2007). Variability, Contingency and Rapid Change in Recent Subarctic Alpine Tree Line Dynamics. *The Journal of Ecology*, *95*(2), 352–363. https://doi.org/10.1111/j.1365-2745.2006.01200.x

Esri Data and Maps. (2021). USA States (Generalized). Retrieved from: https://hub.arcgis.com/datasets/esri::usa-states-generalized/about

Government of Canada. (2016). Provinces/Territories, Cartographic Boundary File – 2016 Census. Retrieved from: https://open.canada.ca/data/en/dataset/a883eb14-0c0e-45c4-b8c4-b54c4a819edb

Government of Canada. (2017). Climate data: homogenized surface air temperature data access. Retrieved from https://www.canada.ca/en/environment-climate-change/services/climate-change/science-research-data/climate-trends-variability/adjusted-homogenized-canadian-data/surface-air-temperature-access.html

Government of Canada. (2018). Meteorological Station Catalogue. Retrieved from: https://open.canada.ca/data/en/dataset/9764d6c6-3044-450c-ac5a-383cedbfef17

Government of Canada. (2019a). Canadian Digital Elevation Model, 1945 – 2011. Retrieved from: https://open.canada.ca/data/en/dataset/7f245e4d-76c2-4caa-951a-45d1d2051333#wb-auto-6

Government of Canada. (2019b). Daily Data Report for June 2004. Retrieved from: https://climate.weather.gc.ca/climate_data/daily_data_e.html?hlyRange=%7C&dlyRange=1983-09-01%7C2017-05-30&mlyRange=1983-01-01%7C2007-02-01&StationID=1573&Prov=YT&urlExtension=_e.html&searchType=stnProv&optLimit=specDate&StartYear=1840&EndYear=2020&selRowPerPage=25&Line=24&Month=6&Day=25&lstProvince=YT&timeframe=2&Year=2004

Government of Canada. (2019c). Station Results – 1981 – 2010 Climate Normals and Averages. Retrieved from https://climate.weather.gc.ca/climate_normals/station_select_1981_2010_e.html?searchType=stnProv&lstProvince=YT

Government of Canada. (2021a). Indexes of the National Topographic System of Canada. Retrieved from https://open.canada.ca/data/en/dataset/055919c2-101e-4329-bfd7-1d0c333c0e62

Government of Canada. (2019b). Daily Data Report for June 2004. Retrieved from: https://climate.weather.gc.ca/climate_data/daily_data_e.html?hlyRange=%7C&dlyRange=1983-09-01%7C2017-05-30&mlyRange=1983-01-01%7C2007-02-01&StationID=1573&Prov=YT&urlExtension=_e.html&searchType=stnProv&optLimit=specDate&StartYear=1840&EndYear=2020&selRowPerPage=25&Line=24&Month=6&Day=25&lstProvince=YT&timeframe=2&Year=2004

Government of Canada. (2021c). The UTM Grid - Universal Transverse Mercator Projection. Retrieved from https://www.nrcan.gc.ca/earth-sciences/geography/topographic-information/maps/utm-grid-map-projections/utm-grid-universal-transverse-mercator-projection/9779

Government of Canada, (2022a). Lakes, Rivers and Glaciers in Canada - CanVec Series - Hydrographic Features. https://open.canada.ca/data/en/dataset/9d96e8c9-22fe-4ad2-b5e8-94a6991b744b

Government of Canada. (2022b). Historical Data. Retrieved from https://climate.weather.gc.ca/historical_data/search_historic_data_e.html?hlyRange=%7C&dlyRange=1983-09-01%7C2017-05-30&mlyRange=1983-01-01%7C2007-02-01&urlExtension=_e.html&searchType=stnProv&optLimit=specDate&StartYear=1840&EndYear=2020&selRowPerPage=25&Line=24&Month=6&Day=25&lstProvince=YT&timeframe=2&Year=2004

Government of Yukon. (2009). Yukon Government Climate Change Action Plan. Retrieved from: https://yukon.ca/sites/yukon.ca/files/env/env-yukon-government-climate-change-action-plan.pdf

Government of Yukon. (2018). Climate Change Action Plan Update. Retrieved from: https://yukon.ca/sites/yukon.ca/files/env/env-climate-change-action-plan-update.pdf

International Panel on Climate Change (IPCC). (2019). IPCC Special Report on the Ocean and Cryosphere in a Changing Climate [H.-O. Pörtner, D.C. Roberts, V. Masson-Delmotte, P. Zhai, M. Tignor, E. Poloczanska, K. Mintenbeck, A. Alegría, M. Nicolai, A. Okem, J. Petzold, B. Rama, N.M. Weyer (eds.)]. In press.

Kattel, D., Yao, T., Yang, K., Tian, L., Yang, G., Joswiak, D. (2012). Temperature lapse rate in complex mountain terrain on the southern slope of the central Himalayas. *Theoretical and Applied Climatology, 113,* 671-682. DOI: 10.1007/s00704-012-0816-6

Larsen, P., Goldsmith, S., Smith, O., Wilson, M., Strzepek, K., Chinowsky, P., Saylor, B. (2008). Estimating future costs for Alaska public infrastructure at risk from climate change. *Global Environmental Change, 10, 442 – 457.* DOI: 10.1016/j.gloenvcha.2008.03.005

Lewkowicz, A.G., & Bonnaventure, P. P. (2011). Equivalent Elevation: A New Method to Incorporate Variable Surface Lapse Rates into Mountain Permafrost Modelling. *Permafrost and Periglacial Processes*, *22*(2), 153–162. https://doi.org/10.1002/ppp.720

Lewkowicz, A.G., & Bonnaventure, P.P., Smith, S.L., Kuntz, Z. (2012). Spatial and thermal characteristics of mountain permafrost, northwest Canada. *Geografiska Annaler: Series A, Physical Geography, 94(2),* 195–213. DOI: 10.1111/j.1468-0459.2012.00462.x

Lewkowicz, A.G., & Way, R.G. (2019). Extremes of summer climate trigger thousands of thermokarst landslides in a High Arctic environment *Nature Communications*, *10*(1), 1329–11. https://doi.org/10.1038/s41467-019-09314-7

Melvin, A., Larsen, P., Boehlert, B., Neumann, J., Chinowsky, P., Espinet, X., Martinich, J., Baumann, M., Rennels, L., Bothner, A., Nicolsky, D., Machenko, S. (2016). Climate change damages to Alaska public infrastructure and the economics of proactive adaptation. *Proceedings of the National Academy of Sciences of the United States of America, 114(2), 122.*

National Centers for Environmental Information (NCEI). (n.d.). Data tools: 1981-2010 normals. Retrieved April 6, 2022, from https://www.ncdc.noaa.gov/cdo-web/datatools/normals

Rolland, C. (2003). Spatial and Seasonal Variations of Air Temperature Lapse Rates in Alpine Regions. *Journal of Climate, 16,* 1032-1046. DOI: https://doi.org/10.1175/1520-0442(2003)016<1032:SASVOA>2.0.CO;2

Wahl, H.E., Fraser, D.B., Harvey, R.C. (1987). *Climate of Yukon*. Canadian Government Publishing Center.

CHAPTER 4: FREEZING DEGREE DAY AND THAWING DEGREE DAY MODELLING IN SOUTHERN YUKON AND NORTHERN BRITISH COLUMBIA USING LAPSE RATES AND DEGREE OF CONTINENTALITY

4.1 Abstract

Annual indices of air freezing degree days (FDD) and air thawing degree days (TDD) are a crucial first step in ground temperature modelling using the temperature at the top of permafrost model. FDD and TDD were calculated from air temperature measurements at 83 monitoring sites within seven study areas in southern Yukon and northern British Columbia operating for up to 14 years between 2006 – 2019. Relationships between degree of continentality of the study area and the elevational gradient of the temperature index were used in spatial modelling of FDD and TDD. FDD values were found to be highly influenced by both degree of continentality as well as latitude, whereas TDD values were mainly dependent on elevation, with degree of continentality and latitude playing lesser roles. The study region showed an overall negative MAAT based on the modelled FDD and TDD values, confirming the results of MAAT values derived from mean monthly air temperature (MMAT) models. Differences between the two models are attributed to incomplete datasets, skewing the MMAT and F/TDD values. The models closely correspond to recent historical values of FDD and TDD at specific locations (Climate Atlas of Canada, 2019) and provide components of temperature at top of permafrost (TTOP) modelling for future studies.

4.2 Introduction

Permafrost distribution in the Yukon is complex due to the broad trends in climate superimposed on varied topography (Bonnaventure *et al.,* 2012). Empirical-statistical modelling has shown that climate change will reduce the area underlain by permafrost over the long-term (Bonnaventure and Lewkowicz, 2013). The change in permafrost temperature and the resulting thaw will be expensive to adapt to (Larsen *et al.*, 2008), underlining the need for better understanding of permafrost distribution.

Air temperatures can be used to develop freezing and thawing degree day indices (FDD and TDD, respectively) through the summation of temperatures above or below 0 °C over the course of a year. These indices are basic data for numerical permafrost modeling using the temperature at the top of permafrost (TTOP) method (Smith & Riseborough, 2002). Although the TTOP model is an equilibrium model, its use would be preferable to empirical-statistical solutions such as Bonnaventure *et al.* (2012). This method of permafrost distribution modelling has been implemented for small parts of the study region (Bevington & Lewkowicz, 2015) but has not been applied to the area as a whole. TTOP modelling using FDD and TDD has also been used in other areas at large and small scales including Labrador (Way & Lewkowicz, 2016), the northern hemisphere (Obu *et al.,* 2019), Livingston Island and Antarctica (Ferreira *et al.*, 2016; Obu *et al.*, 2020). While there is a current model of permafrost using the TTOP method that encompasses the entire study area, the grid cells are 1 km^2 in area, which does not allow for a detailed understanding of permafrost distribution, and input data are not based on field measurements (Obu *et al.*, 2019). The goal of this research is to generate updated and larger-scale FDD and TDD maps, which would permit the future development of a TTOP based model of permafrost in the region.

4.3 Methods

Methods have been divided into five sections to explain the sources of data as well as the steps followed during data processing. These sections include workflow overview, Digital Elevation Model and treeline modelling, data processing, and spatial modelling of FDD and TDD, and FDD and TDD model validation. The workflow chart (*Figure 4-1*) gives a general overview of steps taken in the methods and is explained in more detail below.

4.3.1 Methods overview

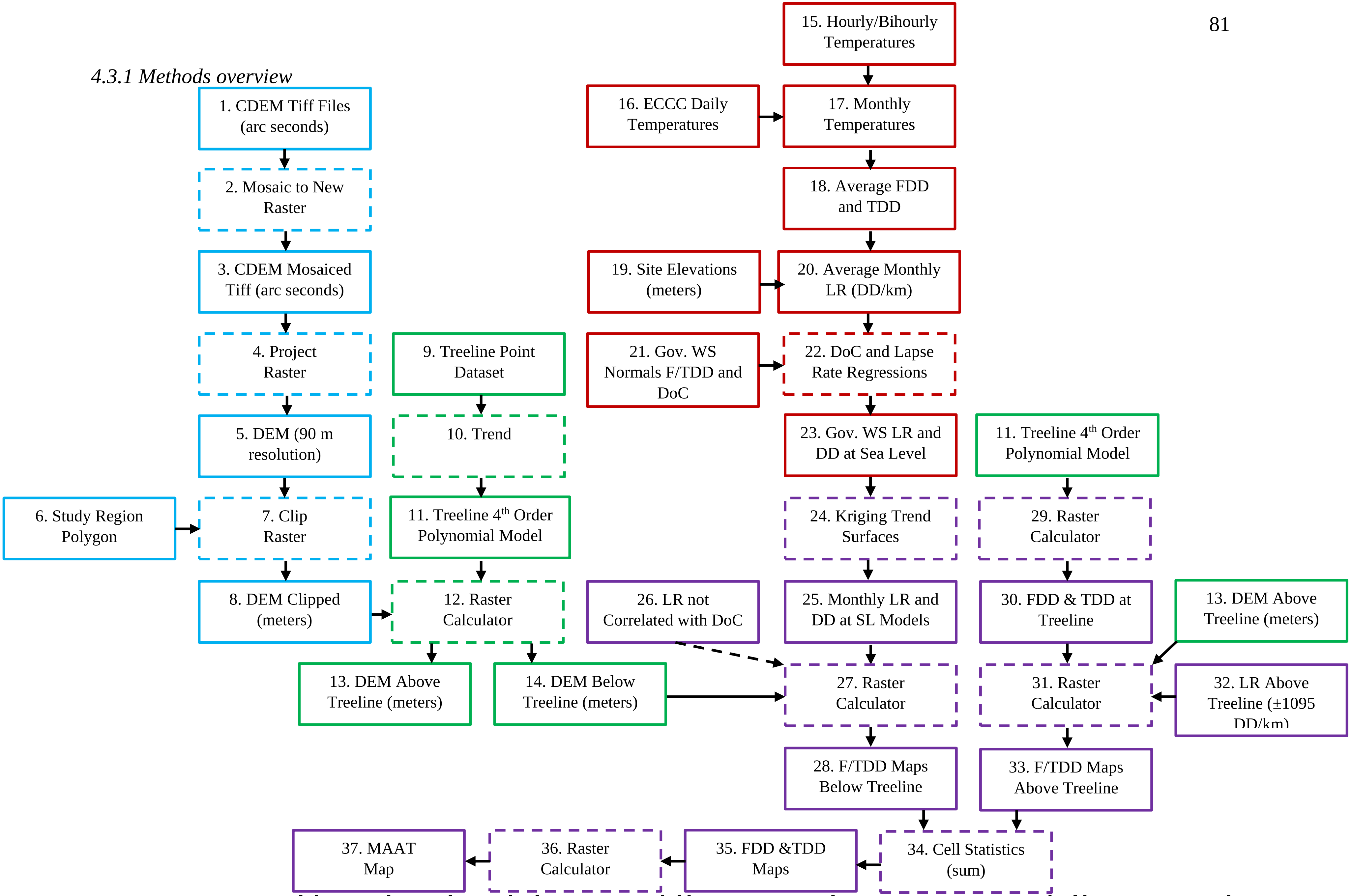

Figure 4-1. Freezing and thawing degree day methods overview. Solid boxes correspond to inputs or outputs. Dashed boxes correspond to ArcGIS Pro tools or Excel calculations. Blue boxes outline the steps of the DEM preparation, green outlines the steps to create a treeline model, red outlines the data processing, and purple outlines the FDD and TDD modelling process.

4.3.2 Digital Elevation and treeline models

Digital elevation and treeline models were prepared following the same methods used in Chapter 3 to create mean monthly air temperature maps. The overview steps for these methods are shown in the workflow chart (*Figure 4-1,* 1-14).

4.3.3 Data processing

Daily mean temperatures were calculated as described in Chapter 3 (*Figure 4-1,* 15-17). Any months missing 7 or fewer days of data were infilled with the mean monthly air temperature value for the missing dates. This allowed the month to be used as part of the complete freezing or thawing season dataset needed for calculating freezing and thawing degree days. Freezing degree days were calculated as the absolute sum of all temperatures below 0 ºC (*Figure 4-1,* 18). The sum of freezing degree days spanned winters rather than calendar years. Therefore, the sum of negative temperatures was calculated from August 1st to July 31st each year. Thawing degree days were calculated as the sum of all temperatures greater than 0 ºC within a calendar year. A breakdown of the amount of data missing from excluded months can be found in Appendix A.

If a month was missing more than 7 days of data, the freezing or thawing degree days calculation was omitted from the averaged FDD and TDD calculations. However, if the month had only positive or only negative temperatures, only the affected FDD or TDD value was removed from average calculations. For example, if January at a particular site was missing 8 or more days of data one year, the FDD value for that year would be excluded from the average FDD for that site. The TDD value would be included since the missing January temperatures could be assumed to leave TDD unaffected. Average FDD and TDD for 20 individual stations not in clusters were also calculated to be used later to test the accuracy of the FDD and TDD spatial models (*Figure 4-2*).

The average FDD and TDD values for the nearest homogenized ECCC station were used to constrain the model at lower elevations where most ECCC stations are located.

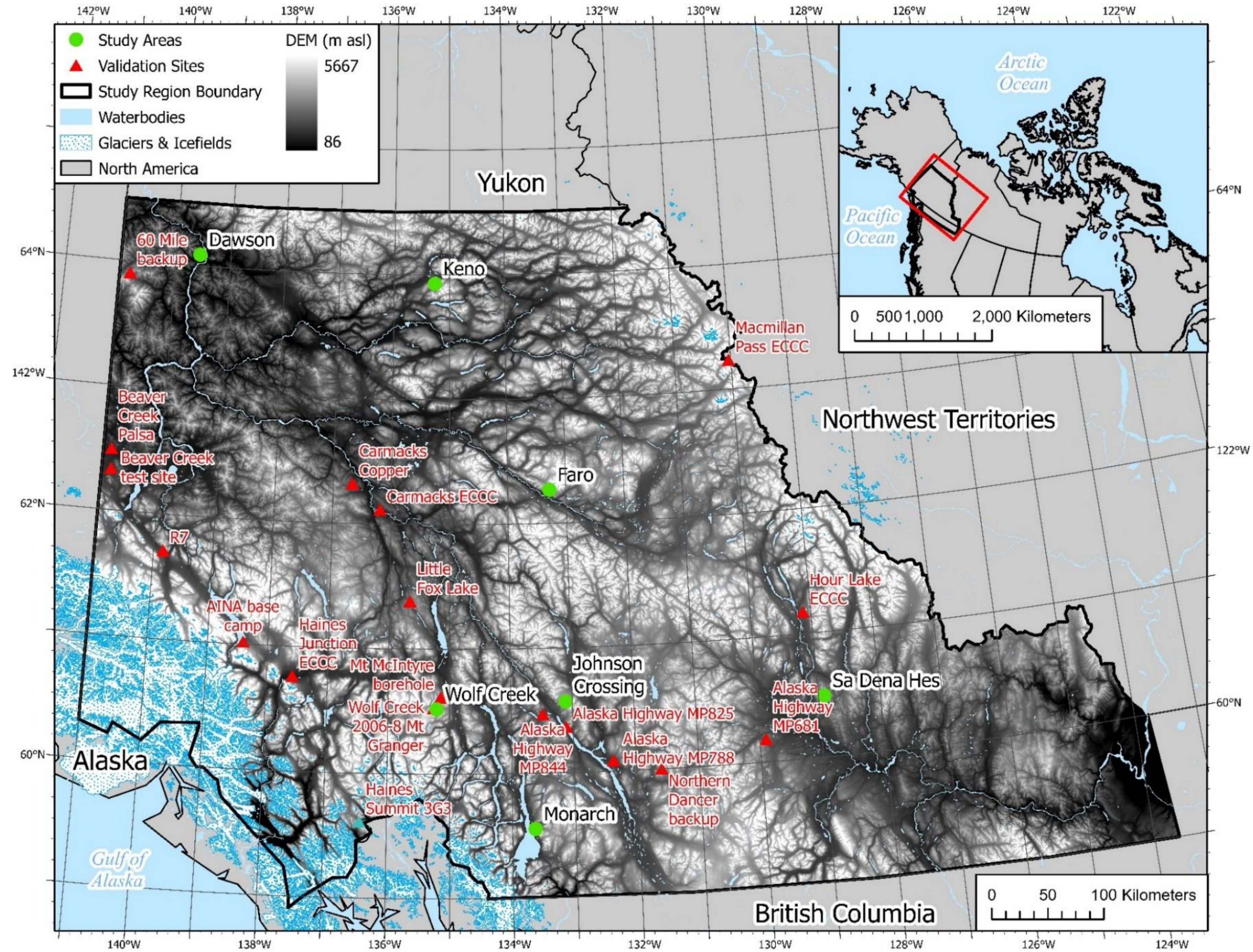

Figure 4-2. Study regions and validation sites in study area of southern Yukon and northern British Columbia, Canada. Study region locations are based on geographic centers of the individual sites within a study region (Government of Canada, 2016; ESRI Data and Maps, 2021; Government of Canada, 2018; ArcGIS Pro, 2020).

Data from all sites below treeline within an area were used to create a linear model of the FDD and TDD against elevation for each complete year, resulting in multiple linear models of the FDD and TDD lapse rates (*Figure 4-1*, 18-20). This was done by regressing the FDD and TDD for a given year across all sites within an area against the elevation of each site. The regressions were run in Excel using the Data Analysis tool for each year's data in each of the seven study areas to determine the statistical significance of the relationship using a p-value of 0.1 as the threshold of significance. Averages of the slopes and y-intercepts of the statistically significant linear models were then used to estimate the FDD and TDD lapse rates for that area.

Annual and many monthly lapse rates are correlated with degree of continentality (Lewkowicz & Bonnaventure, 2011; Chapter 3). Degree of continentality is calculated by finding the difference in mean temperature for the warmest and coldest months of the year. This relationship was assessed for FDD and TDD by testing linear regressions with the degree of continentality of each of the seven study areas as the independent variable (*Figure 4-1*, 21-23). Regressions were tested at the 0.1 significance level.

Degree of continentality and FDD lapse rates show a negative correlation (*Figure 4-3A*). As DOC increases, the lapse rate decreases from zero to more negative values. Therefore, the more continental an area, the stronger the lapse rate for FDD. Areas with higher DOC show greater decreases in FDD as elevation increases.

Degree of continentality and TDD lapse rates show a positive correlation (*Figure 4-3B*). As DOC increases, the TDD lapse rate increases towards zero. The higher the DOC, the lower the TDD lapse rate. Therefore, the more continental an area, the weaker the lapse rate for TDD. Areas with higher DOC will show slower increases in TDD as elevation increases.

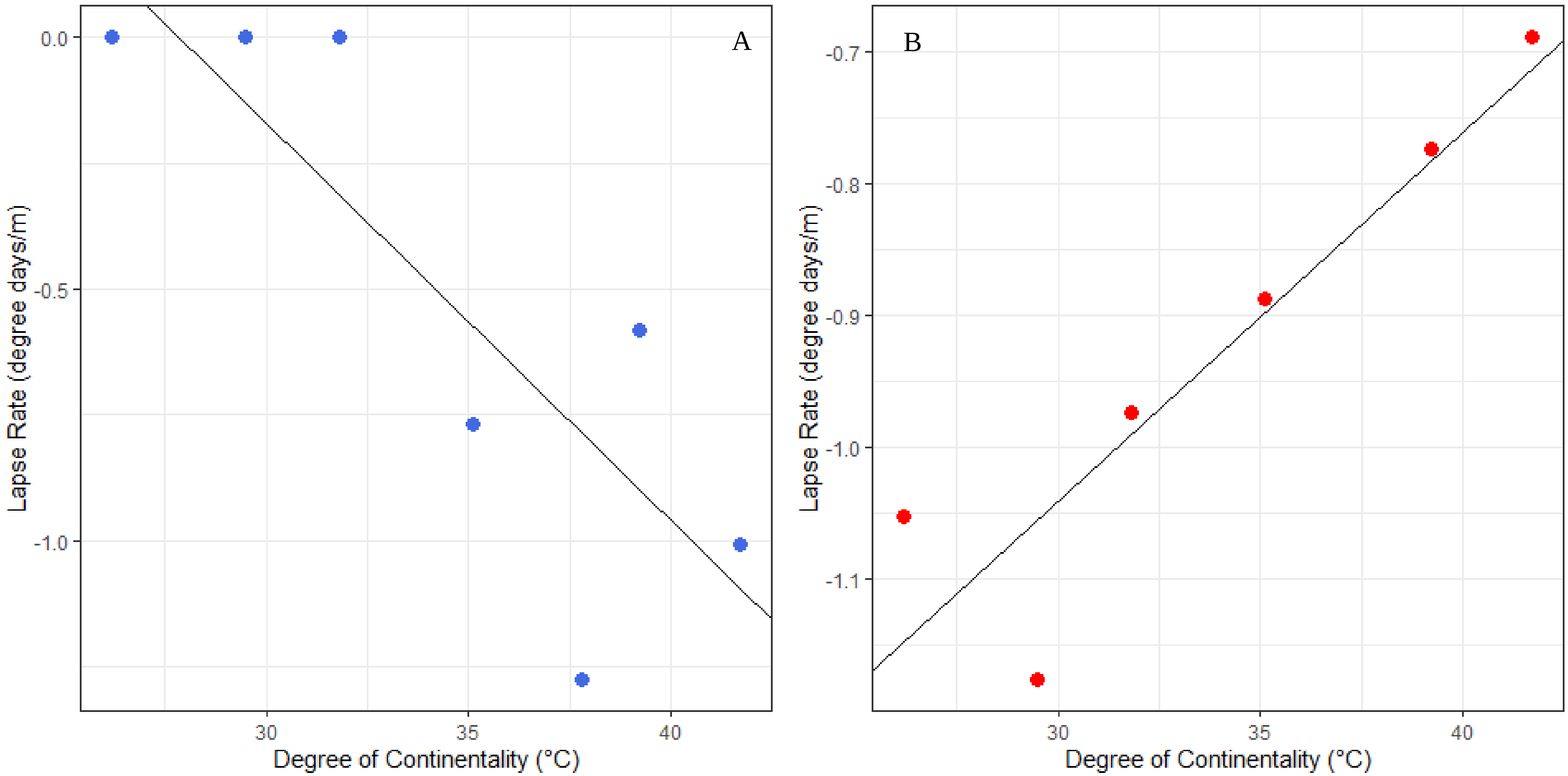

Figure 4-3. Measured FDD (A) and TDD (B) lapse rates below treeline and degree of continentality at seven study areas. The linear regression line for the two variables is shown. Regressions are significant at p = 0.1. FDD and DOC regression slope = -0.079. TDD and DOC regression slope = 0.028. Three areas (Johnson's Crossing, Wolf Creek, Monarch) were found to have no significant FDD lapse rate below treeline, these sites were given a lapse rate of 0 degree days/m. Sa Dena Hes was excluded from the calculation of TDD lapse rate due to a lack of data.

If the elevation range of the active stations was less than 400 m, that year was excluded. This was done to ensure that temperature index change along the elevation gradient could be attributed to more than instrumental inaccuracies. This criterion was chosen to maximize the number of years of record while limiting the impact of logger measurement error and the influence of local topography and microclimates on lapse rates.

Data from 23 government climate stations from ECCC with 30-year climate normals (1981-2010) were used to increase the number of station locations across the study region available to create predictive trend surfaces of FDD and TDD. The 30-year normal FDD and TDD values for each year were retrieved and imported into Excel.

Predicted FDD and TDD lapse rates below treeline for each of the government climate stations were calculated using the linear regression between lapse rate and degree of continentality (*Figure 4-1*, 23). An example of this using the Beaver Creek ECCC station FDD is shown below.

$$Degree\ of\ Continentality\ Regression\ Slope\ =\ -0.079\frac{\frac{degree\ days}{m}}{degree\ days} =\ -0.079\ \mathrm{m}^{-1}$$

$$Degree\ of\ Continentality\ Regression\ Intercept =\ 2.21\ degree\ days/m$$

$$Degree\ of\ Continentality\ of\ Beaver\ Creek =\ 39.3\ degree\ days$$

$$Predicted\ FDD\ LR = (DoC\ Regression\ Slope) * (DoC) + DoC\ Regression\ Intercept$$

$$Predicted\ FDD\ LR = (-0.079\ m^{-1}) * (39.3\ degree\ days/m) + 2.21\ degree\ days$$

$$Predicted\ FDD\ LR = -0.89\ degree\ days/m$$

FDD and TDD at 0 m asl were calculated using the predicted lapse rates at each of the government weather stations as well as the 30-year normal values and elevation. This provided the sea level values for the spatial model of FDD and TDD that could be built up to treeline with the lapse rate and Digital Elevation Model. An example of this calculation using the Beaver Creek ECCC station FDD is shown below. The 30-year normal FDD for the Beaver Creek ECCC station is known as well as the elevation of the station. Using these values and the predicted FDD lapse rate, the linear equation can be rearranged to calculate the temperature at sea level, by solving for the Y intercept.

$FDD = 3321.8\ degree\ days$

$FDD\ Lapse\ Rate = -0.89\ degree\ days/m$

$Elevation = 649\ m$

$FDD = (FDD\ Lapse\ Rate) * (Elevation) + FDD\ at\ Sea\ Level$

$FDD\ at\ Sea\ Level = (-FDD\ Lapse\ Rate) * (Elevation) + FDD$

$FDD\ at\ Sea\ Level = (0.89\ degree\ days/m) * (649\ m) + 3321.8\ degree\ days$

$FDD\ at\ Sea\ Level = 3902.5\ degree\ days$

4.3.4 Spatial modelling of FDD and TDD

No 30-year FDD and TDD normals were available for Alaskan government weather station sites, so the overall modelling of FDD and TDD was based on 23 Canadian sites (*Figure 4-4*) (*Appendix C, Table C-1*). Spatial modelling of FDD and TDD was completed using the methodology described in Chapter 3.3.5 (*Figure 4-1*, 24-27), with the modelled FDD and TDD lapse rates used below treeline and a constant lapse rate value of -6 ºC/km above treeline. Any modelled TDD values below zero were added to the modelled FDD values to maintain a consistent annual air temperature lapse rate. A MAAT map was created from these values by finding the difference between FDD and TDD totals and dividing by 365.

To determine how lapse rates above treeline would affect FDD and TDD, two pairs of sites were used to compare the change in FDD and TDD from a site at high elevation close to treeline and a site above treeline (*Table 4-1*). The differences between FDD and TDD at the near treeline and above treeline sites were not consistent between the pairs. It was decided that an even split between FDD and TDD would be used. Using a lapse rate of -6 ºC/km, a total of 2190 degree days were possible in a year. Split evenly, this would mean a reduction of 1095 thawing degree days/km and an increase of 1095 freezing degree days/km (*Figure 4-1*, 29-32).

FDD and TDD above (*Figure 4-1*, 29) and below (*Figure 4-1*, 28) treeline were combined to create a continuous model of FDD and TDD (*Figure 4-1*, 30-31). These maps were then used to calculate MAAT by finding the difference between FDD and TDD values and dividing by 365 (*Figure 4-1*, 36-37).

Table 4-1. FDD, TDD, and difference values for two pairs of sites spanning treeline.

Degree Days	Dawson 8	60 Mile Backup	Difference	Mount McIntyre	Mount Granger	Difference
FDD	2443	2751	-308	2096	2765	-669
TDD	1368	976	392	882	450	432

4.3.5 FDD and TDD model validation

FDD, TDD and MAAT values were validated using the same validation sites (*Figure 4-4 and Appendix E, Table E-1*) and methodology described in Chapter 3.3.6.

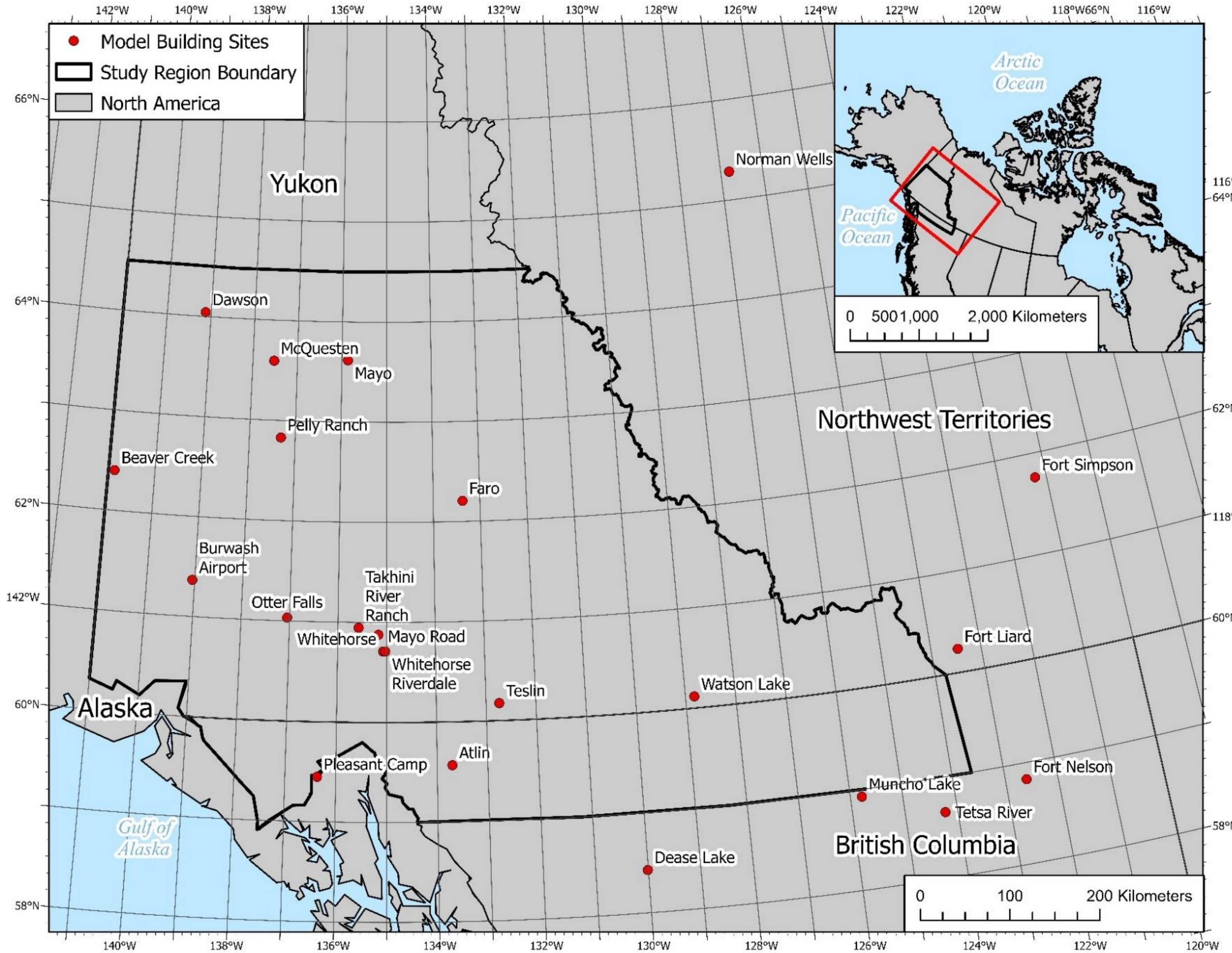

Figure 4-4. Government weather stations (Appendix C, Table C-1) within the study region as well as surrounding areas used to build the models of freezing and thawing degree days based on calculated FDD and TDD lapse rates and values at sea level and treeline. (Government of Canada, 2016; Government of Canada, 2019; ESRI Data and Maps, 2021).

4.4 Results

4.4.1 Freezing and Thawing Degree Day maps

The freezing and thawing degree day maps show very different ranges in values. The overall range for FDD is 11,185 degree days spanning from a low of 330 to a high of 11,515 (*Figure 4-4*). Thawing degree days showed a much smaller range with a low of 0 and a high of 2500 (*Figure 4-5*). FDD that exceed TDD indicate negative MAAT which is the case for the majority of the study region. Very high FDD values (and correspondingly zero TDD) are due to the extremely cold conditions predicted for high elevations.

The FDD values are modelled to be greatest in the terrain immediately surrounding the icefields and glaciers in the southwest Yukon. However, a latitudinal gradient combined with a trend due to the degree of continentality is also evident in the spatial pattern (*Figure 4-4*). These trends result in FDD values exceeding 3500 degree days in the low-elevation valleys adjacent to the Alaska border.

As expected, TDD values are greatest in valley bottoms and in the southeast part of the study region where summer temperatures are highest (*Figure 4-5*). Valley-bottom inversions mainly occur in the winter months when temperatures for the entire study region are below freezing so they do not affect TDD values. Although latitude and degree of continentality have an effect on TDD values, elevation is the greatest influence on the spatial pattern (*Figure 4-5*).

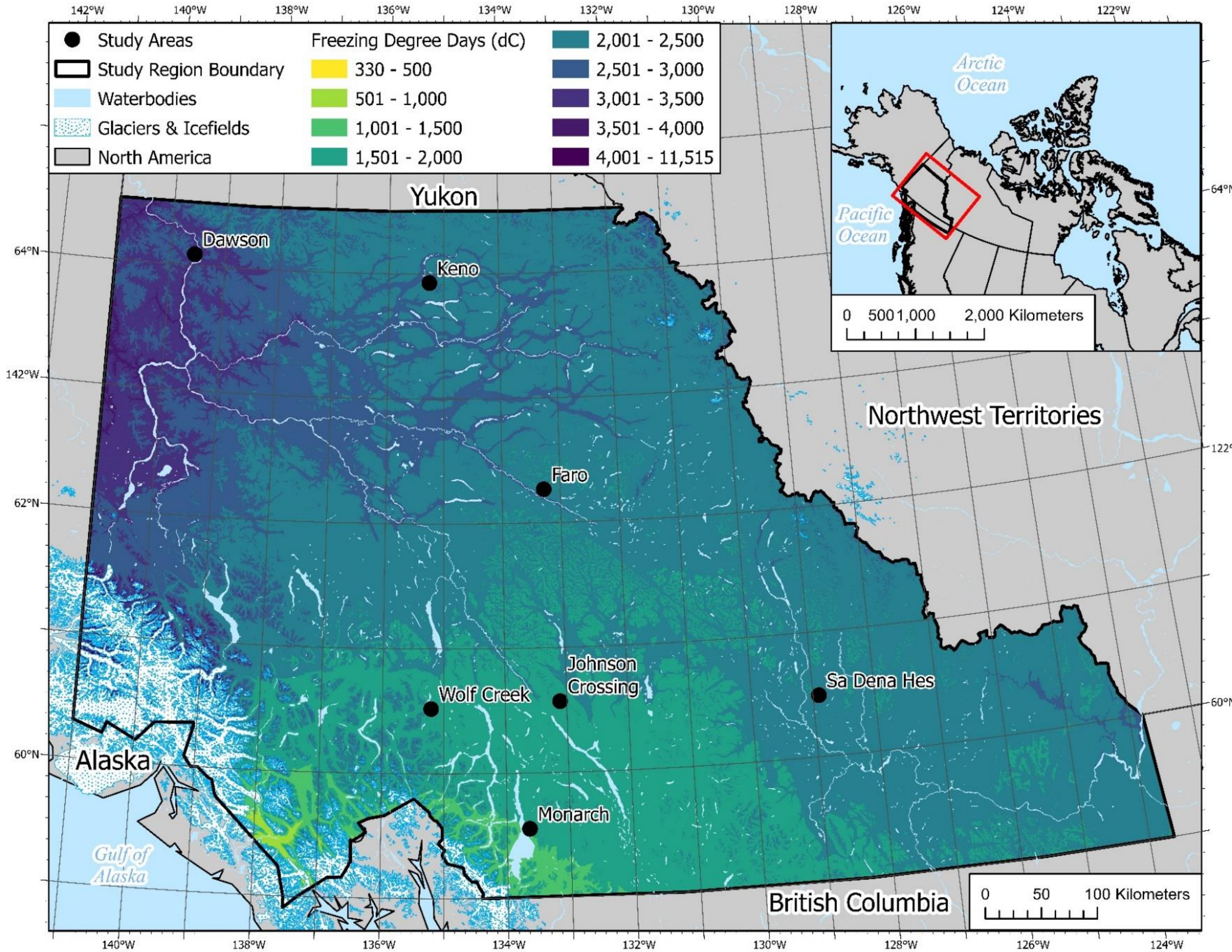

Figure 4-5. Predicted freezing degree days (FDD) across study region in northern British Columbia and Southern Yukon, from 59 – 64.5º N. The seven study areas used in building the model are shown. Whitehorse (not shown) is located approximately 10 km northeast of Wolf Creek. Average FDD across the study region was calculated to be 2272 degree days.

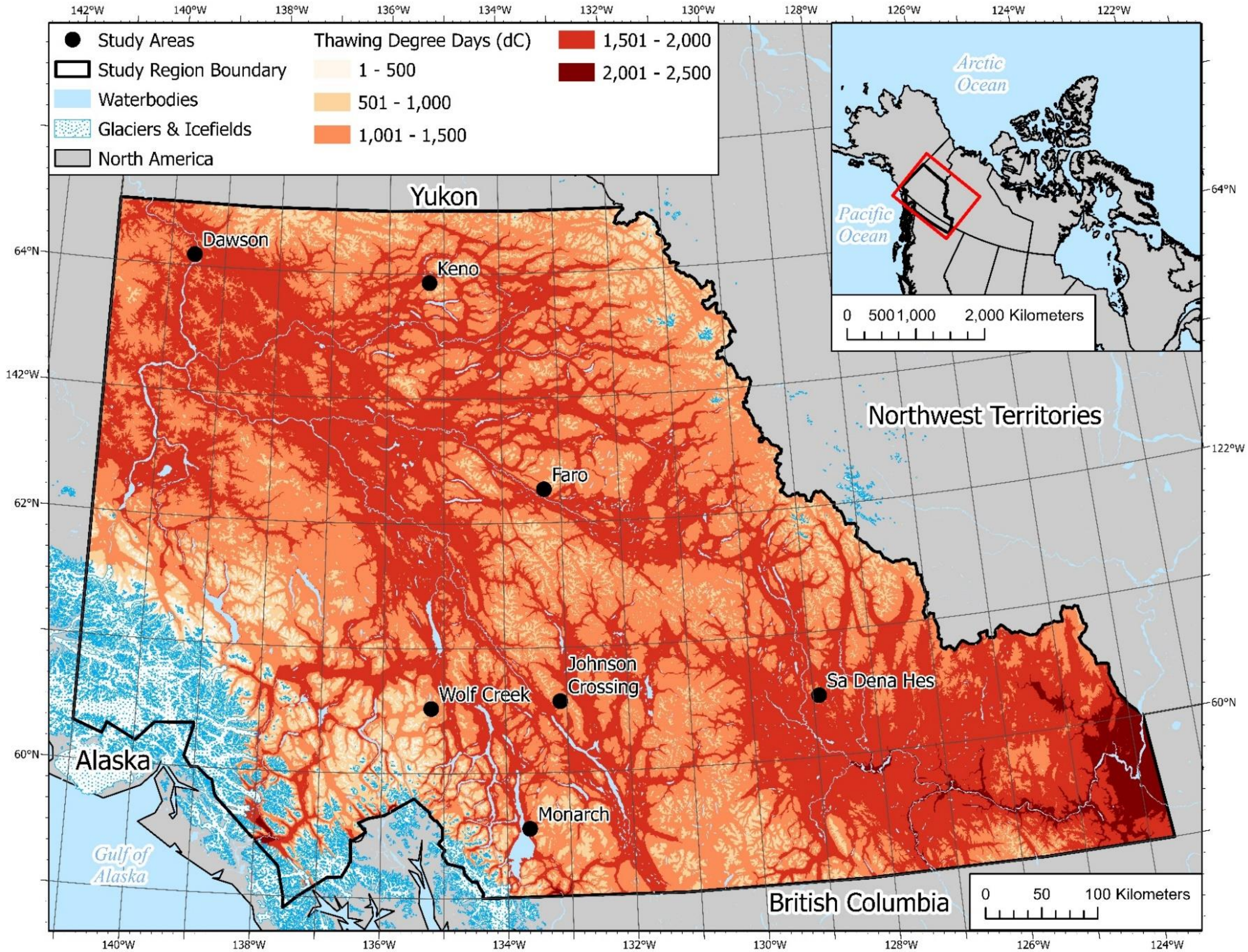

Figure 4-6. Predicted thawing degree days (TDD) across study region in northern British Columbia and Southern Yukon, from 59 – 64.5° N. The seven study areas used in building the model are shown. Whitehorse (not shown) is located approximately 10 km northeast of Wolf Creek. Average TDD across the study region was calculated to be 1399 degree days.

4.4.2 Evaluation of FDD and TDD models

FDD and TDD were validated using 20 sites, including both ECCC and University of Ottawa sites. These sites had a minimum record of three years of data. The measured and modelled FDD and TDD values are shown in *Figure 4-6* with a 1:1 line to make visual comparison easier.

Modelled FDD values showed more deviation from measured indices than TDD values (*Figure 4-6*). Three points were notably further from the 1:1 line for FDD: one high above the 1:1 line and two close together below the 1:1 line. The outlier above the 1:1 line is Alpine Burwash Backup (1809 m, asl), a validation site located above treeline that had a difference of -947 degree days between modelled and measured values. The two outliers below the 1:1 line are Alaska Highway MP681 (848 m asl, below treeline) and Macmillan Pass ECCC (1379 m asl, below treeline) with respective differences of 759 and 830 degree days between measured and modelled values. The average absolute difference between measured and modelled FDD values is 254 degree days.

Modelled TDD values were much more similar to measured TDD values, falling more closely to the 1:1 line. The most noticeable outlier (388, 798), with a difference of 410 degree days is Alpine Burwash Backup site. This site also had a poorly modelled FDD value. The average absolute difference between measured and modelled TDD values is 200 degree days.

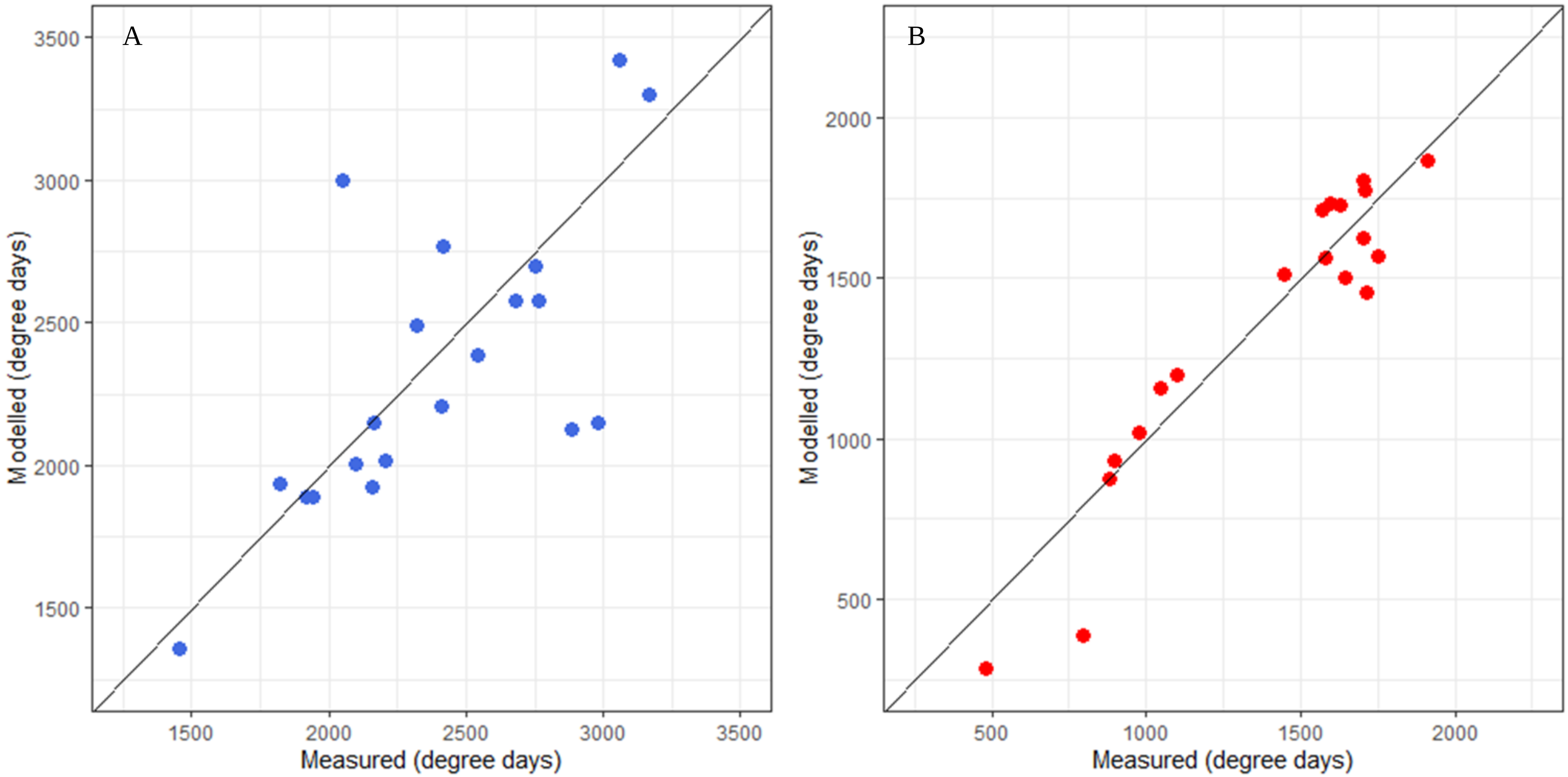

Figure 4-7. Measured and modelled (A) FDD and (B) TDD values at the 20 validation sites. A 1:1 reference line is shown as a comparison guide. One validation site below treeline, Alaska Highway MP681 (848 m asl), did not have a measured value for comparison and was therefore excluded.

Four sites below treeline and four sites above treeline are presented as sample comparisons (*Table 4-2*, *Table 4-3*). These eight sites include both strong and poor relationships between the predicted and modelled FDD and TDD values. Difference values were calculated by subtracting measured values from modelled values. Positive difference values indicate predicted values higher than measured and negative difference values indicate lower predicted than measured values.

Below treeline, all sites were predicted reasonably well. The measured FDD and TDD were neither consistently above nor below the modelled values and differences were small given the overall range in values. FDD values across the study region range from 330 – 11,515 degree days (*Figure 4-5)* whereas TDD values range from 1 – 2500 degree days (*Figure 4-6*).

Table 4-2. Modelled and measured FDD and TDD values for four sites below treeline. Difference values were calculated as measured minus modelled.

Validation Site	Modelled FDD	Measured FDD	Difference	%	Modelled TDD	Measured TDD	Difference	%
AINA Base Camp	2699	2408	-291	-0.1	1016	1449	433	0.3
Beaver Creek Palsa	3420	3057	-363	-0.1	1570	1749	179	0.1
Carmacks ECCC	2575	2679	104	0.0	1869	1914	45	0.0
Hour Lake ECCC	2384	2542	158	0.1	1734	1599	-135	-0.1

Above treeline, Alpine Burwash Backup and Macmillan Pass ECCC FDD and TDD were poorly predicted (*Table 4-3*). These two validation sites are located near the edge of the study area, suggesting that edge effects are present in the model. Alpine Burwash Backup, located in the southwest part of the study area, was predicted to be much colder than measured values, while the reverse is the case for Macmillan Pass ECCC in the northwest part of the study area. Northern Dancer Backup and Sixty Mile Backup have similar modelled and measured FDD and TDD values, indicating that the model predicted well in those areas (*Table 4-3*). These two sites are located below treeline although relatively close to the periphery of the study region.

Table 4-3. Modelled and measured FDD and TDD values for four sites above treeline. Difference values were calculated as modelled minus measured.

Validation Site	Modelled FDD	Measured FDD	Difference	%	Modelled TDD	Measured TDD	Difference	%
Alpine Burwash Backup	2997	2050	-947	-0.5	388	798	410	0.5
Macmillan Pass ECCC	2149	2978	829	0.3	1196	1098	-98	-0.1
Northern Dancer Backup	1889	1918	29	0.0	930	895	-35	0.0
Sixty Mile Backup	2699	2751	52	0.0	1016	976	-40	0.0

The root mean square error (RMSE) was calculated based on the difference between the modelled and measured FDD and TDD values (*Table 4-4*). RMSE is larger for FDD than TDD, in part because of generally greater FDD values. Regression slope coefficient values in *Table 4-4* show the linear relationship between measured (x) and modelled (y) values. The regression slope coefficients show a strong positive relationship between measured and modelled FDD, TDD, and MAAT values. This is especially true for MAAT and TDD. The coefficient for FDD indicates the measured values were on average higher than the modelled values for the validation sites. Conversely, the coefficient for TDD indicates the measured values were on average lower than the modelled values.

Table 4-4. RMSE and slope coefficient.

Month	RMSE	Regression Slope Coefficient
FDD	367.77	0.80
TDD	150.17	1.07
MAAT	1.25	1.00

In all aspects of the FDD and TDD model validation, FDD were not predicted as well as TDD. This was evident in the difference values of modelled and measured FDD and TDD both above and below treeline (*Table 4-2, 4-3*), as well as the RMSE and the regression slope coefficient (*Table 4-4*).

The remainder of the measured and modelled FDD and TDD at the 20 validation sites are presented in Appendix D.

4.4.3 Mean Annual Air Temperature

Mean annual air temperature calculated from the FDD and TDD models ranged between -34.4 ºC and 6 ºC (*Figure 4-8*). However, the lowest temperatures are predicted for the southwestern portion of the study region, an area that is largely unmodelled due to the presence of ice fields and glaciers. Most of the remainder of the study region has modelled mean annual air temperatures ranging from -6 ºC to 0 ºC. The average MAAT across the entire study region was -2.4 ºC. A south-north gradient in mean annual air temperature dominates the spatial pattern (*Figure 4-8*) with the influence from degree of continentality mainly in the west.

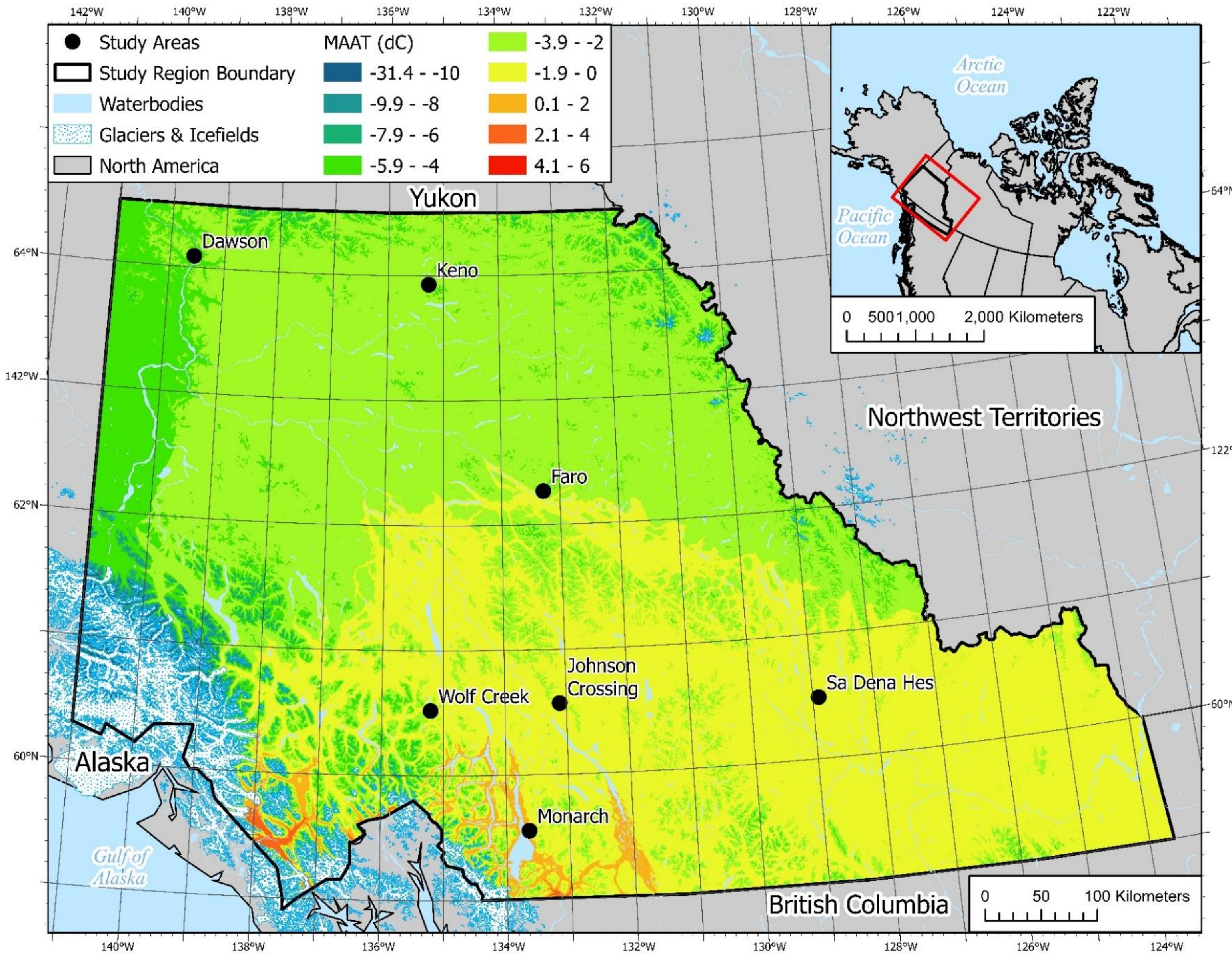

Figure 4-8. Predicted mean annual air temperature (MAAT) values across study region in northern British Columbia and Southern Yukon, from 59 – 64.5º N. Calculated from modelled FDD and TDD values. Whitehorse (not shown) is located approximately 10 km northeast of Wolf Creek. Average MAAT across the study region was calculated to be -2.4 ºC.

4.5 Discussion

4.5.1 Factors affecting model validity

Model validation showed the model for FDD did not perform as well as the model for TDD. However, the range of TDD was not as large as the range of FDD values, so the differences in validity could be related to the scale of the data. Edge effects were present in the model as seen by the difference between measured and modelled values at Alpine Burwash Backup as well as Macmillan Pass ECCC, most notably for freezing degree days. Alpine Burwash Backup is located near the ice fields in the southwest part of the study region and may be influenced by the temperature profiles above and around them. No lapse rate data were available from the glaciers and ice fields, increasing uncertainty in the predictions of FDD and TDD changes with elevation. Conversely, Macmillan Pass ECCC is located along the northeast border of the study region where there is also no direct coverage from the sites used to build the model. The distance from the model building sites could have negatively impacted the strength of the model in that area. The models of FDD and TDD performed better below treeline than above treeline, potentially as a result of the selection of lapse rates for FDD and TDD above treeline.

Edge effects for the model were potentially more problematic for the FDD and TDD models than they were for MMAT models in Chapter 3 because FDD and TDD values were not available for Alaska. The western border of the study region as well as the coastal south-east area were the most affected by this lack of FDD and TDD at government weather stations.

As discussed in Chapter 3, although measures were taken to avoid errors in the field data, it is possible not all issues were caught, resulting in some negative impacts on the model. However, the impact of one year of rime accumulation on a temperature shield, for example, would have had minimal impacts on the overall models of FDD, TDD, or validation data, given that a minimum of three years of data were required to ensure a particularly warm or colder year did not have a substantial impact on temperature values.

Factors such as elevation, latitude, and longitude of validation sites did not appear to have any relationship to the difference between measured and modelled temperatures. Overall, the differences were likely a result of model inputs being unequally distributed across the study region and surroundings as well as variable lengths of data collection periods for input and validation data. A more consistent record of data for both model building and validation would have been preferable but was prevented by a combination of site setup dates as well as temperature logger failures.

4.5.2 Comparison with other FDD and TDD maps

Current freezing and thawing degree day maps for the study region are not easily compared due to varying data collection periods. The Climate Atlas of Canada presents FDD for the country as an interactive map interface (Climate Atlas of Canada, 2019). However, the time periods for the model include the recent past (1976 – 2005), the immediate future (2021 – 2050), and the near future (2051 – 2080) and thawing degree days are not shown. The only potentially comparable set of values from this dataset is the recent past model, given that FDD values modelled were based on actual temperatures, not predicted future temperatures. The study region is also not the entirety of the Yukon and contains part of British Columbia, therefore the average FDD in the Yukon cannot be directly compared using the Climate Atlas of Canada. The much higher latitudes in the Yukon from the Climate Atlas of Canada would have a positive influence on the FDD value whereas lower latitude values in the study region would influence the FDD values negatively. The FDD values shown in the Climate Atlas of Canada also models the FDD values based on government weather stations. As previously mentioned, government weather stations in the Yukon territory are located at lower elevations which do not provide a complete representation of the topographic effects in the study region.

However, the recent past data shows an average of 3476 freezing degree days between 1976 and 2005 (Climate Atlas of Canada, 2019). The study area FDD modelled values had an average of 2272 freezing degree days based on data from 2006 – 2019 (*Figure 4-5*). The higher latitudes of Yukon Territory included in the Climate Atlas of Canada data (2019) combined with the exclusion of lower latitudes of the study region, would explain, at least in part, the discrepancies between the FDD values.

Fourteen sites within the study region had specific FDD data available through the Climate Atlas of Canada (2019) based on temperatures collected from 1976 – 2005. The Climate Atlas of Canada sites were government weather station locations and comparison data values were pulled from the modelled FDD map using the coordinates of the stations (*Figure 4-9*). On average, the FDD values from the Climate Atlas of Canada (2019) were 275 freezing degree days colder than the modelled values. The largest difference of +735 degree days was at Elsa, a site near Mayo

ECCC where the coordinates of the government weather station could not be determined, and an estimated location was used. The lack of specific coordinates could be the cause of such a large difference between Climate Atlas of Canada and modelled values. The smallest difference between Climate Atlas of Canada and modelled FDD values was at Beaver Creek. The difference between the two value was -25 degree days, the only site where the modelled FDD value was greater than the Climate Atlas of Canada value.

The higher FDD values from Climate Atlas of Canada can likely be explained by four factors: 1) data collection period length, 2) timeframe of data collection, 3) different methodology and 4) scale. Although the length of data collection likely has more influence on the FDD values, it is unlikely the entire difference between Climate Atlas of Canada and modelled values can be attributed to the length of data collection. The shorter time period (14 years) used in the modelled FDD values in comparison with the Climate Atlas of Canada values (30 years) could indicate that the natural presence of warmer and colder years was not represented as fully in the sorted data collection period of 14 years.

The time frame of data collection was also different between the Climate Atlas of Canada and modelled FDD values. Climate Atlas of Canada FDD values were based on data collected from 1976 – 2005, ending prior to the beginning of data collection for modelled FDD values. given regional warming, we would expect to see FDD values increase through time, but not at the rate that the differences show (*Figure 4-9*). Therefore, the time frame of data collection is not likely to explain much of the difference between FDD values.

The difference in FDD modelling between Climate Atlas of Canada and modelled FDD values can contribute to the differences. The Climate Atlas of Canada values were based on the average of 24 models of FDD (Climate Atlas of Canada, 2019). The worldwide FDD value modelling done to create Climate Atlas of Canada would likely have resulted in edge effects as well as issues modelling in areas where extreme values are found. The study region would be fairly peripheral in relation to the rest of the world as well as showing higher FDD values. The combination of these two factors could skew the averaged models to predict accurate trends but less precise values of FDD across the study region.

Lastly, the scale of the FDD models is vastly different. While the Climate Atlas of Canada FDD values are available for the entire world, there are concessions that had to be made. The biggest difference between the two models was the scale. Both in overall area covered as well as grid cell size that was feasible. Although the modelled FDD values were only able to cover a small part of the world in comparison to the Climate Atlas of Canada FDD values, the grid cell size was greatly reduced. Climate Atlas of Canada FDD values were represented on a 10 km^2 cell size, significantly different than the 90 m^2 cell size used for modelled FDD values. Neither source of FDD values will be a perfect representation, however the spatial variability in FDD values in Yukon territory indicates that the accuracy of the Climate Atlas of Canada FDD values will be low relative to modelled FDD values.

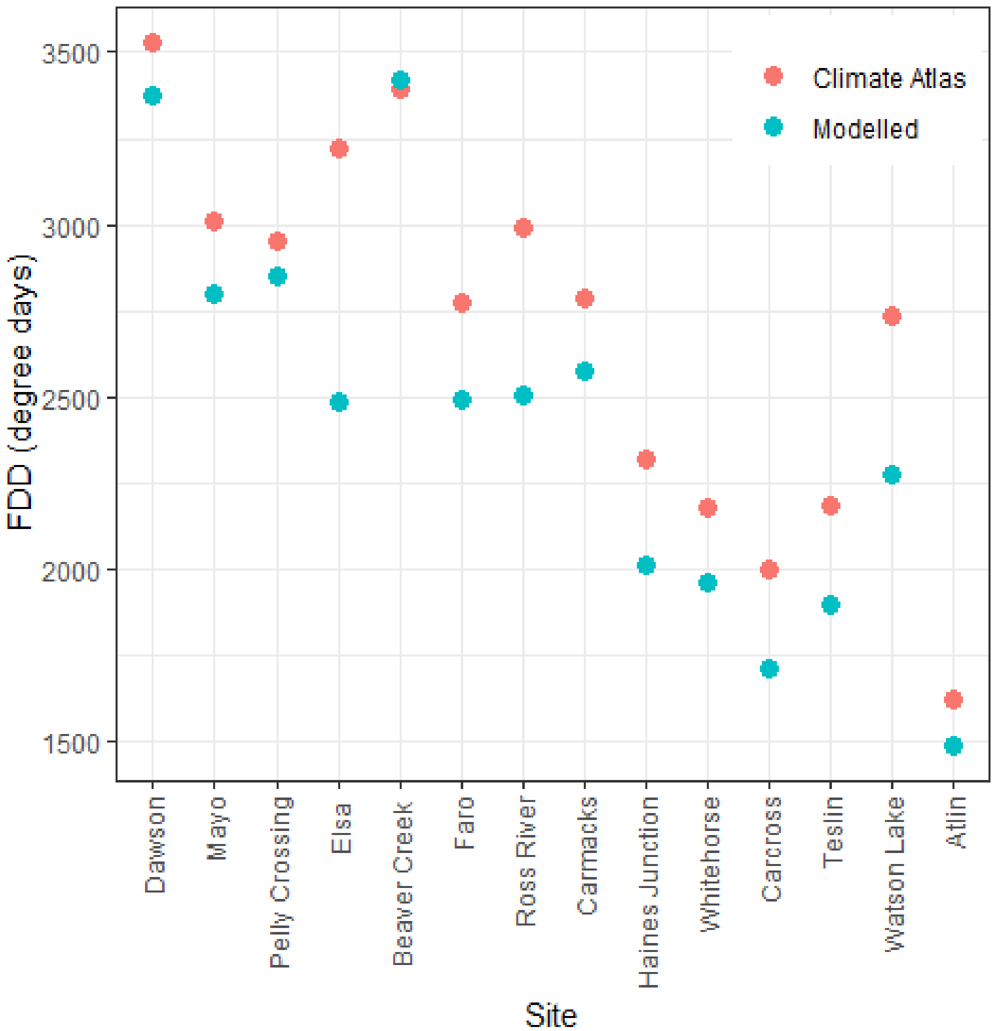

Figure 4-9. Climate Atlas of Canada FDD days in comparison to modelled FDD days at 14 sites in Yukon and British Columbia. Climate Atlas of Canada based on FDD values calculated from data collected between 1976 – 2005. Modelled FDD values calculated from data collected between 2006 – 2019. Average difference calculated to be 275 freezing degree days.

4.5.3 MAAT maps

The mean annual air temperature map created from FDD and TDD values was very similar to the MAAT map created by Lewkowicz *et al. (2012)* even though the calculation methods and the field data were not the same (*Figure 4-10*). The map by Lewkowicz *et al.* (2012) showed the majority of the study region having a MAAT between -6 ºC and -1 ºC (*Figure 4-10A*). The new MAAT map however, showed the majority of MAAT values between -4 ºC and 0 ºC (*Figure 4-10B*). Both maps showed higher MAAT values in the southern portion of the study region, extending up the centre of the study region, with lower MAAT values extending towards the east and west boundaries (*Figure 4-10*). In both cases, the highest MAAT values were found in low elevations near Monarch as well as within the coastal, and therefore very maritime area, of the ice fields. These values in the latter case may be a result of edge effects and a lack of knowledge of temperature patterns within the ice fields as no temperature loggers used in creating these models were located in this region.

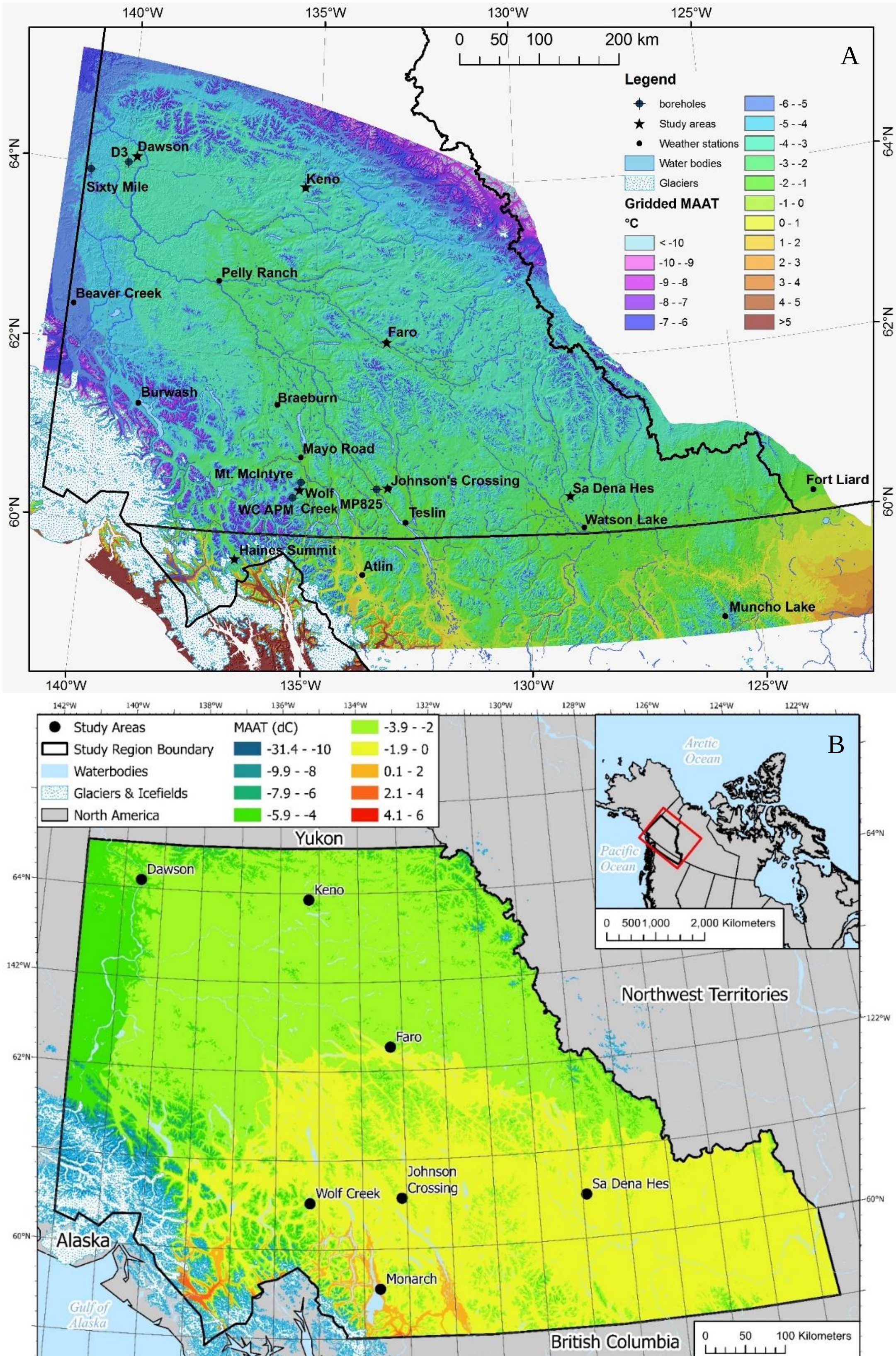

Figure 4-10. MAAT map calculated using MMAT values (A) by Lewkowicz et al. (2012) and MAAT map calculated using FDD and TDD values (B).

The mean annual air temperatures within the study region derived from freezing and thawing degree days can be compared to those calculated from MMAT (see Chapter 3). The difference between the two maps was assessed by subtracting the former from the latter. Positive differences indicate where the MMAT-based MAAT is warmer than that based on FDD and TDD, and negative values indicate the opposite (*Figure 4-11*).

The average MAAT calculated from FDD and TDD values was -2.4 ºC, whereas the average MAAT calculated from MMAT values was -2.8 ºC giving an average difference between the two models of -0.4 ºC. The largest positive differences between the two models are in the southwest part of the study region in the ice fields (*Figure 4-11*). Conversely, the areas where the FDD and TDD-based MAAT model predicts higher temperatures are found in the eastern portion of the study region, surrounding and slightly north of Sa Dena Hes. MAAT temperatures in the study region are within ±1 ºC for 86 % of the grid cells (*Table 4-5*). A total of 14 % of the study region showed a difference of more than ±1 ºC between the two models with less than 1 % showing a difference exceeding ±2 ºC.

Table 4-5. Percent area of difference between MAAT maps created using MMAT and FDD and TDD values.

Temperature (°C)	Percent Area
1 - 1.99	0.2
0 - 0.99	18.8
0 - -0.99	67.1
-1 - -1.99	13.3
< -2	0.6

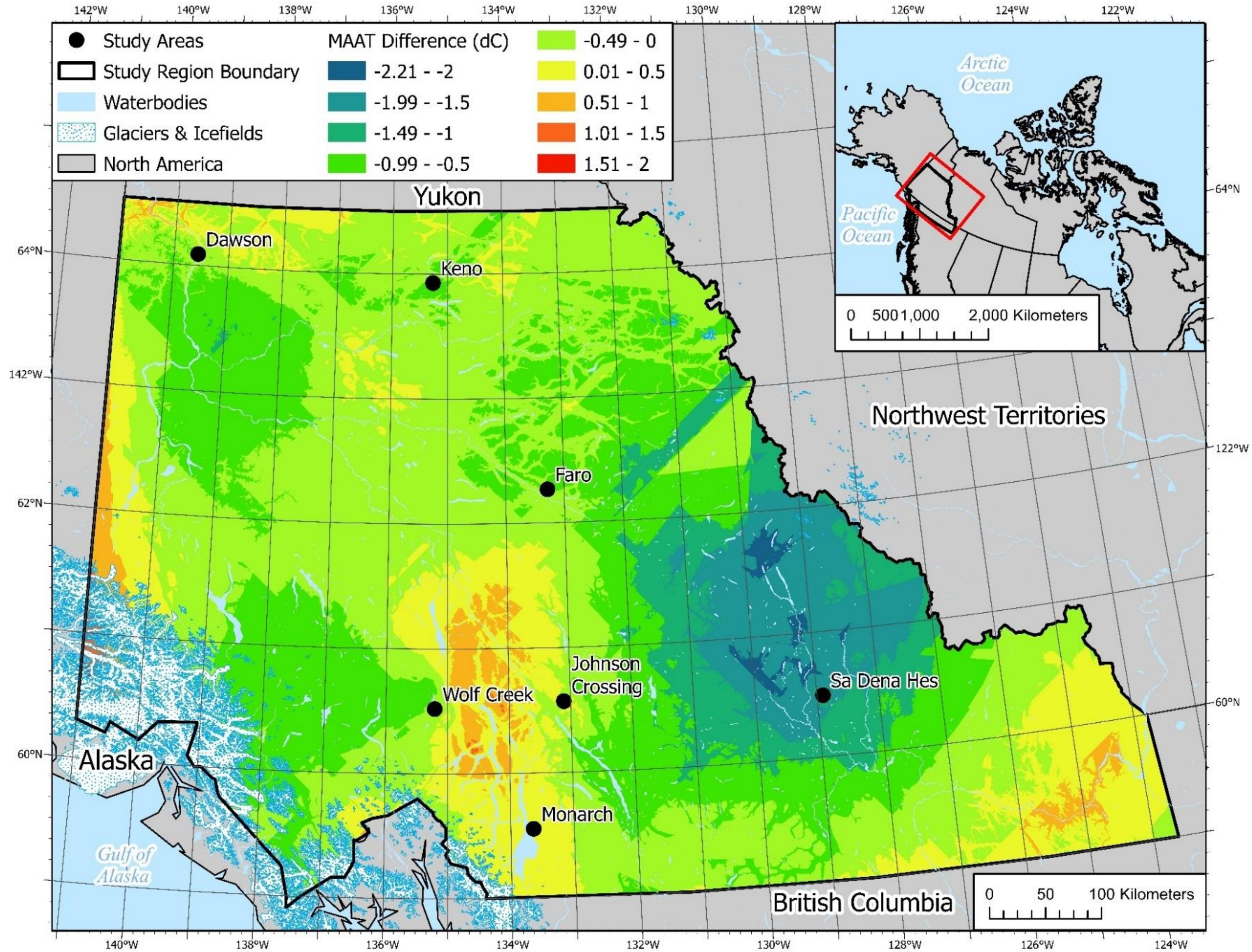

Figure 4-11. Difference in mean annual air temperature predictions calculated by subtracting the FDD and TDD-based MAAT values from the MMAT-based MAAT values. Whitehorse (not shown) is located approximately 10 km northeast of Wolf Creek. The average difference in MAAT models across the study region was calculated to be -0.4 ºC.

4.6 Conclusions

The results of this study are unique to the study region, adding a new understanding of lapse rate trends across Yukon territory. FDD and TDD values have not been calculated previously with as much detail as presented here. The relationship below treeline between FDD and TDD with the degree of continentality made extrapolation of FDD and TDD across a larger area possible.

Lapse rates of TDD and FDD have not been calculated and made available for this region before, likely as a result of a lack of elevation gradient data. Further understanding of FDD and TDD lapse rates in the study region and how they relate to DOC will allow for their use in TTOP modelling (Ferrarria *et al.*, 2016).

Updated and regional scale FDD and TDD maps will allow for a better understanding of how FDD and TDD values are changing over time. They provide both a comparison point to historical data as well as a source for future comparisons. Current FDD and TDD values can be used to develop a better understanding of how permafrost is changing across the study region when compared to historical FDD and TDD values.

4.7 References

Bevington, A. (2015). *Towards a TTOP-Model of Permafrost Distribution for Three Areas in Yukon and Northern British Columbia*. Thesis (M.Sc.) – University of Ottawa.

Bonnaventure, P., & Lewkowicz, A. (2012). Permafrost probability modeling above and below treeline, Yukon, Canada. *Cold Regions Science and Technology, 79-80,* 92-106. DOI: 10.1016/j.coldregions.2012.03.004

Bonnaventure, P., & Lewkowicz, A. (2013). Impacts of mean annual air temperature change on a regional permafrost probability model for the southern Yukon and northern British Columbia, Canada. *The Cryosphere*, *7*, 935–946. DOI: 10.5194/tc-7-935-2013

Climate Atlas of Canada. (2019). Freezing Degree Days. Retrieved from https://climateatlas.ca/map/canada/fdd_baseline#

Esri Data and Maps. (2021). USA States (Generalized). Retrieved from: https://hub.arcgis.com/datasets/esri::usa-states-generalized/about

Ferreira, A., Vieira, G., Ramos, M., Nieuwendam, A. (2017). Ground temperature and permafrost distribution in Hurd Peninsula (Livingston Island, Maritime Antarctic): An assessment using freezing indexes and TTOP modelling. *Catena*, *149*(2), 560–571. DOI: https://doi.org/10.1016/j.catena.2016.08.027

Government of Canada. (2016). Provinces/Territories, Cartographic Boundary File – 2016 Census. Retrieved from: https://open.canada.ca/data/en/dataset/a883eb14-0c0e-45c4-b8c4-b54c4a819edb

Government of Canada. (2018). Meteorological Station Catalogue. Retrieved from: https://open.canada.ca/data/en/dataset/9764d6c6-3044-450c-ac5a-383cedbfef17

Government of Canada. (2021). The UTM Grid - Universal Transverse Mercator Projection. Retrieved from https://www.nrcan.gc.ca/earth-sciences/geography/topographic-information/maps/utm-grid-map-projections/utm-grid-universal-transverse-mercator-projection/9779

Larsen, P., Goldsmith, S., Smith, O., Wilson, M., Strzepek, K., Chinowsky, P., Saylor, B. (2008). Estimating future costs for Alaska public infrastructure at risk from climate change. *Global Environmental Change*, *10, 442 – 457*. DOI: 10.1016/j.gloenvcha.2008.03.005

Lewkowicz, A.G., & Bonnaventure, P.P. (2011). Equivalent Elevation: A New Method to Incorporate Variable Surface Lapse Rates into Mountain Permafrost Modelling. *Permafrost and Periglacial Processes*, *22*(2), 153–162. https://doi.org/10.1002/ppp.720

Lewkowicz, A.G., & Bonnaventure, P.P., Smith, S.L., Kuntz, Z. (2012). Spatial and thermal characteristics of mountain permafrost, northwest Canada. *Geografiska Annaler: Series A, Physical Geography, 94(2),* 195–213. DOI: 10.1111/j.1468-0459.2012.00462.x

Obu, J., Westermann, S., Bartsch, A., Berdnikov, N., Christiansen, H., Dashtseren, A., Delaloye, R., Elberling, B., Etzelmüller, B., Kholodov, A., Khomutov, A., Kääb, A., Leibman, M. O., Lewkowicz, A. G., Panda, S. K., Romanovsky, V., Way, R. (2019). Northern Hemisphere permafrost map based on TTOP modelling for 2000–2016 at 1 km2 scale. *Earth-Science Reviews*, *193*, 299–316. DOI: https://doi.org/10.1016/j.earscirev.2019.04.023

Obu, J., Westermann, S., Vieira, G., Abramov, A., Balks, M.R., Bartsch, A., Hrbáček, F., Kääb, A., Ramos, M. (2020). Pan-Antarctic map of near-surface permafrost temperatures at 1 km2 scale. *The Cryosphere*, *14(2)*, 497–519. DOI: https://doi.org/10.5194/tc-14-497-2020

Smith, M., & Riseborough, D. (2002). Climate and the limits of permafrost: a zonal analysis. *Permafrost and Periglacial Processes*, *13*(1), 1–15. DOI: https://doi.org/10.1002/ppp.410

Way, R., & Lewkowicz, A. (2016). Modelling the spatial distribution of permafrost in Labrador–Ungava using the temperature at the top of permafrost. *Canadian Journal of Earth Sciences*, *53*(10), 1010–1028. DOI: https://doi.org/10.1139/cjes-2016-0034

CHAPTER 5: CONCLUSIONS

5.1 Introduction

Mean monthly air temperatures and freezing and thawing degree day models were developed for the complex terrain of the study region. Climate data from the 83 temperature monitoring stations used in the model as well as a number of stations above treeline that were not used in the models were processed and made available to the Government of Northwest Territories, allowing for further research with the same data. Two mean annual air temperature maps based on MMAT and F/TDD were created and compared for the study region to evaluate against previous MAAT models as well as each other.

5.2 Summary of findings

Lapse rate inversions were found to occur across the study region in the colder months (*Figure 3-4*) with the strongest inversions occurring in the study areas with a higher degree of continentality. Lapse rates remained inverted for a maximum of five months (November – March) at the more continental sites, Dawson (42 ºC) and Sa Dena Hes (38 ºC). Relatively stable lapse rates occurred between April and October, with negative values at all seven study areas. Lapse rates were weaker than the global annual average of -6.5 ºC/km in all months of the year. Lapse rates were found to be significantly correlated ($p < 0.1$) with degree of continentality from November through April, and August. In the months of the year that degree of continentality was related to lapse rates, the degree of continentality was used to create lapse rate trend surfaces for the region (Chapter 3.3.4).

Mean monthly air temperature maps as well as seasonal mean air temperature maps were created for the study region, showing strong similarities but more detail than MMAT maps created by Wahl *et al.* (1987). The maps were modelled at 90 x 90 meter resolution, greatly increasing the detail from the 1987 MMAT maps that were created using apparently hand-drawn isotherms. More complex MMAT patterns were seen in colder months when inversions occurred and more homogenous MMAT patterns were seen in warmer months. Three components of the model had influence on the pattern of temperatures throughout the study area: 1) degree of continentality, 2) elevation, and 3) latitude. In the winter (*Figure 3-6*), the degree of continentality shows the strongest influence on MMAT with inversions in lapse rates being most obvious in the northwest near Dawson. In the spring (*Figure 3-10*), the influence of degree of continentality decreases from March through May with elevation taking a dominant role in the MMAT patterns. Summer MMAT (*Figure 3-14*) were mainly influenced by elevation and latitude with elevation being the most influential, highlighting the complex terrain within the study region. Autumn MMAT (*Figure 3-18*) shows a decrease in the influence of latitude and elevation on temperatures and a progressive increase in the influence of degree of continentality from September through November. Validation of MMAT models showed lower RMSE in warmer months where temperature patterns are more homogenous (*Table 3-1*) than in winter months. The highest RMSE between modelled and measured temperatures at the 20 validation sites was in January (4.4 °C) and lowest in June (0.7 °C).

Freezing and thawing degree day maps combined gave an overall negative MAAT for the study region as expected. Although degree of continentality was significantly correlated with FDD and TDD ($p < 0.1$), visually elevation and latitude are more influential on FDD, and elevation alone appears influential on TDD values. When comparing the validation sites and RMSE values, the TDD model performs better. However, the range of FDD values is larger, showing greater variation of winter temperatures within the study region.

Mean annual air temperature maps created from MMAT and F/TDD were compared to previous models of MAAT (Wahl *et al.*, 1987; Lewkowicz *et al*., 2012) and showed slightly warmer temperatures across the study region. In comparison to each other, the MAAT maps were very similar, predicting within ±1 ºC for 86% of the grid cells and within ±2 ºC for all but 0.2 % of the area. Most of the study region had a MAAT between -6 °C and 0 °C. RMSE between modelled and measured MMAT at the 20 validation sites was slightly lower for the MAAT model created from MMAT (1.18 °C) than for the model created from FDD and TDD (1.25 °C).

5.3 Research limitations

Data from the 83 University of Ottawa sites used in building the MMAT, FDD and TDD models was collected between 2006 and 2019, however not all months in that time period were complete enough to be used (Appendix A). A minimum of 3 years of data were needed for a site to be included in modelling MMAT or F/TDD while the maximum number of years of data that was used in the model was 14 years. The inclusion of one or more anomalously cold or warm months could have affected shorter data collection averages while impacts on the longer records would have been much less.

While missing data is influential on the models, the actual years of collection could also have impacted the models. Data collection periods at the study areas were as long as 13 years from 2006-2019 (Johnson Crossing, Dawson and Keno) to 3 years in length (Sa Dena Hes and Faro; 2006-2009). The variable periods of data collection could also have influenced warm and cold years were included in a site dataset.

Edge effects in the model were most prominent in the northeast and southwest of the study region. The northeast part of the study region lacked data collection stations, decreasing the region-specific data in that area and increasing the amount of estimation for the models. The southwest of the study region in and around the icefields along the Alaska border also lacked data collection stations. The lack of data combined with the unknown variable of lapse rates and temperature patterns over and surrounding the ice fields, increased prediction uncertainty in the southwest.

5.4 Future research

Future research in this area should include continued monitoring of air temperatures at varying elevations to allow further evaluation of lapse rates. The addition of sites well above treeline would be beneficial to establish lapse rate behaviour for this elevation range as well as within low altitude clouds. A comparison of historical climate normals with current data collection at the government weather stations would give more insight into the apparent changes in mean monthly air temperature indicated by the new maps. A longer data collection period in some areas, especially in Monarch where lapse rates are the least variable would be beneficial to further supporting these findings. Continued research in our northern regions will assist us in better understanding the changing physical environment and the corresponding changes to species ranges over time.

BIBLIOGRAPHY

Bevington, A. (2015). *Towards a TTOP-Model of Permafrost Distribution for Three Areas in Yukon and Northern British Columbia*. Thesis (M.Sc.) – University of Ottawa.

Bonnaventure, P., & Lewkowicz, A. (2012). Permafrost probability modeling above and below treeline, Yukon, Canada. *Cold Regions Science and Technology, 79-80,* 92-106. DOI: 10.1016/j.coldregions.2012.03.004

Bonnaventure, P., & Lewkowicz, A. (2013). Impacts of mean annual air temperature change on a regional permafrost probability model for the southern Yukon and northern British Columbia, Canada. *The Cryosphere*, *7*, 935–946. DOI: 10.5194/tc-7-935-2013

Bush, E. & Lemmen, D.S., editors. (2019). Canada's Changing Climate Report; Government of Canada, Ottawa, ON. 444 p.

Chaput, M., & Gawjewski, K. (2014). Analysis of Daily Air Temperatures across a Topographically Complex Alpine Region of Southwestern Yukon, Canada. *Arctic*, *67*(4), 537–553. https://doi.org/10.14430/arctic4427

Climate Atlas of Canada. (2019). Freezing Degree Days. Retrieved from https://climateatlas.ca/map/canada/fdd_baseline#

Danby, R.K., & Hik, D.S. (2007). Variability, Contingency and Rapid Change in Recent Subarctic Alpine Tree Line Dynamics. *The Journal of Ecology*, *95*(2), 352–363. https://doi.org/10.1111/j.1365-2745.2006.01200.x

Daubenmire, R. (1954). ALPINE TIMBERLINES IN THE AMERICAS AND THEIR INTERPRETATION. *Butler University Botanical Studies*, *11*(8/17), 119–136.

D'Odorico, He, Y., Collins, S., De Wekker, S. F. J., Engel, V., & Fuentes, J. D. (2013). Vegetation-microclimate feedbacks in woodland-grassland ecotones. Global Ecology and Biogeography, 22(4), 364–379. https://doi.org/10.1111/geb.12000

Encyclopædia Britannica, Inc. (n.d.). *Lapse rate*. Encyclopædia Britannica. Retrieved November 1, 2022, from https://www.britannica.com/science/lapse-rate

Esri Data and Maps. (2021). USA States (Generalized). Retrieved from: https://hub.arcgis.com/datasets/esri::usa-states-generalized/about

Ferreira, A., Vieira, G., Ramos, M., Nieuwendam, A. (2017). Ground temperature and permafrost distribution in Hurd Peninsula (Livingston Island, Maritime Antarctic): An assessment using freezing indexes and TTOP modelling. *Catena*, *149*(2), 560–571. DOI: https://doi.org/10.1016/j.catena.2016.08.027

Government of Canada. (2016). Provinces/Territories, Cartographic Boundary File – 2016 Census. Retrieved from: https://open.canada.ca/data/en/dataset/a883eb14-0c0e-45c4-b8c4-b54c4a819edb

Government of Canada. (2017). Climate data: homogenized surface air temperature data access. Retrieved from https://www.canada.ca/en/environment-climate-change/services/climate-change/science-research-data/climate-trends-variability/adjusted-homogenized-canadian-data/surface-air-temperature-access.html

Government of Canada. (2018). Meteorological Station Catalogue. Retrieved from: https://open.canada.ca/data/en/dataset/9764d6c6-3044-450c-ac5a-383cedbfef17

Government of Canada. (2019a). Canadian Digital Elevation Model, 1945 – 2011. Retrieved from: https://open.canada.ca/data/en/dataset/7f245e4d-76c2-4caa-951a-45d1d2051333#wb-auto-6

Government of Canada. (2019b). Daily Data Report for June 2004. Retrieved from: https://climate.weather.gc.ca/climate_data/daily_data_e.html?hlyRange=%7C&dlyRange=1983-09-01%7C2017-05-30&mlyRange=1983-01-01%7C2007-02-01&StationID=1573&Prov=YT&urlExtension=_e.html&searchType=stnProv&optLimit=specDate&StartYear=1840&EndYear=2020&selRowPerPage=25&Line=24&Month=6&Day=25&lstProvince=YT&timeframe=2&Year=2004

Government of Canada. (2019c). Station Results – 1981 – 2010 Climate Normals and Averages. Retrieved from https://climate.weather.gc.ca/climate_normals/station_select_1981_2010_e.html?searchType=stnProv&lstProvince=YT

Government of Canada. (2021a). Indexes of the National Topographic System of Canada. Retrieved from https://open.canada.ca/data/en/dataset/055919c2-101e-4329-bfd7-1d0c333c0e62

Government of Canada. (2021b). The UTM Grid - Universal Transverse Mercator Projection. Retrieved from https://www.nrcan.gc.ca/earth-sciences/geography/topographic-information/maps/utm-grid-map-projections/utm-grid-universal-transverse-mercator-projection/9779

Government of Canada, (2022a). Lakes, Rivers and Glaciers in Canada - CanVec Series - Hydrographic Features. https://open.canada.ca/data/en/dataset/9d96e8c9-22fe-4ad2-b5e8-94a6991b744b

Government of Canada. (2022b). Historical Data. Retrieved from https://climate.weather.gc.ca/historical_data/search_historic_data_e.html?hlyRange=%7C&dlyRange=1983-09-01%7C2017-05-30&mlyRange=1983-01-01%7C2007-02-01&urlExtension=_e.html&searchType=stnProv&optLimit=specDate&StartYear=1840&EndYear=2020&selRowPerPage=25&Line=24&Month=6&Day=25&lstProvince=YT&timeframe=2&Year=2004

Government of Yukon. (2009). Yukon Government Climate Change Action Plan. Retrieved from: https://yukon.ca/sites/yukon.ca/files/env/env-yukon-government-climate-change-action-plan.pdf

Government of Yukon. (2018). Climate Change Action Plan Update. Retrieved from: https://yukon.ca/sites/yukon.ca/files/env/env-climate-change-action-plan-update.pdf

Harris. (1982). Cold Air Drainage West of Fort Nelson, British Columbia. Arctic, 35(4), 537–541. https://doi.org/10.14430/arctic2362 Cambridge University Press, Cambridge, UK, and New York, NY, USA, pp. 1-19

International Panel on Climate Change (IPCC). (2012). Summary for Policymakers. In: Managing the Risks of Extreme Events and Disasters to Advance Climate Change Adaptation [Field, C.B., V. Barros, T.F. Stocker, D. Qin, D.J. Dokken, K.L. Ebi, M.D. Mastrandrea, K.J. Mach, G.-K. Plattner, S.K. Allen, M. Tignor, and P.M. Midgley (eds.)].

International Panel on Climate Change (IPCC). (2019). IPCC Special Report on the Ocean and Cryosphere in a Changing Climate [H.-O. Pörtner, D.C. Roberts, V. Masson-Delmotte, P. Zhai, M. Tignor, E. Poloczanska, K. Mintenbeck, A. Alegría, M. Nicolai, A. Okem, J. Petzold, B. Rama, N.M. Weyer (eds.)]. In press.

Karunaratne, & Burn, C. R. (2004). Relations between air and surface temperature in discontinuous permafrost terrain near Mayo, Yukon Territory. Canadian Journal of Earth Sciences, 41(12), 1437–1451. https://doi.org/10.1139/e04-082

Kattel, D., Yao, T., Yang, K., Tian, L., Yang, G., Joswiak, D. (2013). Temperature lapse rate in complex mountain terrain on the southern slope of the central Himalayas. *Theoretical and Applied Climatology, 113,* 671-682. DOI: 10.1007/s00704-012-0816-6

Laughlin. (1982). Minimum temperature and lapse rate in complex terrain: Influencing factors and prediction. Archives for Meteorology, Geophysics, and Bioclimatology Series B, 30(1-2), 141–152. https://doi.org/10.1007/BF02323400

Larsen, P., Goldsmith, S., Smith, O., Wilson, M., Strzepek, K., Chinowsky, P., Saylor, B. (2008). Estimating future costs for Alaska public infrastructure at risk from climate change. *Global Environmental Change, 10, 442 – 457.* DOI: 10.1016/j.gloenvcha.2008.03.005

Lewkowicz, A.G., & Bonnaventure, P.P. (2011). Equivalent Elevation: A New Method to Incorporate Variable Surface Lapse Rates into Mountain Permafrost Modelling. *Permafrost and Periglacial Processes, 22*(2), 153–162. https://doi.org/10.1002/ppp.720

Lewkowicz, A.G., Bonnaventure, P.P., Smith, S.L., Kuntz, Z. (2012). Spatial and thermal characteristics of mountain permafrost, northwest Canada. *Geografiska Annaler: Series A, Physical Geography, 94(2),* 195–213. DOI: 10.1111/j.1468-0459.2012.00462.x

Lewkowicz, A.G., & Way, R.G. (2019). Extremes of summer climate trigger thousands of thermokarst landslides in a High Arctic environment *Nature Communications, 10*(1), 1329–11. https://doi.org/10.1038/s41467-019-09314-7

Melvin, A., Larsen, P., Boehlert, B., Neumann, J., Chinowsky, P., Espinet, X., Martinich, J., Baumann, M., Rennels, L., Bothner, A., Nicolsky, D., Machenko, S. (2016). Climate change damages to Alaska public infrastructure and the economics of proactive adaptation. *Proceedings of the National Academy of Sciences of the United States of America, 114(2), 122.*

National Centers for Environmental Information (NCEI). (n.d.). Data tools: 1981-2010 normals. Retrieved April 6, 2022, from https://www.ncdc.noaa.gov/cdo-web/datatools/normals

Obu, J., Westermann, S., Bartsch, A., Berdnikov, N., Christiansen, H., Dashtseren, A., Delaloye, R., Elberling, B., Etzelmüller, B., Kholodov, A., Khomutov, A., Kääb, A., Leibman, M. O., Lewkowicz, A. G., Panda, S. K., Romanovsky, V., Way, R. (2019). Northern Hemisphere permafrost map based on TTOP modelling for 2000–2016 at 1 km2 scale. *Earth-Science Reviews*, *193*, 299–316. DOI: https://doi.org/10.1016/j.earscirev.2019.04.023

Obu, J., Westermann, S., Vieira, G., Abramov, A., Balks, M.R., Bartsch, A., Hrbáček, F., Kääb, A., Ramos, M. (2020). Pan-Antarctic map of near-surface permafrost temperatures at 1 km2 scale. *The Cryosphere, 14(2),* 497–519. DOI: https://doi.org/10.5194/tc-14-497-2020

Rolland, C. (2003). Spatial and Seasonal Variations of Air Temperature Lapse Rates in Alpine Regions. *Journal of Climate, 16,* 1032-1046. DOI: https://doi.org/10.1175/1520-0442(2003)016<1032:SASVOA>2.0.CO;2

Rowland, E., Fresco, N., Reid, D., Cooke, H. (2016). Examining climate-biome (“cliome”) shifts for Yukon and its protected areas. *Global Ecology and Conservation, 6,* 1-17. DOI: https://doi.org/10.1016/j.gecco.2016.07.006

Scudder, G.G.E. (1997). Environment of the Yukon. *Danks & Downes (Eds.) Insects of the Yukon, Biological Survey of Canada (Terrestrial Arthropods), Ottawa, ON*, 13-57.

Smith, M., & Riseborough, D. (2002). Climate and the limits of permafrost: a zonal analysis. *Permafrost and Periglacial Processes*, *13*(1), 1–15. DOI: https://doi.org/10.1002/ppp.410

Vincent, L. A., Wang, X. L., Milewska, E. J., Wan, H., Yang, F., Swail, V. (2012). A second generation of homogenized Canadian monthly surface air temperature for climate trend analysis. *Journal of Geophysical Research, 117*, DOI:10.1029/2012JD017859.

Wahl, H.E., Fraser, D.B., Harvey, R.C. (1987). *Climate of Yukon*. Canadian Government Publishing Center.

Walsh, J.E. (2014). Intensified warming of the Arctic: Causes and impacts on middle latitudes. *Glob. and Plan. Chang*. 117, 52-63.

Way, R., & Lewkowicz, A. (2016). Modelling the spatial distribution of permafrost in Labrador–Ungava using the temperature at the top of permafrost. *Canadian Journal of Earth Sciences*, *53*(10), 1010–1028. DOI: https://doi.org/10.1139/cjes-2016-0034

APPENDICES

Appendix A: Excluded data statistics

Table A-1. Months missing data excluded from MMAT, FDD, and TDD calculations. Months were only excluded if missing more than 8 days of data. The number of months missing data is across all 83 sites collecting data from 2006 – 2019.

Days Missing	Number of Months	Percentage of Months Missing Data
8 - 14	76	36.2
15 - 21	73	34.8
22 - 28	61	29.0

Table A-2. Excluded or missing data from Dawson sites located below treeline used in lapse rate modelling. Green indicates data that was used. Red indicates missing data where a minimum of 8 days of data was missing. No fill indicates time outside of the data collection period for the site.

Year	Month	D1	D3	D4	D5	D6	D7	D8	D9	D10	D11	D12	D13
2007	J												
	F												
	M												
	A												
	M												
	J												
	J												
	A												
	S												
	O												
	N												
	D												
2008	J												
	F												
	M												
	A												
	M												
	J												
	J												
	A												
	S												
	O												
	N												
	D												
2009	J												
	F												
	M												
	A												
	M												
	J												
	J												
	A												
	S												
	O												
	N												
	D												

Table A-2. Continued.

Year	Month	D1	D3	D4	D5	D6	D7	D8	D9	D10	D11	D12	D13
2010	J												
	F												
	M												
	A												
	M												
	J												
	J												
	A												
	S												
	O												
	N												
	D												
2011	J												
	F												
	M												
	A												
	M												
	J												
	J												
	A												
	S												
	O												
	N												
	D												
2012	J												
	F												
	M												
	A												
	M												
	J												
	J												
	A												
	S												
	O												
	N												
	D												

Table A-2. Continued.

Year	Month	D1	D3	D4	D5	D6	D7	D8	D9	D10	D11	D12	D13
2013	J												
	F												
	M												
	A												
	M												
	J												
	J												
	A												
	S												
	O												
	N												
	D												
2014	J												
	F												
	M												
	A												
	M												
	J												
	J												
	A												
	S												
	O												
	N												
	D												
2015	J												
	F												
	M												
	A												
	M												
	J												
	J												
	A												
	S												
	O												
	N												
	D												

Table A-2. Continued.

Year	Month	D1	D3	D4	D5	D6	D7	D8	D9	D10	D11	D12	D13
2016	J												
	F												
	M												
	A												
	M												
	J												
	J												
	A												
	S												
	O												
	N												
	D												
2017	J												
	F												
	M												
	A												
	M												
	J												
	J												
	A												
	S												
	O												
	N												
	D												
2018	J												
	F												
	M												
	A												
	M												
	J												
	J												
	A												
	S												
	O												
	N												
	D												

Table A-2. Continued.

Year	Month	D1	D3	D4	D5	D6	D7	D8	D9	D10	D11	D12	D13
2019	J												
	F												
	M												
	A												
	M												
	J												
	J												
	A												
	S												
	O												
	N												
	D												

Table A-3. Excluded or missing data from Faro sites located below treeline used in lapse rate modelling. Green indicates data that was used. Red indicates missing data where a minimum of 8 days of data was missing. No fill indicates time outside of the data collection period for the site.

Year	Month	F1	F2	F3	F4	F5	F6	F7	F8	F9	F10	F11	F12	F13
2006	J													
	F													
	M													
	A													
	M													
	J													
	J													
	A													
	S													
	O													
	N													
	D													
2007	J													
	F													
	M													
	A													
	M													
	J													
	J													
	A													
	S													
	O													
	N													
	D													
2008	J													
	F													
	M													
	A													
	M													
	J													
	J													
	A													
	S													
	O													
	N													
	D													

Table A-3. Continued.

Year	Month	F1	F2	F3	F4	F5	F6	F7	F8	F9	F10	F11	F12	F13
2009	J													
	F													
	M													
	A													
	M													
	J													
	J													
	A													
	S													
	O													
	N													
	D													

Table A-4. Excluded or missing data from Johnson Crossing sites located below treeline used in lapse rate modelling. Green indicates data that was used. Red indicates missing data where a minimum of 8 days of data was missing. No fill indicates time outside of the data collection period for the site.

Year	Month	JC1	JC2	JC3	JC4	JC5	JC8	JC9	JC10	JC11	JC12	JC13
2006	J											
	F											
	M											
	A											
	M											
	J											
	J											
	A											
	S											
	O											
	N											
	D											
2007	J											
	F											
	M											
	A											
	M											
	J											
	J											
	A											
	S											
	O											
	N											
	D											
2008	J											
	F											
	M											
	A											
	M											
	J											
	J											
	A											
	S											
	O											
	N											
	D											

Table A-4. Continued.

Year	Month	JC1	JC2	JC3	JC4	JC5	JC8	JC9	JC10	JC11	JC12	JC13
2009	J											
	F											
	M											
	A											
	M											
	J											
	J											
	A											
	S											
	O											
	N											
	D											
2010	J											
	F											
	M											
	A											
	M											
	J											
	J											
	A											
	S											
	O											
	N											
	D											
2011	J											
	F											
	M											
	A											
	M											
	J											
	J											
	A											
	S											
	O											
	N											
	D											

Table A-4. Continued.

Year	Month	JC1	JC2	JC3	JC4	JC5	JC8	JC9	JC10	JC11	JC12	JC13
2012	J											
	F											
	M											
	A											
	M											
	J											
	J											
	A											
	S											
	O											
	N											
	D											
2013	J											
	F											
	M											
	A											
	M											
	J											
	J											
	A											
	S											
	O											
	N											
	D											
2014	J											
	F											
	M											
	A											
	M											
	J											
	J											
	A											
	S											
	O											
	N											
	D											

Table A-4. Continued.

Year	Month	JC1	JC2	JC3	JC4	JC5	JC8	JC9	JC10	JC11	JC12	JC13
2015	J											
	F											
	M											
	A											
	M											
	J											
	J											
	A											
	S											
	O											
	N											
	D											
2016	J											
	F											
	M											
	A											
	M											
	J											
	J											
	A											
	S											
	O											
	N											
	D											
2017	J											
	F											
	M											
	A											
	M											
	J											
	J											
	A											
	S											
	O											
	N											
	D											

Table A-4. Continued.

Year	Month	JC1	JC2	JC3	JC4	JC5	JC8	JC9	JC10	JC11	JC12	JC13
2018	J											
	F											
	M											
	A											
	M											
	J											
	J											
	A											
	S											
	O											
	N											
	D											

Table A-5. Excluded or missing data from Keno sites located below treeline used in lapse rate modelling. Green indicates data that was used. Red indicates missing data where a minimum of 8 days of data was missing. No fill indicates time outside of the data collection period for the site.

Year	Month	K1	K2	K3	K4	K5	K6	K7	K8	K9	K10	K11	K12	K13
2006	J													
	F													
	M													
	A													
	M													
	J													
	J													
	A													
	S													
	O													
	N													
	D													
2007	J													
	F													
	M													
	A													
	M													
	J													
	J													
	A													
	S													
	O													
	N													
	D													
2008	J													
	F													
	M													
	A													
	M													
	J													
	J													
	A													
	S													
	O													
	N													
	D													

Table A-5. Continued.

Year	Month	K1	K2	K3	K4	K5	K6	K7	K8	K9	K10	K11	K12	K13
2009	J													
	F													
	M													
	A													
	M													
	J													
	J													
	A													
	S													
	O													
	N													
	D													
2010	J													
	F													
	M													
	A													
	M													
	J													
	J													
	A													
	S													
	O													
	N													
	D													
2011	J													
	F													
	M													
	A													
	M													
	J													
	J													
	A													
	S													
	O													
	N													
	D													

Table A-5. Continued.

Year	Month	K1	K2	K3	K4	K5	K6	K7	K8	K9	K10	K11	K12	K13
2012	J													
	F													
	M													
	A													
	M													
	J													
	J													
	A													
	S													
	O													
	N													
	D													
2013	J													
	F													
	M													
	A													
	M													
	J													
	J													
	A													
	S													
	O													
	N													
	D													
2014	J													
	F													
	M													
	A													
	M													
	J													
	J													
	A													
	S													
	O													
	N													
	D													

Table A-5. Continued.

Year	Month	K1	K2	K3	K4	K5	K6	K7	K8	K9	K10	K11	K12	K13
2015	J													
	F													
	M													
	A													
	M													
	J													
	J													
	A													
	S													
	O													
	N													
	D													
2016	J													
	F													
	M													
	A													
	M													
	J													
	J													
	A													
	S													
	O													
	N													
	D													
2017	J													
	F													
	M													
	A													
	M													
	J													
	J													
	A													
	S													
	O													
	N													
	D													

Table A-5. Continued.

Year	Month	K1	K2	K3	K4	K5	K6	K7	K8	K9	K10	K11	K12	K13
2018	J													
	F													
	M													
	A													
	M													
	J													
	J													
	A													
	S													
	O													
	N													
	D													

Table A-6. Excluded or missing data from Monarch sites located below treeline used in lapse rate modelling. Green indicates data that was used. Red indicates missing data where a minimum of 8 days of data was missing. No fill indicates time outside of the data collection period for the site.

Year	Month	M1	M2	M3	M4	M5	M6	School
2010	J							
	F							
	M							
	A							
	M							
	J							
	J							
	A							
	S							
	O							
	N							
	D							
2011	J							
	F							
	M							
	A							
	M							
	J							
	J							
	A							
	S							
	O							
	N							
	D							
2012	J							
	F							
	M							
	A							
	M							
	J							
	J							
	A							
	S							
	O							
	N							
	D							

Table A-6. Continued.

Year	Month	M1	M2	M3	M4	M5	M6	School
2013	J							
	F							
	M							
	A							
	M							
	J							
	J							
	A							
	S							
	O							
	N							
	D							
2014	J							
	F							
	M							
	A							
	M							
	J							
	J							
	A							
	S							
	O							
	N							
	D							
2015	J							
	F							
	M							
	A							
	M							
	J							
	J							
	A							
	S							
	O							
	N							
	D							

Table A-6. Continued.

Year	Month	M1	M2	M3	M4	M5	M6	School
2016	J							
	F							
	M							
	A							
	M							
	J							
	J							
	A							
	S							
	O							
	N							
	D							
2017	J							
	F							
	M							
	A							
	M							
	J							
	J							
	A							
	S							
	O							
	N							
	D							
2018	J							
	F							
	M							
	A							
	M							
	J							
	J							
	A							
	S							
	O							
	N							
	D							

Table A-6. Continued.

Year	Month	M1	M2	M3	M4	M5	M6	School
2019	J							
	F							
	M							
	A							
	M							
	J							
	J							
	A							
	S							
	O							
	N							
	D							
2020	J							
	F							
	M							
	A							
	M							
	J							
	J							
	A							
	S							
	O							
	N							
	D							

Table A-7. Excluded or missing data from Sa Dena Hes sites located below treeline used in lapse rate modelling. Green indicates data that was used. Red indicates missing data where a minimum of 8 days of data was missing. No fill indicates time outside of the data collection period for the site.

Year	Month	S1	S2	S3	S4	S5	S6	S7	S8	S9	S10	S11	S12	S13
2006	J													
	F													
	M													
	A													
	M													
	J													
	J													
	A													
	S													
	O													
	N													
	D													
2007	J													
	F													
	M													
	A													
	M													
	J													
	J													
	A													
	S													
	O													
	N													
	D													
2008	J													
	F													
	M													
	A													
	M													
	J													
	J													
	A													
	S													
	O													
	N													
	D													

Table A-7. Continued.

Year	Month	S1	S2	S3	S4	S5	S6	S7	S8	S9	S10	S11	S12	S13
2009	J													
	F													
	M													
	A													
	M													
	J													
	J													
	A													
	S													
	O													
	N													
	D													

Table A-8. Excluded or missing data from Wolf Creek sites located below treeline used in lapse rate modelling. Green indicates data that was used. Red indicates missing data where a minimum of 8 days of data was missing. No fill indicates time outside of the data collection period for the site.

Year	Month	P9	WC 1	WC 2	WC 3	WC 4	WC 5	WC 6	WC 7	WC 9	WC 11	WC 12	APM	CR1	CR2	CR3	CR4	DL	T1	T2	T3	T4
2006	J																					
	F																					
	M																					
	A																					
	M																					
	J																					
	J																					
	A																					
	S																					
	O																					
	N																					
	D																					
2007	J																					
	F																					
	M																					
	A																					
	M																					
	J																					
	J																					
	A																					
	S																					
	O																					
	N																					
	D																					

Table A-8. Continued.

Year	Month	P9	WC 1	WC 2	WC 3	WC 4	WC 5	WC 6	WC 7	WC 9	WC 11	WC 12	APM	CR1	CR2	CR3	CR4	DL	T1	T2	T3	T4
2008	J																					
	F																					
	M																					
	A																					
	M																					
	J																					
	J																					
	A																					
	S																					
	O																					
	N																					
	D																					
2009	J																					
	F																					
	M																					
	A																					
	M																					
	J																					
	J																					
	A																					
	S																					
	O																					
	N																					
	D																					

Table A-8. Continued.

Year	Month	P9	WC 1	WC 2	WC 3	WC 4	WC 5	WC 6	WC 7	WC 9	WC 11	WC 12	APM	CR1	CR2	CR3	CR4	DL	T1	T2	T3	T4
2010	J																					
	F																					
	M																					
	A																					
	M																					
	J																					
	J																					
	A																					
	S																					
	O																					
	N																					
	D																					
2011	J																					
	F																					
	M																					
	A																					
	M																					
	J																					
	J																					
	A																					
	S																					
	O																					
	N																					
	D																					

Table A-8. Continued.

Year	Month	P9	WC 1	WC 2	WC 3	WC 4	WC 5	WC 6	WC 7	WC 9	WC 11	WC 12	APM	CR1	CR2	CR3	CR4	DL	T1	T2	T3	T4
2012	J																					
	F																					
	M																					
	A																					
	M																					
	J																					
	J																					
	A																					
	S																					
	O																					
	N																					
	D																					
2013	J																					
	F																					
	M																					
	A																					
	M																					
	J																					
	J																					
	A																					
	S																					
	O																					
	N																					
	D																					

Table A-8. Continued.

Year	Month	P9	WC 1	WC 2	WC 3	WC 4	WC 5	WC 6	WC 7	WC 9	WC 11	WC 12	APM	CR1	CR2	CR3	CR4	DL	T1	T2	T3	T4
2014	J																					
	F																					
	M																					
	A																					
	M																					
	J																					
	J																					
	A																					
	S																					
	O																					
	N																					
	D																					
2015	J																					
	F																					
	M																					
	A																					
	M																					
	J																					
	J																					
	A																					
	S																					
	O																					
	N																					
	D																					

Table A-8. Continued.

Year	Month	P9	WC 1	WC 2	WC 3	WC 4	WC 5	WC 6	WC 7	WC 9	WC 11	WC 12	APM	CR1	CR2	CR3	CR4	DL	T1	T2	T3	T4
2016	J																					
	F																					
	M																					
	A																					
	M																					
	J																					
	J																					
	A																					
	S																					
	O																					
	N																					
	D																					
2017	J																					
	F																					
	M																					
	A																					
	M																					
	J																					
	J																					
	A																					
	S																					
	O																					
	N																					
	D																					

Appendix B: Lapse rate values

Table B-1. Monthly lapse rate at the seven study areas used to create kriging trend surfaces of lapse rate for MMAT modelling across the study region. The global average annual value is -6.5°C/km.

Study Area	J	F	M	A	M	J	J	A	S	O	N	D
Dawson	10.4	9.6	2.3	-3.7	-4.1	-3.9	-3.9	-3.6	-2.7	-1.3	4.6	9.8
Keno	7.9	5.4	-1.1	-5.8	-5.8	-5.5	-5.2	-5.1	-4.6	-2.8	4.3	7.3
Sa Dena Hes	14.2	6.8	0.8	-4.3	-6.7	-6.7	-6.0	-5.7	-5.7	-4.6	5.8	13.9
Faro	11.0	6.9	-0.3	-4.4	-4.8	-5.2	-5.2	-5.3	-4.0	-2.7	5.3	10.2
Johnson Crossing	5.3	2.5	-2.8	-4.8	-5.1	-5.2	-5.6	-5.8	-5.4	-5.5	-1.5	5.3
Wolf Creek	5.2	1.4	-3.7	-7.4	-7.1	-6.8	-7.0	-6.7	-6.0	-4.8	-0.6	4.9
Monarch	1.8	1.7	-3.0	-6.1	-5.0	-5.5	-4.8	-5.5	-5.5	-5.4	-4.3	-0.3
Average	8.0	4.9	-1.1	-5.2	-5.5	-5.5	-5.4	-5.4	-4.8	-3.9	2.0	7.3

Appendix C: Government weather station data

Table C-1. Environment and Climate Change Canada (Government of Canada, 2022b) weather station elevations and coordiates (WGS 1984).

Province	Site	Elevation (m asl)	Latitude	Longitude
BC	Atlin	673.6	59.57	-133.70
YT	Beaver Creek	649.0	62.40	-140.87
YT	Blanchard River	836.0	60.00	-136.77
YT	Burwash Airport	806.2	61.37	-139.05
YT	Carcross	660.0	60.17	-134.70
YT	Dawson	370.3	64.04	-139.13
BC	Dease Lake	806.6	58.43	-130.01
YT	Drury Creek	609.0	62.20	-134.39
YT	Faro	716.3	62.21	-133.37
NWT	Fort Liard	216.0	60.24	-123.47
BC	Fort Nelson	381.9	58.84	-122.60
NWT	Fort Simpson	169.2	61.76	-121.24
YT	Mayo	503.8	63.62	-135.87
YT	Mayo Road	655.0	60.88	-135.17
YT	McQuesten	458.2	63.59	-137.52
BC	Muncho Lake	836.5	58.93	-125.78
NWT	Norman Wells	72.5	65.28	-126.80
YT	Otter Falls	829.7	61.03	-137.05
YT	Pelly Ranch	445.0	62.83	-137.31
BC	Pleasant Camp	274.3	59.45	-136.37
YT	Stewart Crossing	480.1	63.38	-136.68
YT	Takhini River Ranch	671.0	60.95	-135.57
YT	Teslin	705.0	60.17	-132.74
BC	Tetsa River	810.0	58.65	-124.24
YT	Whitehorse	706.2	60.71	-135.07
YT	Whitehorse Riverdale	640.1	60.71	-135.03

Table C-2. National Centers for Environmental Information (NCEI, n.d.) weather station elevations and coordinates (WGS 1984).

State	Site	Elevation (m asl)	Latitude	Longitude
AK	Auke Bay	13.4	58.38	-134.65
AK	Chicken	548.6	64.09	-141.92
AK	Cordova North	7.6	60.56	-145.75
AK	Eagle Airport	276.8	64.78	-141.15
AK	Eagle River 5 SE	151.8	61.30	-149.44
AK	Eagle River Gakona Circle	172.8	61.32	-149.54
AK	Eagle River Nature Center	158.5	61.23	-149.27
AK	Elfin Cove	6.1	58.19	-136.34
AK	Glacier Bay	13.7	58.46	-135.87
AK	Gulkana Airport	476.1	62.16	-145.46
AK	Haines 40 NW	249.9	59.45	-136.36
AK	Haines Airport	4.6	59.24	-135.51
AK	Haines Number 2	25.0	59.23	-135.47
AK	Hoonah	39.6	58.11	-135.43
AK	Juneau Downtown	7.6	58.30	-134.41
AK	Juneau International Airport	4.9	58.36	-134.56
AK	McCarthy 3 SW	681.0	61.42	-143.00
AK	Nabesna	862.9	62.40	-143.00
AK	Northway Airport	522.1	62.96	-141.99
AK	Skagway Airport	6.1	59.46	-135.32
AK	Tok	493.8	63.33	-143.04
AK	Valdez Airport	33.5	61.13	-146.24
AK	Valdez Weather Service Office	7.0	61.13	-146.35
AK	Yakutat Airport	10.1	59.51	-139.67

Appendix D: Measured and modelled MMAT

Table D-1. Elevation (m asl) and coordinates (WGS 1984) for the validations sites.

Site	Elevation (m asl)	Latitude	Longitude
60 Mile Backup	1450.0	63.91	-140.81
AINA Base Camp	770.0	61.03	-138.41
Alaska Highway MP681	848.0	60.19	-129.90
Alaska Highway MP788	773.0	60.09	-132.37
Alaska Highway MP825	728.0	60.37	-133.11
Alaska Highway MP844	821.0	60.48	-133.48
Alpine Burwash Backup	1809.0	61.45	-139.41
Beaver Creek Palsa	619.0	62.50	-140.86
Beaver Creek Test Site	700.0	62.34	-140.84
Carmacks Copper	863.0	62.32	-136.67
Carmacks ECCC	542.9	62.12	-136.19
Haines Junction ECCC	595.3	60.77	-137.58
Haines Summit 3G3	1030.0	59.62	-136.43
Hour Lake ECCC	890.0	61.18	-129.13
Little Fox Lake	943.0	61.39	-135.66
MacMillan Pass ECCC	1379.0	63.24	-130.04
Mt McIntyre Borehole	1569.0	60.62	-135.14
Northern Dancer Backup	1627.0	60.01	-131.60
R7	788.0	61.71	-139.84
Wolf Creek 2006-8 Mt Granger	2077.0	60.54	-135.26

Table D-2. Measured MMAT and MAAT values at 20 validation sites within the study region. Measured values are based on either ECCC or University of Ottawa temperature monitoring stations. Data was collected between 2006 – 2019, with a minimum of 3 years of data.

Validation Site	J	F	M	A	M	J	J	A	S	O	N	D	MMAT
60 Mile Backup	-16.1	-14.7	-14.2	-5.7	2.9	8.2	9.6	7.2	1.3	-7.1	-14.5	-16.2	-4.9
AINA Base Camp	-17.9	-15.2	-11.8	-1.7	6.2	10.7	12.1	10.4	5.9	-1.4	-12.7	-17.4	-2.7
Alaska Highway MP681	-20.4	-16.1	-13.2	-0.9	6.6	NA	NA	10.5	4.9	-2.8	-15.7	-22.3	NA
Alaska Highway MP788	-13.4	-12.8	-8.3	0.8	8.0	11.8	13.3	11.5	6.6	-0.1	-11.2	-16.5	-0.9
Alaska Highway MP825	-13.7	-12.5	-7.9	0.8	7.5	11.5	13.4	11.9	6.9	0.4	-8.7	-15.6	-0.5
Alaska Highway MP844	-16.0	-14.1	-8.6	0.1	7.4	11.2	12.9	11.0	5.7	-1.4	-11.2	-17.9	-1.8
Alpine Burwash Backup	-10.9	-10.4	-12.0	-5.7	1.4	5.3	7.8	6.5	1.7	-4.7	-11.2	-10.8	-3.6
Beaver Creek Palsa	-22.0	-19.1	-13.2	-0.2	8.6	13.2	14.6	12.3	5.8	-4.1	-17.2	-22.6	-3.7
Beaver Creek Test Site	-22.8	-19.3	-13.2	-1.1	8.1	12.5	14.0	11.2	5.2	-5.1	-17.9	-23.2	-4.3
Carmacks Copper	-17.2	-13.8	-9.1	0.2	8.8	12.7	13.9	12.1	6.0	-2.4	-13.6	-18.1	-1.7
Carmacks ECCC	-21.0	-17.9	-9.7	1.1	8.6	13.6	15.5	12.9	7.4	-1.1	-14.6	-20.7	-2.2
Haines Junction ECCC	-16.6	-14.0	-8.5	0.3	7.0	11.1	13.3	11.3	6.6	-0.6	-12.1	-17.1	-1.6
Haines Summit 3G3	-8.8	-8.7	-8.2	-2.5	3.8	6.9	8.9	8.4	4.4	-1.2	-8.7	-8.7	-1.2
Hour Lake ECCC	-17.5	-16.2	-11.9	-1.4	6.5	11.1	13.6	11.5	6.5	-1.4	-14.4	-19.5	-2.8
Little Fox Lake	-12.8	-15.1	-9.3	0.3	7.8	11.4	12.9	11.1	5.5	-1.6	-13.0	-16.3	-1.6
Macmillan Pass ECCC	-17.6	-18.2	-17.3	-7.7	2.6	9.2	10.8	8.8	3.1	-5.8	-15.6	-17.4	-5.4
Mt McIntyre Borehole	-11.0	-11.0	-11.4	-4.7	2.7	6.5	8.2	5.0	2.0	-4.2	-11.2	-12.6	-3.5
Northern Dancer Backup	-10.0	-11.1	-10.8	-4.5	2.9	6.4	8.4	7.2	2.7	-3.5	-10.4	-11.5	-2.8
R7	-17.5	-14.1	-9.5	0.3	8.3	12.3	13.9	12.1	6.2	-3.1	-15.7	-17.9	-2.1
Wolf Creek 2006-8 Mt Granger	-12.8	-14.4	-14.7	-9.1	-1.4	2.7	4.7	3.3	-1.6	-7.2	-13.6	-14.2	-6.5

Table D-3. Modelled MMAT and MAAT values at 20 validation sites within the study region. Modelled values were based on values from Chapter 3.4.

Validation Site	J	F	M	A	M	J	J	A	S	O	N	D	MMAT
60 Mile Backup	-19.5	-16.1	-13.1	-5.0	2.6	8.1	9.6	7.9	0.9	-9.6	-13.7	-14.9	-5.2
AINA Base Camp	-18.4	-14.6	-9.4	-1.2	5.7	10.5	12.8	10.3	5.5	-2.1	-13.5	-16.1	-2.5
Alaska Highway MP681	-21.7	-16.1	-8.5	0.6	6.6	11.7	14.2	12.2	6.6	-0.5	-14.1	-19.6	-2.3
Alaska Highway MP788	-17.4	-14.3	-7.3	0.6	6.8	11.4	13.8	11.8	7.1	0.7	-10.9	-14.0	-1.0
Alaska Highway MP825	-17.6	-13.4	-7.1	0.6	6.9	11.7	14.3	12.1	7.2	0.6	-10.1	-12.9	-0.6
Alaska Highway MP844	-17.4	-12.9	-7.1	0.2	6.4	11.2	14.1	11.7	6.8	0.2	-9.4	-12.0	-0.7
Alpine Burwash Backup	-21.2	-17.3	-13.8	-7.0	-0.2	4.6	7.4	4.7	-0.2	-8.5	-17.0	-17.9	-7.2
Beaver Creek Palsa	-25.6	-19.9	-12.2	-0.6	7.0	12.6	14.3	11.7	5.2	-5.1	-18.2	-23.1	-4.5
Beaver Creek Test Site	-24.5	-18.9	-11.8	-1.1	6.3	11.9	13.9	11.1	4.7	-5.1	-17.4	-22.0	-4.4
Carmacks Copper	-19.7	-14.8	-9.5	-0.6	6.2	11.4	13.2	11.2	5.3	-3.4	-15.2	-16.1	-2.7
Carmacks ECCC	-21.8	-15.2	-9.1	0.6	7.6	12.8	14.3	12.4	6.5	-2.0	-15.5	-17.5	-2.3
Haines Junction ECCC	-17.3	-13.9	-8.5	-0.2	6.8	12.0	13.4	11.5	6.4	-0.8	-12.4	-15.5	-1.6
Haines Summit 3G3	-10.1	-7.5	-5.1	-2.6	4.1	8.1	10.7	8.0	5.3	0.4	-7.8	-7.6	-0.3
Hour Lake ECCC	-21.4	-18.6	-10.9	-0.8	5.9	11.5	14.5	12.1	6.1	-2.5	-16.9	-23.4	-3.7
Little Fox Lake	-16.5	-11.7	-8.4	-0.9	5.8	10.8	12.7	10.7	5.4	-2.1	-11.9	-12.7	-1.6
Macmillan Pass ECCC	-8.3	-15.3	-12.1	-4.2	-3.3	8.8	11.8	9.6	3.7	-6.4	-11.1	-16.1	-3.1
Mt McIntyre Borehole	-15.2	-13.3	-9.0	-5.0	2.1	6.9	9.8	7.0	3.0	-3.4	-12.0	-12.4	-3.5
Northern Dancer Backup	-14.7	-13.5	-9.0	-4.1	2.4	6.6	9.5	7.2	3.2	-2.8	-12.1	-12.7	-3.3
R7	-22.5	-17.2	-10.7	-1.1	5.9	10.9	13.4	10.6	5.1	-3.9	-15.7	-17.8	-3.8
Wolf Creek 2006-8 Mt Granger	-18.9	-16.3	-12.0	-8.5	-1.3	3.5	6.4	3.6	-0.3	-6.5	-14.8	-15.3	-6.7

Appendix E: Measured and modelled FDD and TDD

Table E-1. Measured FDD, TDD, amd MAAT values at 20 validation sites within the study region. Measured values are based on either ECCC or University of Ottawa temperature monitoring stations. Data was collected between 2006 – 2019, with a minimum of 3 years of data.

Validation Site	FDD	TDD	MMAT
60 Mile Backup	2751	976	-4.9
AINA Base Camp	2408	1449	-2.6
Alaska Highway MP681	2887	NA	NA
Alaska Highway MP788	1945	1706	-0.7
Alaska Highway MP825	1819	1700	-0.3
Alaska Highway MP844	2158	1567	-1.6
Alpine Burwash Backup	2050	798	-3.4
Beaver Creek Palsa	3057	1749	-3.6
Beaver Creek Test Site	3165	1644	-4.2
Carmacks Copper	2322	1704	-1.7
Carmacks ECCC	2679	1914	-2.1
Haines Junction ECCC	2205	1630	-1.6
Haines Summit 3G3	1457	1045	-1.1
Hour Lake ECCC	2542	1599	-2.6
Little Fox Lake	2164	1581	-1.6
Macmillan Pass ECCC	2978	1098	-5.2
Mt McIntyre Borehole	2096	882	-3.3
Northern Dancer Backup	1918	895	-2.8
R7	2416	1712	-1.9
Wolf Creek 2006-8 Mt Granger	2765	481	-6.3

Table E-2. Modelled FDD, TDD, and MAAT values at 20 validation sites within the study region. Modelled values were based on values from Chapter 4.4.

Validation Site	FDD	TDD	MMAT
60 Mile Backup	2699	1016	-4.6
AINA Base Camp	2205	1514	-1.9
Alaska Highway MP681	2128	1759	-1.0
Alaska Highway MP788	1886	1776	-0.3
Alaska Highway MP825	1934	1807	-0.4
Alaska Highway MP844	1922	1714	-0.6
Alpine Burwash Backup	2997	388	-7.2
Beaver Creek Palsa	3420	1570	-5.1
Beaver Creek Test Site	3300	1500	-4.9
Carmacks Copper	2487	1625	-2.4
Carmacks ECCC	2575	1869	-1.9
Haines Junction ECCC	2016	1727	-0.8
Haines Summit 3G3	1360	1156	-0.6
Hour Lake ECCC	2384	1734	-1.8
Little Fox Lake	2150	1564	-1.6
Macmillan Pass ECCC	2149	1196	-2.6
Mt McIntyre Borehole	2005	875	-3.1
Northern Dancer Backup	1889	930	-2.6
R7	2770	1457	-3.6
Wolf Creek 2006-8 Mt Granger	2579	282	-6.3